Eur. Phys. J. C (2021) 81:178
https://doi.org/10.1140/epjc/s10052-020-08677-2

THE EUROPEAN PHYSICAL JOURNAL C

Regular Article - Experimental Physics

Measurements of WH and ZH production in the $H \to b\bar{b}$ decay channel in pp collisions at 13 TeV with the ATLAS detector

ATLAS Collaboration[*]

CERN, 1211 Geneva 23, Switzerland

Received: 7 July 2020 / Accepted: 16 November 2020 / Published online: 22 February 2021

Abstract Measurements of the Standard Model Higgs boson decaying into a $b\bar{b}$ pair and produced in association with a W or Z boson decaying into leptons, using proton–proton collision data collected between 2015 and 2018 by the ATLAS detector, are presented. The measurements use collisions produced by the Large Hadron Collider at a centre-of-mass energy of $\sqrt{s} = 13$ TeV, corresponding to an integrated luminosity of 139 fb^{-1}. The production of a Higgs boson in association with a W or Z boson is established with observed (expected) significances of 4.0 (4.1) and 5.3 (5.1) standard deviations, respectively. Cross-sections of associated production of a Higgs boson decaying into bottom quark pairs with an electroweak gauge boson, W or Z, decaying into leptons are measured as a function of the gauge boson transverse momentum in kinematic fiducial volumes. The cross-section measurements are all consistent with the Standard Model expectations, and the total uncertainties vary from 30% in the high gauge boson transverse momentum regions to 85% in the low regions. Limits are subsequently set on the parameters of an effective Lagrangian sensitive to modifications of the WH and ZH processes as well as the Higgs boson decay into $b\bar{b}$.

Contents

[*] e-mail: atlas.publications@cern.ch

1 Introduction

The Higgs boson [1–6] was discovered in 2012 by the ATLAS and CMS Collaborations [7,8] with a mass of approximately 125 GeV from the analysis of proton–proton (pp) collisions produced by the Large Hadron Collider (LHC) [9]. Since then, the analysis of data collected at centre-of-mass energies of 7 TeV, 8 TeV and 13 TeV in Runs 1 and 2 of the LHC has led to the observation and measurement of many of the production modes and decay channels predicted by the Standard Model (SM) [10–25].

The most likely decay mode of the SM Higgs boson is into pairs of b-quarks, with an expected branching fraction of 58.2% for a mass of $m_H = 125$ GeV [26,27]. However, large backgrounds from multi-jet production make a search in the dominant gluon–gluon fusion production mode very challenging at hadron colliders [28]. The most sensitive production modes for detecting $H \to b\bar{b}$ decays are the associated production of a Higgs boson and a W or Z boson [29], referred to as the VH channel ($V = W$ or Z), where the leptonic decay of the vector boson enables efficient triggering and a significant reduction of the multi-jet background. As well as probing the dominant decay of the Higgs boson, this measurement allows the overall Higgs boson decay width [30,31] to be constrained, provides the

best sensitivity to the WH and ZH production modes and allows Higgs boson production at high transverse momentum to be probed, which provides enhanced sensitivity to some beyond the SM (BSM) physics models in effective field theories [32]. The $b\bar{b}$ decay of the Higgs boson was observed by the ATLAS [33] and CMS Collaborations [34] using data collected at centre-of-mass energies of 7 TeV, 8 TeV and 13 TeV during Runs 1 and 2 of the LHC. ATLAS also used the same dataset to perform differential measurements of the VH, $H \to b\bar{b}$ cross-section in kinematic fiducial volumes defined in the simplified template cross-section (STXS) framework [35]. These measurements were used to set limits on the parameters of an effective Lagrangian sensitive to anomalous Higgs boson couplings with the electroweak gauge bosons.

This paper updates the measurements of the SM Higgs boson decaying into a $b\bar{b}$ pair in the VH production mode with the ATLAS detector in Run 2 of the LHC presented in Refs. [33,35] and uses the full dataset. Events are categorised in 0-, 1- and 2-lepton channels, based on the number of charged leptons, ℓ (electrons or muons[1]), to explore the $ZH \to \nu\nu b\bar{b}$, $WH \to \ell\nu b\bar{b}$ and $ZH \to \ell\ell b\bar{b}$ signatures, respectively. The dominant background processes after the event selection are V + jets, $t\bar{t}$, single-top-quark and diboson production. Multivariate discriminants, built from variables that describe the kinematics, jet flavour and missing transverse momentum content of the selected events, are used to maximise the sensitivity to the Higgs boson signal. Their output distributions are used as inputs to a binned maximum-likelihood fit, referred to as the global likelihood fit, which allows the yields and kinematics of both the signal and the background processes to be estimated. This method is validated using a diboson analysis, where the nominal multivariate analysis is modified to extract the VZ, $Z \to b\bar{b}$ diboson process. The Higgs boson signal measurement is also cross-checked with a dijet-mass analysis, where the signal yield is measured using the mass of the dijet system as the main observable instead of the multivariate discriminant. Finally, limits are set on the coefficients of effective Lagrangian operators which affect the VH production and the $H \to b\bar{b}$ decay. Limits are reported for both the variation of a single operator and also the simultaneous variation of an orthogonal set of linear combinations of operators to which the analysis is sensitive.

This update uses 139 fb^{-1} of pp collision data collected at a centre-of-mass energy of 13 TeV, to be compared with 79.8 fb^{-1} for the previous result. In addition, several improvements have been implemented: enhanced object calibrations, more coherent categorisation between the event selection and the STXS binning, re-optimised multivariate discriminants including the addition of more information, redefined signal and control regions, a significant increase in the effective number of simulated events and re-derived background modelling uncertainties, including using a multivariate approach to estimate the modelling uncertainty in the dominant backgrounds. A complementary analysis using the same final states, but focussing on regions of higher Higgs boson transverse momentum not accessible using the techniques outlined in this paper, has also been undertaken [36]. The same dataset was used, resulting in some overlap in the events analysed.

[1] This includes electrons and muons produced from the leptonic decay of a τ-lepton.

2 The ATLAS detector

ATLAS [37] is a general-purpose particle detector covering nearly the entire solid angle[2] around the collision point. An inner tracking detector, located within a 2 T axial magnetic field generated by a thin superconducting solenoid, is used to measure the trajectories and momenta of charged particles. The inner layers consist of high-granularity silicon pixel detectors covering a pseudorapidity range $|\eta| < 2.5$, with an innermost layer [38,39] that was added to the detector between Run 1 and Run 2. Silicon microstrip detectors covering $|\eta| < 2.5$ are located beyond the pixel detectors. Outside the microstrip detectors and covering $|\eta| < 2.0$, there are straw-tube tracking detectors, which also provide measurements of transition radiation that are used in electron identification.

A calorimeter system surrounds the inner tracking detector, covering the pseudorapidity range $|\eta| < 4.9$. Within the region $|\eta| < 3.2$, electromagnetic calorimetry is provided by barrel ($|\eta| < 1.475$) and endcap ($1.375 < |\eta| < 3.2$) high-granularity lead/liquid-argon (LAr) sampling calorimeters, with an additional thin LAr presampler covering $|\eta| < 1.8$ to correct for energy loss in material upstream of the calorimeters. Hadronic calorimetry is provided by a steel/scintillator-tile calorimeter within $|\eta| < 1.7$, and copper/LAr endcap calorimeters extend the coverage to $|\eta| = 3.2$. The solid angle coverage for $|\eta|$ between 3.2 and 4.9 is completed with copper/LAr and tungsten/LAr calorimeter mod-

[2] ATLAS uses a right-handed coordinate system with its origin at the nominal interaction point (IP) in the centre of the detector and the z-axis coinciding with the axis of the beam pipe. The x-axis points from the IP towards the centre of the LHC ring, and the y-axis points upward. Cylindrical coordinates (r,ϕ) are used in the transverse plane, ϕ being the azimuthal angle around the z-axis. The pseudorapidity is defined in terms of the polar angle θ as $\eta = -\ln\tan(\theta/2)$. The distance in (η,ϕ) coordinates, $\Delta R = \sqrt{(\Delta\phi)^2 + (\Delta\eta)^2}$, is also used to define cone sizes. Rapidity is defined as $y = (1/2)\ln[(E + p_z)/(E - p_z)]$, where E is the energy and p_z is the z-component of the momentum. Transverse momentum and energy are defined as $p_T = p\sin\theta$ and $E_T = E\sin\theta$, respectively.

ules optimised for electromagnetic and hadronic measurements, respectively.

The outermost part of the detector is the muon spectrometer, which measures the curved trajectories of muons in the magnetic field of three large air-core superconducting toroidal magnets. High-precision tracking is performed within the range $|\eta| < 2.7$ and there are chambers for fast triggering within the range $|\eta| < 2.4$.

A two-level trigger system [40] is used to reduce the recorded data rate. The first level is a hardware implementation aiming to reduce the rate to around 100 kHz, while the software-based high-level trigger provides the remaining rate reduction to approximately 1 kHz.

3 Data and simulated event samples

The data used in this analysis were collected using unprescaled single-lepton or missing transverse momentum triggers at a centre-of-mass energy of 13 TeV during the 2015–2018 running periods. Events are selected for analysis only if they are of good quality and if all the relevant detector components are known to have been in good operating condition, which corresponds to a total integrated luminosity of 139.0 ± 2.4 fb^{-1} [41,42]. The recorded events contain an average of 34 inelastic pp collisions per bunch-crossing.

Monte Carlo (MC) simulated events are used to model most of the backgrounds from SM processes and the VH, $H \to b\bar{b}$ signal processes. A summary of all the generators used for the simulation of the signal and background processes is shown in Table 1. Samples produced with alternative generators are used to estimate systematic uncertainties in the event modelling, as described in Sect. 7. The same event generators as in Ref. [33] are used; however, the number of simulated events in all samples has been increased by at least the factor by which the integrated luminosity grew compared to the previous publication (~ 1.75). In addition, processes which significantly contributed to the statistical uncertainty of the background in the previous publication benefited from a further factor of two increase in the number of simulated events produced.

All simulated processes are normalised using the most accurate theoretical cross-section predictions currently available and were generated to next-to-leading-order (NLO) accuracy at least, except for the $gg \to ZH$ and $gg \to VV$ processes, which were generated at LO. All samples of simulated events were passed through the ATLAS detector simulation [43] based on GEANT [44]. The effects of multiple interactions in the same and nearby bunch crossings (pile-up) were modelled by overlaying minimum-bias events, simulated using the soft QCD processes of PYTHIA 8.186 [45] with the A3 [46] set of tuned parameters (tune) and NNPDF2.3LO [47] parton distribution functions (PDF). For all samples of simulated events, except for those generated using SHERPA [48], the EVTGEN V1.6.0 program [49] was used to describe the decays of bottom and charm hadrons.

4 Object and event selection

The event topologies characteristic of VH, $H \to b\bar{b}$ processes contain zero, one or two charged leptons, and two 'b-jets' containing particles from b-hadron decays. The object and event selections broadly follow those of Ref. [33] but with updates to the definition of the signal and control regions.

4.1 Object reconstruction

Tracks measured in the inner detector are used to reconstruct interaction vertices [85], of which the one with the highest sum of squared transverse momenta of associated tracks is selected as the primary vertex of the hard interaction.

Electrons are reconstructed from topological clusters of energy deposits in the electromagnetic calorimeter and matched to a track in the inner detector [86]. Following Refs. [86,87], *loose* electrons are required to have $p_{\mathrm{T}} > 7$ GeV and $|\eta| < 2.47$, to have small impact parameters,[3] to fulfil a loose track isolation requirement, and to meet a 'LooseLH' quality criterion computed from shower shape, track quality and track–cluster matching variables. In the 1-lepton channel, *tight* electrons are selected using a 'TightLH' likelihood requirement and a calorimeter-based isolation in addition to the track-based isolation.

Muons are required to be within the acceptance of the muon spectrometer $|\eta| < 2.7$, to have $p_{\mathrm{T}} > 7$ GeV, and to have small impact parameters. *Loose* muons are selected using a 'loose' quality criterion [88] and a loose track isolation requirement. In the 1-lepton channel, *tight* muons fulfil the 'medium' quality criterion and a stricter track isolation requirement.

Hadronically decaying τ-leptons [89,90] are required to have $p_{\mathrm{T}} > 20$ GeV and $|\eta| < 2.5$, to be outside the transition region between the barrel and endcap electromagnetic calorimeters $1.37 < |\eta| < 1.52$, and to meet a 'medium' quality criterion [90]. Reconstructed hadronic τ-leptons are not directly used in the event selection, but are utilised in the missing transverse momentum calculation and are also used to avoid double-counting hadronic τ-leptons as other objects.

Jets are reconstructed from the energy in topological clusters of calorimeter cells [91] using the anti-k_t algorithm [92] with radius parameter $R = 0.4$. Jet cleaning criteria are used

[3] Transverse and longitudinal impact parameters are defined relative to the primary vertex position, where the beam line is used to approximate the primary vertex position in the transverse plane.

Table 1 The generators used for the simulation of the signal and background processes. Samples are generated considering decays into all three lepton (ℓ) flavours. If not specified, the order of the cross-section calculation refers to the expansion in the strong coupling constant (α_S). The acronyms ME, PS and UE stand for matrix element, parton shower and underlying event, respectively. ($\star$) The events were generated using the first PDF in the NNPDF3.0NLO set and subsequently reweighted to the PDF4LHC15NLO set [50] using the internal algorithm in POWHEG- BOX v2. (†) The NNLO(QCD)+NLO(EW) cross-section calculation for the $pp \to ZH$ process includes the $gg \to ZH$ contribution. The $qq \to ZH$ process is normalised using the cross-section for the $pp \to ZH$ process, after subtracting the $gg \to ZH$ contribution. An additional scale factor is applied to the $qq \to VH$ processes as a function of the transverse momentum of the vector boson, to account for electroweak (EW) corrections at NLO. This makes use of the VH differential cross-section computed with HAWK [51,52]. Contributions from photon-induced processes are also included for $pp \to WH$ [53]. (‡) For the diboson samples the cross-sections are calculated by the Monte Carlo generator at NLO accuracy in QCD

Process	ME generator	ME PDF	PS and Hadronisation	UE model tune	Cross-section order
Signal, mass set to 125 GeV and $b\bar{b}$ branching fraction to 58%					
$qq \to WH$	POWHEG- BOX v2 [54] +	NNPDF3.0NLO$^{(\star)}$ [55]	PYTHIA 8.212 [45]	AZNLO [56]	NNLO(QCD)$^{(\dagger)}$+
$\to \ell\nu b\bar{b}$	GOSAM [57] + MINLO [58,59]				NLO(EW) [60–66]
$qq \to ZH$	POWHEG- BOX v2 +	NNPDF3.0NLO$^{(\star)}$	PYTHIA 8.212	AZNLO	NNLO(QCD)$^{(\dagger)}$+
$\to \nu\nu b\bar{b}/\ell\ell b\bar{b}$	GOSAM + MINLO				NLO(EW)
$gg \to ZH$	POWHEG- BOX v2	NNPDF3.0NLO$^{(\star)}$	PYTHIA 8.212	AZNLO	NLO+
$\to \nu\nu b\bar{b}/\ell\ell b\bar{b}$					NLL [67–71]
Top quark, mass set to 172.5 GeV					
$t\bar{t}$	POWHEG- BOX v2 [72]	NNPDF3.0NLO	PYTHIA 8.230	A14 [73]	NNLO+NNLL [74]
s-channel single top	POWHEG- BOX v2 [75]	NNPDF3.0NLO	PYTHIA 8.230	A14	NLO [76]
t-channel single top	POWHEG- BOX v2 [75]	NNPDF3.0NLO	PYTHIA 8.230	A14	NLO [77]
Wt	POWHEG- BOX v2 [78]	NNPDF3.0NLO	PYTHIA 8.230	A14	Approximate NNLO [79]
Vector boson + jets					
$W \to \ell\nu$	SHERPA 2.2.1 [48,80,81]	NNPDF3.0NNLO	SHERPA 2.2.1 [82,83]	Default	NNLO [84]
$Z/\gamma^* \to \ell\ell$	SHERPA 2.2.1	NNPDF3.0NNLO	SHERPA 2.2.1	Default	NNLO
$Z \to \nu\nu$	SHERPA 2.2.1	NNPDF3.0NNLO	SHERPA 2.2.1	Default	NNLO
Diboson					
$qq \to WW$	SHERPA 2.2.1	NNPDF3.0NNLO	SHERPA 2.2.1	Default	NLO$^{(\ddagger)}$
$qq \to WZ$	SHERPA 2.2.1	NNPDF3.0NNLO	SHERPA 2.2.1	Default	NLO$^{(\ddagger)}$
$qq \to ZZ$	SHERPA 2.2.1	NNPDF3.0NNLO	SHERPA 2.2.1	Default	NLO$^{(\ddagger)}$
$gg \to VV$	SHERPA 2.2.2	NNPDF3.0NNLO	SHERPA 2.2.2	Default	NLO$^{(\ddagger)}$

to identify jets arising from non-collision backgrounds or noise in the calorimeters [93], and events containing such jets are removed. Jets are required to have $p_{\mathrm{T}} > 20\,\mathrm{GeV}$ in the central region ($|\eta| < 2.5$), and $p_{\mathrm{T}} > 30\,\mathrm{GeV}$ outside the tracker acceptance ($2.5 < |\eta| < 4.5$). A jet vertex tagger [94] is used to remove jets with $p_{\mathrm{T}} < 120\,\mathrm{GeV}$ and $|\eta| < 2.5$ that are identified as not being associated with the primary vertex of the hard interaction. Simulated jets are labelled as b-, c- or light-flavour jets according to which hadrons with $p_{\mathrm{T}} > 5\,\mathrm{GeV}$ are found within a cone of size $\Delta R = 0.3$ around their axis [95]. In the central region, jets are identified as b-jets (b-tagged) using a multivariate discriminant [95] (MV2), with the selection tuned to produce an average efficiency of 70% for b-jets in simulated $t\bar{t}$ events, which corresponds to light-flavour (u-, d-, s-quark and gluon) jet and c-jet misidentification efficiencies of 0.3% and 12.5% respectively.

Simulated V+jets events are categorised according to the two b-tagged jets that are required in the event: $V + ll$ when they are both light-flavour jets, $V + cl$ when there is one c-jet and one light-flavour jet, and $V +$ HF (heavy flavour) in all other cases (which after the b-tagging selection mainly consist of events with two b-jets).

In practice, b-tagging is not applied directly to simulated events containing light-flavour jets or c-jets, because the substantial MV2 rejection results in a significant statistical uncertainty for these background processes. Instead, all events with c-jets or light-flavour jets are weighted by the probability that these jets pass the b-tagging requirement [87]. This is an expansion of the weighting technique compared to the previous analysis, where only jets in the $V + ll$, $V + cl$ and WW processes were treated in this manner. Applying the same treatment to all light-flavour jets and c-jets significantly increases the number of simulated events present after the full event selection, reducing the statistical uncertainty of the $V +$ HF ($t\bar{t}$) background by $\sim$ 65–75% ($\sim$ 25%). When comparing the direct application of the b-tagging to the weighting technique, differences were observed in a particular subset of events with a small angular separation between the jets, but it was verified that this has a negligible impact on the result.

In addition to the standard jet energy scale calibration [96], b-tagged jets receive additional flavour-specific corrections to improve their energy measurement (scale and resolution): if any muons are found within a p_{T}-dependent cone around the jet axis, the four-momentum of the closest muon is added to that of the jet. In addition, a residual correction is applied to equalise the response to jets with leptonic or hadronic decays of heavy-flavour hadrons and to correct for resolution effects. This improves the resolution of the dijet mass by up to $\sim$ 20% [87]. Alternatively, in the 2-lepton channel for events with two or three jets, a per-event kinematic likelihood uses the complete reconstruction of all final-state objects to improve the estimate of the energy of the b-jets. This improves the resolution of the dijet mass by up to $\sim$ 40%.

The missing transverse momentum, $\boldsymbol{E}_{\mathrm{T}}^{\mathrm{miss}}$, is reconstructed as the negative vector sum of the transverse momenta of leptons, photons, hadronically decaying τ-leptons and jets, and a 'soft-term', $\boldsymbol{p}_{\mathrm{T}}^{\mathrm{miss,st}}$. The soft-term is calculated as the vectorial sum of the p_{T} of tracks matched to the primary vertex but not associated with a reconstructed lepton or jet [97]. The magnitude of $\boldsymbol{E}_{\mathrm{T}}^{\mathrm{miss}}$ is referred to as $E_{\mathrm{T}}^{\mathrm{miss}}$. The track-based missing transverse momentum, $\boldsymbol{p}_{\mathrm{T}}^{\mathrm{miss}}$, is calculated using only tracks reconstructed in the inner tracking detector and matched to the primary vertex.

An overlap removal procedure is applied to avoid any double-counting between leptons, including hadronically decaying τ-leptons, and jets.

4.2 Event selection and categorisation

Events are categorised into 0-, 1- and 2-lepton channels (referred to as the n-lepton channels) depending on the number of selected electrons and muons, to target the $ZH \to \nu\nu b\bar{b}$, $WH \to \ell\nu b\bar{b}$ and $ZH \to \ell\ell b\bar{b}$ signatures, respectively. In all channels, events are required to have exactly two b-tagged jets, which form the Higgs boson candidate. At least one b-tagged jet is required to have p_{T} greater than 45 GeV. Events are further split into 2-jet or 3-jet categories, where the 3-jet category includes events with one or more untagged jets. In the 0- and 1-lepton channels, only one untagged jet is allowed, as the $t\bar{t}$ background is much larger in events with four jets or more. In the 2-lepton channel any number of untagged jets are accepted in the 3-jet category (referred to as the $\geq$ 3-jet category when discussing only the 2-lepton channel), which increases the signal acceptance in this category by 100%.

The reconstructed transverse momentum of the vector boson, p_{T}^{V}, corresponds to $E_{\mathrm{T}}^{\mathrm{miss}}$ in the 0-lepton channel, the vectorial sum of $\boldsymbol{E}_{\mathrm{T}}^{\mathrm{miss}}$ and the charged-lepton transverse momentum in the 1-lepton channel, and the transverse momentum of the 2-lepton system in the 2-lepton channel. Since the signal-to-background ratio increases for large p_{T}^{V} values [98,99], the analysis focuses on two high-p_{T}^{V} regions defined as $150\,\mathrm{GeV} < p_{\mathrm{T}}^{V} < 250\,\mathrm{GeV}$ and $p_{\mathrm{T}}^{V} > 250\,\mathrm{GeV}$. In the 2-lepton channel, an additional fiducial measurement region is studied via the inclusion of a medium-p_{T}^{V} region with $75\,\mathrm{GeV} < p_{\mathrm{T}}^{V} < 150\,\mathrm{GeV}$.

The event selection for the three lepton channels is outlined in Table 2 with details provided below.

0-lepton channel The online selection uses $E_{\mathrm{T}}^{\mathrm{miss}}$ triggers with thresholds that varied from 70 GeV to 110 GeV between the 2015 and 2018 data-taking periods. Their efficiency is measured in W+jets, Z+jets and $t\bar{t}$ events using single-muon

Table 2 Summary of the event selection and categorisation in the 0-, 1- and 2-lepton channels

Selection	0-lepton	1-lepton		2-lepton
		e sub-channel	μ sub-channel	
Trigger	$E_{\mathrm{T}}^{\mathrm{miss}}$	Single lepton	$E_{\mathrm{T}}^{\mathrm{miss}}$	Single lepton
Leptons	0 *loose* leptons	Exactly 1 *tight* electron	Exactly 1 *tight* muon	Exactly 2 *loose* leptons
		0 additional *loose* leptons	0 additional *loose* leptons	$p_{\mathrm{T}} > 27$ GeV
		$p_{\mathrm{T}} > 27$ GeV	$p_{\mathrm{T}} > 25$ GeV	Same-flavour
				Opposite-sign charges ($\mu\mu$)
$E_{\mathrm{T}}^{\mathrm{miss}}$	> 150 GeV	> 30 GeV	–	–
$m_{\ell\ell}$	–	–	–	$81\ \mathrm{GeV} < m_{\ell\ell} < 101\ \mathrm{GeV}$
Jet p_{T}		> 20 GeV for $\lvert\eta\rvert < 2.5$		
		> 30 GeV for $2.5 < \lvert\eta\rvert < 4.5$		
b-jets		Exactly 2 b-tagged jets		
Leading b-tagged jet p_{T}		> 45 GeV		
Jet categories	Exactly 2/Exactly 3 jets	Exactly 2/Exactly 3 jets		Exactly 2/$\geq$ 3 jets
H_{T}	> 120 GeV (2 jets), >150 GeV (3 jets)	–		–
$\min[\Delta\phi(\boldsymbol{E}_{\mathrm{T}}^{\mathrm{miss}}, \mathbf{jets})]$	$> 20°$ (2 jets), $> 30°$ (3 jets)	–		–
$\Delta\phi(\boldsymbol{E}_{\mathrm{T}}^{\mathrm{miss}}, \boldsymbol{bb})$	$> 120°$	–		–
$\Delta\phi(\boldsymbol{b_1}, \boldsymbol{b_2})$	$< 140°$	–		–
$\Delta\phi(\boldsymbol{E}_{\mathrm{T}}^{\mathrm{miss}}, \boldsymbol{p}_{\mathrm{T}}^{\mathrm{miss}})$	$< 90°$	–		–
p_{T}^{V} regions	–	–		$75\ \mathrm{GeV} < p_{\mathrm{T}}^{V} < 150\ \mathrm{GeV}$
	$150\ \mathrm{GeV} < p_{\mathrm{T}}^{V} < 250\ \mathrm{GeV}$	$150\ \mathrm{GeV} < p_{\mathrm{T}}^{V} < 250\ \mathrm{GeV}$		$150\ \mathrm{GeV} < p_{\mathrm{T}}^{V} < 250\ \mathrm{GeV}$
	$p_{\mathrm{T}}^{V} > 250$ GeV	$p_{\mathrm{T}}^{V} > 250$ GeV		$p_{\mathrm{T}}^{V} > 250$ GeV
Signal regions		$\Delta R(\boldsymbol{b_1}, \boldsymbol{b_2})$ signal selection		
Control regions		High and low $\Delta R(\boldsymbol{b_1}, \boldsymbol{b_2})$ side-bands		

triggered data, which effectively selects events with large trigger-level $E_{\mathrm{T}}^{\mathrm{miss}}$ values as muons are not included in the trigger $E_{\mathrm{T}}^{\mathrm{miss}}$ calculation. The resulting trigger correction factors that are applied to the simulated events range from 0.95 at the offline $E_{\mathrm{T}}^{\mathrm{miss}}$ threshold of 150 GeV to a negligible deviation from unity at $E_{\mathrm{T}}^{\mathrm{miss}}$ values above 200 GeV. A requirement on the scalar sum of the transverse momenta of the jets, H_{T}, removes a small part of the phase space (less than 1%) where the trigger efficiency depends mildly on the number of jets in the event. Events with any *loose* lepton are rejected. High $E_{\mathrm{T}}^{\mathrm{miss}}$ in multi-jet events typically arises from mismeasured jets in the calorimeters. Such events are efficiently removed by requirements on the angular separation of the $\boldsymbol{E}_{\mathrm{T}}^{\mathrm{miss}}$, jets, and $\boldsymbol{p}_{\mathrm{T}}^{\mathrm{miss}}$.

1-lepton channel In the electron sub-channel, events are required to satisfy a logical OR of single-electron triggers with p_{T} thresholds that started at 24 GeV in 2015 and increased to 26 GeV in 2016–2018.[4] The muon sub-channel uses the same $E_{\mathrm{T}}^{\mathrm{miss}}$ triggers and correction factors as the 0-lepton channel. As these triggers effectively select on p_{T}^{V}, given that muons are not included in the trigger $E_{\mathrm{T}}^{\mathrm{miss}}$ calculation, they perform more efficiently than the single-muon triggers in the analysis phase space, which have a lower efficiency due to the more limited coverage of the muon trigger system in the central region. Events are required to have exactly one *tight* muon with $p_{\mathrm{T}} > 25$ GeV or one *tight* electron with $p_{\mathrm{T}} > 27$ GeV and no additional *loose* leptons. In the electron sub-channel an additional selection of $E_{\mathrm{T}}^{\mathrm{miss}} > 30$ GeV is applied to reduce the background from multi-jet production.

2-lepton channel The trigger selection in the electron sub-channel is the same as in the 1-lepton channel. In the muon sub-channel, an OR of single-muon triggers is used, with lowest p_{T} thresholds increasing from 2016–2018 and ranging from 20 GeV to 26 GeV. Events must have exactly two same-flavour *loose* leptons, one of which must have $p_{\mathrm{T}} > 27$ GeV, and the invariant mass of the lepton pair must be close to the Z boson mass. In dimuon events, the two muons are required to have opposite-sign charge. This is not used in the electron sub-channel, where the charge misidentification rate is not negligible.

Signal and control regions The three n-lepton channels, two jet categories and two (0-lepton, 1-lepton) or three (2-lepton) p_{T}^{V} regions result in a total of 14 analysis regions. Each analysis region is further split into a signal region (SR) and two control regions (CRs), resulting in a total of 42 regions. The CRs are enriched in either V + HF or $t\bar{t}$ events and defined using a continuous selection on the ΔR between the two b-tagged jets, $\Delta R(\boldsymbol{b}_1, \boldsymbol{b}_2)$, as a function of p_{T}^{V}, with the b-tagged jets labelled in decreasing p_{T} as b_1 and b_2. A lower

[4] Additional identification and isolation requirements are applied to the trigger object to allow a low p_{T} threshold to be maintained throughout Run 2.

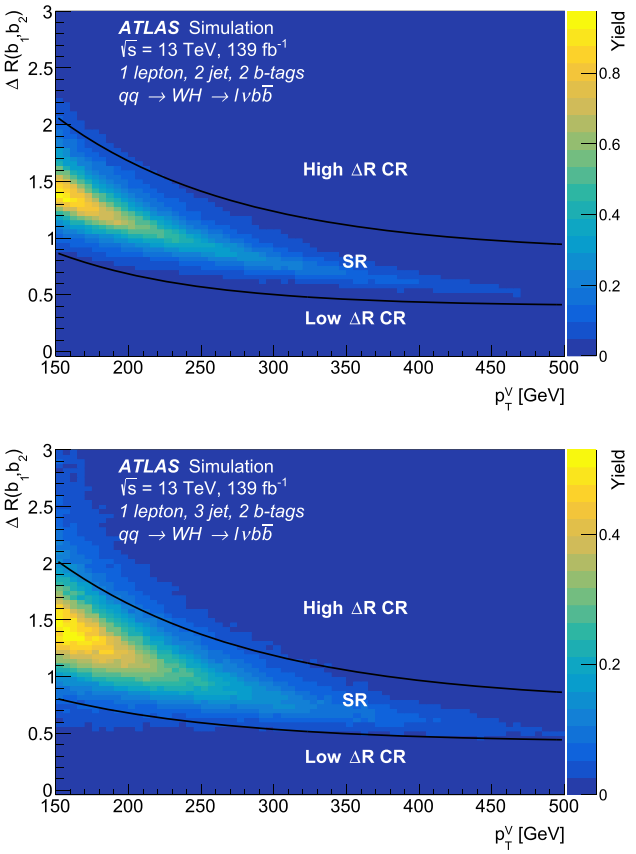

Fig. 1 The signal yield distribution of the ΔR between the two b-tagged jets, $\Delta R(\boldsymbol{b}_1, \boldsymbol{b}_2)$, as a function of p_{T}^{V} in the 1-lepton channel for 2-b-tag events, in the 2-jet (top) and exactly 3-jet (bottom) categories in the high-p_{T}^{V} region. The lines demonstrate the continuous lower and upper selection on $\Delta R(\boldsymbol{b}_1, \boldsymbol{b}_2)$ used to categorise the events into the signal and control regions

Table 3 The cross-section (σ) times branching fraction (B) and acceptance obtained from the simulated signal samples for the three channels at $\sqrt{s} = 13$ TeV. The qq- and gg-initiated ZH processes are shown separately. The branching fractions are calculated considering only decays into muons and electrons for $Z \to \ell\ell$ and decays into all three lepton flavours for $W \to \ell\nu$. The acceptance is calculated as the fraction of events remaining in the combined signal and control regions after the full event selection

Process	$\sigma \times B$ [fb]	Acceptance [%]		
		0-lepton	1-lepton	2-lepton
$qq \to ZH \to \ell\ell b\bar{b}$	29.9	< 0.1	0.2	6.4
$gg \to ZH \to \ell\ell b\bar{b}$	4.8	< 0.1	0.3	14.5
$qq \to WH \to \ell\nu b\bar{b}$	269.0	0.2	1.1	–
$qq \to ZH \to \nu\nu b\bar{b}$	89.1	1.9	–	–
$gg \to ZH \to \nu\nu b\bar{b}$	14.3	3.5	–	–

Table 4 The simplified template cross-section regions used for measurements and the corresponding reconstructed analysis regions that are most sensitive. The current analysis is not sensitive to the regions WH, $p_{\mathrm{T}}^{W,\mathrm{t}} < 150$ GeV and ZH, $p_{\mathrm{T}}^{Z,\mathrm{t}} < 75$ GeV, and their cross-sections are fixed to the SM prediction within their theoretical uncertainties. All leptonic decays of the weak gauge bosons (including $Z \to \tau\tau$ and $W \to \tau\nu$, which are extrapolated from the electron and muon channel measurements) are considered for the STXS definition

STXS region		Corresponding reconstructed analysis regions		
Process	$p_{\mathrm{T}}^{V,\mathrm{t}}$ interval (GeV)	Number of leptons	p_{T}^{V} interval (GeV)	Number of jets
WH	150–250	1	150–250	2, 3
WH	> 250	1	> 250	2, 3
ZH	75–150	2	75–150	2, ≥ 3
ZH	150–250	0	150–250	2, 3
		2	150–250	2, $\geq$3
ZH	> 250	0	> 250	2, 3
		2	> 250	2, $\geq$3

and upper requirement on $\Delta R(\boldsymbol{b}_1, \boldsymbol{b}_2)$ is applied, creating two CRs, referred to as the low and high ΔR CRs, shown in Fig. 1. In the 1-lepton channel, the high ΔR selection was tuned such that the SR and low ΔR CR contain 95% (85%) of the signal in the 2-jet (3-jet) categories, whilst the low ΔR selection was tuned such that the SR contains 90% of the diboson yield, to ensure that a sufficient number of these events remain when conducting the diboson validation analysis. The same ΔR selection is applied in all three n-lepton channels and keeps over 93% of the signal in the 2-jet categories and over 81% (68%) of the signal in the 3-jet ($\geq$ 3-jet) categories.[5]

The acceptances in the three n-lepton channels after the event selection, as well as the predicted cross-sections times branching fractions for $(W/Z)H$ with $W \to \ell\nu$, $Z \to \ell\ell$, $Z \to \nu\nu$, and $H \to b\bar{b}$ are given in Table 3. The non-negligible acceptance for the $qq \to WH$ process in the 0-lepton channel is mostly due to events with a hadronically decaying τ-lepton produced in the W decay, which are not explicitly vetoed and which could also be misidentified as a jet or subsequently decay to a low-p_{T} electron or muon that fails to satisfy the selection criteria. The larger acceptance for the $gg \to ZH$ process compared with $qq \to ZH$ is due to the harder p_{T}^{V} spectrum of the gluon-induced process.

4.3 Simplified template cross-section categories

Cross-section measurements are conducted in the reduced $VH, V \to$ leptons stage-1.2 STXS region scheme [100,101] described in Ref. [35] and summarised in Table 4. In this scheme, $qq \to ZH$ and $gg \to ZH$ are treated as a single ZH process, since there is currently not enough sensitivity to distinguish between them. The expected signal distributions and acceptance times efficiencies for each STXS region are estimated from the simulated signal samples by selecting events using information from the generator's 'truth' record, in particular the truth p_{T}^{V}, denoted by $p_{\mathrm{T}}^{V,\mathrm{t}}$. The signal yield in each reconstructed-event category for each STXS region is shown in Fig. 2a, with the corresponding fraction of signal events shown in Fig. 2b. The key improvement compared to the previous publication is the addition of a reconstructed-event category with $p_{\mathrm{T}}^{V} > 250$ GeV. This region is more aligned with the STXS regions and significantly reduces the correlation between the STXS measurements in the two highest $p_{\mathrm{T}}^{V,\mathrm{t}}$ bins. The acceptance times efficiency for WH events with $p_{\mathrm{T}}^{W,\mathrm{t}} < 150$ GeV or ZH events with $p_{\mathrm{T}}^{Z,\mathrm{t}} < 75$ GeV is at the level of 0.1% or smaller. Given the lack of sensitivity to these regions, the signal cross-section in these regions is constrained to the SM prediction, within the theoretical uncertainties. These regions contribute only marginally to the selected event sample and the impact on the final results is negligible.

5 Multivariate discriminants

A multivariate discriminant is used to improve the sensitivity of the analysis. Two sets of boosted decision trees (BDTs) are trained using the same input variables. A nominal set, referred to as BDT_{VH}, is designed to discriminate the VH signal from the background processes. A second set, referred to as BDT_{VZ}, which aims to separate the $VZ, Z \to b\bar{b}$ diboson process from the VH signal and other background processes, is used to validate the VH analysis. In each set, BDTs are trained in eight regions, obtained by merging some of the 14 analysis regions. In particular, the 150 GeV $< p_{\mathrm{T}}^{V} <$ 250 GeV and $p_{\mathrm{T}}^{V} >$ 250 GeV analysis regions in each lepton channel and jet category are merged for the training, as no increase in sensitivity was found when undertaking separate trainings in the two regions. The outputs of the BDTs, evaluated in each signal region, are used as final discriminating variables.

The BDT input variables used in the three lepton channels are detailed in Table 5. The separation of two b-tagged jets in pseudorapidity is denoted by $|\Delta\eta(\boldsymbol{b_1}, \boldsymbol{b_2})|$. In 3-jet events, the third jet is labelled as jet_3 and the mass of the 3-jet system is denoted m_{bbj}. The azimuthal angle between the vector boson and the system of the Higgs boson candidate formed from the two b-tagged jets is denoted $\Delta\phi(\boldsymbol{V}, \boldsymbol{bb})$, and their pseudorapidity separation is denoted $\Delta\eta(\boldsymbol{V}, \boldsymbol{bb})$. In the 0-lepton channel, m_{eff} is defined as the scalar sum of the transverse

[5] Although the higher jet multiplicity categories have a lower signal efficiency than the 2-jet categories, any reduction in the sensitivity in these categories is less than 5%.

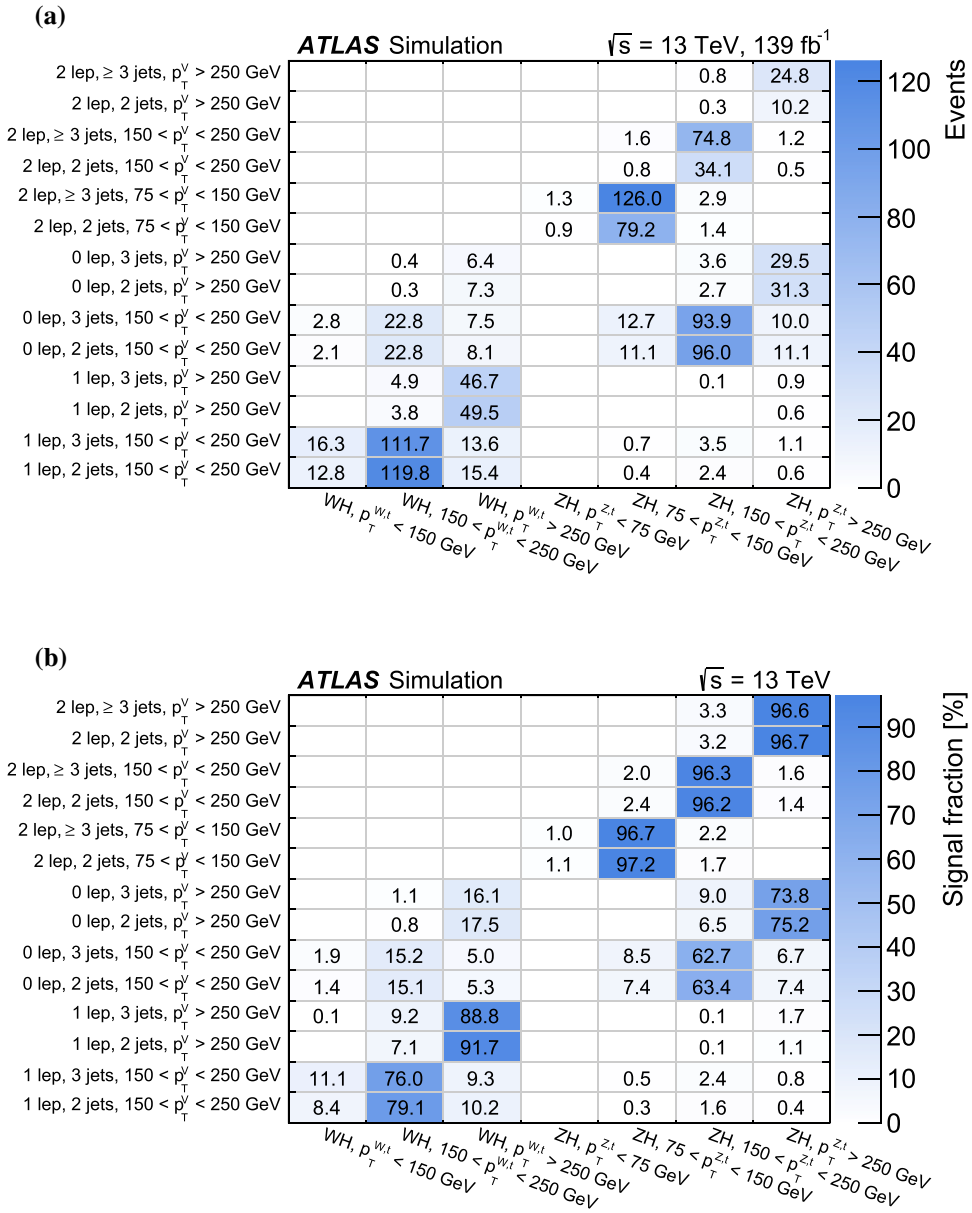

Fig. 2 For each of the STXS regions, **a** the predicted signal event yield for VH, $V \to$ leptons, $H \to b\bar{b}$ events of each reconstructed-analysis region (y-axis) for each STXS signal region (x-axis); **b** the predicted fraction of signal events passing all selection criteria (in percent) in every reconstructed-event category (y-axis) from each STXS signal region (x-axis). Entries with event yield below 0.1 or signal fractions below 0.1% are not shown

momenta of all jets and the $E_{\mathrm{T}}^{\mathrm{miss}}$ ($m_{\mathrm{eff}} = H_{\mathrm{T}} + E_{\mathrm{T}}^{\mathrm{miss}}$). In the 1-lepton channel, the angle between the lepton and the closest b-tagged jet in the transverse plane is denoted $\min(\Delta\phi(\boldsymbol{\ell}, \boldsymbol{b}))$ and two variables are used to improve the rejection of the $t\bar{t}$ background: the rapidity difference between the W and Higgs boson candidates, $|\Delta y(\boldsymbol{V}, \boldsymbol{bb})|$ and, assuming that the event is $t\bar{t}$, the reconstructed top quark mass, m_{top}. The latter is calculated as the invariant mass of the lepton, the reconstructed neutrino and the b-tagged jet that yields the lower mass value. For both variables, the transverse component of the neutrino momentum is identified with $\boldsymbol{E}_{\mathrm{T}}^{\mathrm{miss}}$, and the longitudinal component is obtained by applying a W-mass constraint to the lepton–neutrino system. The variable $E_{\mathrm{T}}^{\mathrm{miss}}/\sqrt{S_{\mathrm{T}}}$, where S_{T} is the scalar sum of transverse momenta of the charged leptons and jets in the event, is defined for use in the 2-lepton channel.

In addition to the above, which were all used in the previous iteration of the analysis [33], the following variables are also input to the BDTs:

- Binned MV2 b-tagging discriminant: The MV2 discriminant for the two b-tagged jets is input to the BDT. The MV2 discriminant is grouped into two bins corresponding to efficiencies of 0–60% and 60–70%, which are calibrated to data [95,102,103]. This variable provides additional rejection against backgrounds where a c-jet or light-flavour jet has been misidentified as a b-jet, especially $W \to cq$ in the $t\bar{t}$ and Wt backgrounds. This improves the sensitivity in the 1-lepton (0-lepton) channel by $\sim$ 10% ($\sim$ 7%). The binned MV2 discriminant does not provide any additional sensitivity in the 2-lepton

Table 5 Variables used for the multivariate discriminant in each of the channels, where the × symbol indicates the inclusion of a variable

Variable	0-lepton	1-lepton	2-lepton
m_{bb}	×	×	×
$\Delta R(\boldsymbol{b_1}, \boldsymbol{b_2})$	×	×	×
$p_{\mathrm{T}}^{b_1}$	×	×	×
$p_{\mathrm{T}}^{b_2}$	×	×	×
p_{T}^{V}	$\equiv E_{\mathrm{T}}^{\mathrm{miss}}$	×	×
$\Delta\phi(\boldsymbol{V}, \boldsymbol{bb})$	×	×	×
MV2(b_1)	×	×	
MV2(b_2)	×	×	
$\lvert\Delta\eta(\boldsymbol{b_1}, \boldsymbol{b_2})\rvert$	×		
m_{eff}	×		
$p_{\mathrm{T}}^{\mathrm{miss,st}}$	×		
$E_{\mathrm{T}}^{\mathrm{miss}}$	×	×	
$\min[\Delta\phi(\boldsymbol{\ell}, \boldsymbol{b})]$		×	
m_{T}^{W}		×	
$\lvert\Delta y(\boldsymbol{V}, \boldsymbol{bb})\rvert$		×	
m_{top}		×	
$\lvert\Delta\eta(\boldsymbol{V}, \boldsymbol{bb})\rvert$			×
$E_{\mathrm{T}}^{\mathrm{miss}}/\sqrt{S_{\mathrm{T}}}$			×
$m_{\ell\ell}$			×
$\cos\theta(\boldsymbol{\ell^-}, \boldsymbol{Z})$			×
	Only in 3-jet events		
$p_{\mathrm{T}}^{\mathrm{jet}_3}$	×	×	×
m_{bbj}	×	×	×

channel, where the backgrounds are dominated by processes containing two b-jets.

- Magnitude of the track-based $E_{\mathrm{T}}^{\mathrm{miss}}$ soft-term, $p_{\mathrm{T}}^{\mathrm{miss,st}}$: In the 0-lepton channel this provides additional rejection against the $t\bar{t}$ background, which may contain unreconstructed objects, such as leptons or b-jets, due to kinematic and detector acceptance. The presence of such objects in an event will result in a larger $p_{\mathrm{T}}^{\mathrm{miss,st}}$ for $t\bar{t}$ events than for signal events. This improves the sensitivity in the 0-lepton channel by $\sim$ 2%–3%.
- Z boson polarisation, $\cos\theta(\boldsymbol{\ell^-}, \boldsymbol{Z})$: The $\cos\theta(\boldsymbol{\ell^-}, \boldsymbol{Z})$ is calculated as the cosine of the polar angle between the lepton (ℓ^-) direction in the Z rest frame and the flight direction of the Z boson in the laboratory frame. The Z bosons from the ZH signal process are expected to have a different polarisation compared to those from the dominant Z+jets background [104], which provides additional background rejection in the 2-lepton channel. This improves the sensitivity in the 2-lepton channel by $\sim$ 7%.

The distributions of all input variables of the BDTs are compared between data and simulation, and good agreement is found within the uncertainties. The same training procedures and BDT output binning transformation as those detailed in Ref. [33] are used, with the exception that the training algorithm was updated to use gradient boosting in the TMVA [105] framework.

6 Background modelling

The simulated event samples summarised in Sect. 3 are used to model all background processes, except for the $t\bar{t}$ background in the 2-lepton channel[6] and the multi-jet background in the 1-lepton channel, which are both estimated using data-driven techniques, as discussed below.

6.1 Data-driven $t\bar{t}$ background estimation

In the 2-lepton channel a high-purity control region, over 99% pure in $t\bar{t}$ and single-top-quark Wt events (jointly referred to as the top background), is defined using the nominal event selection, but replacing the same-flavour lepton selection with a requirement of exactly one electron and one muon. This region is referred to as the $e\mu$-control region, $e\mu$-CR. As these top background events typically contain two W bosons which decay into leptons, they are symmetric in lepton flavour. The events in the $e\mu$-CR are directly used to model the shape and normalisation of the same-flavour lepton top background in the nominal selection. Any bias caused from the lepton trigger, reconstruction, identification or acceptance, is determined by comparing the yield of simulated top background events in the nominal selection with that in the $e\mu$ control region. No significant bias in the shape or normalisation is observed for any of the important kinematic variables, including the BDT discriminant. A ratio of the top yield in the analysis region to that in the $e\mu$-CR of 1.00 ± 0.01 (1.01 ± 0.01) is determined using simulation, for the 2-jet ($\geq$ 3-jet) region, where the uncertainty in the ratio is the statistical uncertainty resulting from the simulated samples. As no evaluated theoretical or experimental uncertainties create any bias beyond the statistical uncertainty of the ratio, the latter is assigned as an extrapolation uncertainty. This method has the advantage that all the experimental and theoretical uncertainties are eliminated, resulting in the data statistics in the $e\mu$-CR becoming the dominant uncertainty source for the data-driven top background estimate.

6.2 Multi-jet background estimation

Multi-jet (MJ) event production has a large cross-section and thus, despite not being a source of genuine missing transverse

[6] The $t\bar{t}$ background in the 2-lepton channel was modelled using simulated event samples in the previous publication [33].

momentum or prompt leptons, has the potential to contribute a non-negligible amount of background. Using the same techniques detailed in Ref. [33], the MJ background was demonstrated to be negligible in both the 0- and 2-lepton channels.

In the 1-lepton channel, the MJ background is reduced to the percent level and is predicted using the same method as described in Ref. [33] with minor changes to account for the use of the MV2(b_j) variables in the BDT. The MJ background is modelled from data in an MJ-enriched control region (MJ-CR), from which all simulated backgrounds are subtracted. The MJ-CR is defined by applying the nominal event selection, except for the stricter lepton isolation requirement, which is inverted. The requirement on the number of b-tagged jets is relaxed from two (2-b-tag MJ-CR) to one (1-b-tag MJ-CR) to increase the statistical precision. To correctly estimate the 2-b-tag MJ BDT shape, the values of both the MV2(b_1) and MV2(b_2) BDT input variables in the 1-b-tag events, are replaced with values emulated from a joint MV2(b_1) and MV2(b_2) probability distribution derived from the 2-b-tag MJ-CR. The normalisation of the MJ background is then determined from a template fit to the m_{T}^{W} distribution after applying the nominal selection with a 2-b-tag requirement, using the MJ shape predicted from the 1-b-tag MJ-CR and the shapes of the other backgrounds from simulation.

7 Systematic uncertainties

The sources of systematic uncertainty can be broadly divided into three groups: those of an experimental nature, those related to the modelling of the backgrounds and those associated with the Higgs boson signal simulation. The estimation of the uncertainties closely follows the methodology outlined in Refs. [35,87] and is briefly summarised below.

7.1 Experimental uncertainties

The dominant experimental uncertainties originate from the b-tagging correction factors, jet energy scale calibration and the modelling of the jet energy resolution. The b-tagging correction factors, determined from the difference between the efficiencies measured in data and simulation, are evaluated in five MV2 discriminant bins and are derived separately for b-jets, c-jets and light-flavour jets [95,102,103]. All of the correction factors for the three jet flavours have uncertainties estimated from multiple measurements, which are decomposed into uncorrelated components that are then treated independently. The uncertainties in the jet energy scale and resolution are based on their respective measurements [96,106].

Uncertainties in the reconstruction, identification, isolation and trigger efficiencies of muons [88] and electrons [107] are considered, along with the uncertainty in their energy scale and resolution. These are found to have only a small impact on the result. The uncertainties in the energy scale and resolution of the jets and leptons are propagated to the calculation of $E_{\mathrm{T}}^{\mathrm{miss}}$, which also has additional uncertainties from the modelling of the underlying event and momentum scale, momentum resolution and reconstruction efficiency of the tracks used to compute the soft-term [97,108]. An uncertainty is assigned to the $E_{\mathrm{T}}^{\mathrm{miss}}$ trigger correction factors, determined from the ratio of the trigger efficiency in data and simulation, to account for the statistical uncertainty in the measured correction factors and for differences between the correction factors determined from W + jets, Z + jets and $t\bar{t}$ events. The uncertainty in the combined 2015–2018 integrated luminosity is 1.7%. It is derived following a methodology similar to that detailed in Ref. [41], and using the LUCID-2 detector for the baseline luminosity measurements [42]. The average number of interactions per bunch crossing in the simulation is rescaled by 1.03 to improve agreement between simulation and data, based on the measurement of the visible cross-section in minimum-bias events [109], and an uncertainty, as large as the correction, is included.

7.2 Background uncertainties

Modelling uncertainties are derived for the simulated samples and broadly cover three areas: normalisations (referred to as normalisation uncertainties), acceptance differences that affect the relative normalisations between regions with a common underlying normalisation (referred to as relative acceptance uncertainties), and the shapes of the differential distributions of the kinematic variables (referred to as shape uncertainties).

The overall cross-sections and associated normalisation uncertainties for the background processes are taken from the currently most accurate calculations as detailed in Table 1, apart from the main backgrounds (Z + HF, W + HF, $t\bar{t}$) whose normalisations are left unconstrained (floated) in the global likelihood fit.

The relative acceptance and shape uncertainties are derived from either particle-level or reconstruction-level comparisons between nominal and alternative simulated samples, or from comparisons with data in control regions. The alternative samples are produced either by different generators or by altering the nominal generator's parameter values. When relative acceptance uncertainties are estimated, the nominal and alternative samples are normalised using the same production cross-section. Shape uncertainties are estimated within a signal region, an analysis region or a set of analysis regions, depending on the distribution being varied, with the nominal and alternative samples scaled to have the same normalisation in the studied area. Shape uncertainties over regions with different acceptance, can affect not only the shape, but also cause event migration between regions

(referred to as a shape plus migration uncertainty) as opposed to an uncertainty that only alters the shape within a single SR (referred to as just a shape uncertainty). Unless stated otherwise, the uncertainty is taken from the alternative sample that differs most in shape from the nominal sample.

Shape uncertainties for Z + HF, single-top and diboson backgrounds are derived for the m_{bb} and p_{T}^{V} variables, as it was found sufficient to consider the changes induced in these variables to cover the overall shape variation of the BDT discriminant. For W + HF and $t\bar{t}$ backgrounds, a more sophisticated multidimensional parameterisation method is introduced to estimate the shape uncertainties of the final discriminant [110]. In this method, a BDT (referred to as BDT_S) is trained to discriminate the nominal sample from an alternative sample, using the kinematic variables from the BDT_{VH} (Table 5) as input variables, except for the p_{T}^{V}. Before training, the p_{T}^{V} distribution of the nominal sample is reweighted to match that of the alternative sample. The p_{T}^{V} difference is considered as a separate, uncorrelated uncertainty, in a manner similar to that for the other backgrounds. The ratio of the BDT_S distributions evaluated for the alternative and nominal samples provide a reweighting function (referred to as $\mathrm{R_{BDT}}$), which can be used to correct the nominal sample to match the alternative sample. This method simultaneously maps the n-dimensional space formed by the kinematic variables of the two generators onto each other. It is verified that, after being reweighted by $\mathrm{R_{BDT}}$, the input variable distributions for the nominal sample are in good agreement with those of the alternative sample.

The systematic uncertainties affecting the modelling of the background samples are summarised in Tables 6 and 7, and key details of the treatment of the backgrounds are reported below.

***V*+jets production** The V + jets backgrounds are subdivided into three different components based upon the jet flavour labels of the two b-tagged jets in the event. The main background contributions ($V+bb$, $V+bc$, $V+bl$ and $V+cc$) are jointly considered as the V + HF background. Their overall normalisations are free to float in the global likelihood fit, separately in the 2- and 3-jet categories. For the Z + HF background, the normalisations are also floated separately in the 75 GeV $< p_{\mathrm{T}}^{V} <$ 150 GeV and $p_{\mathrm{T}}^{V} >$ 150 GeV regions. The remaining flavour components, $V+cl$ and $V+ll$, constitute less than $\sim$ 1% of the background in each analysis region and only normalisation uncertainties are included.

Uncertainties are estimated for the relative normalisation of the four heavy-flavour components that constitute the V + HF background. These are taken as uncertainties in the bc, cc and bl yields compared with the dominant bb yield and are estimated separately in each lepton channel in a manner similar to the acceptance systematic uncertainties. Relative acceptance uncertainties for the W + HF background are estimated for the ratio of the event yield in the 0-lepton channel to that in the 1-lepton channel. For the Z + HF background, there is a relative acceptance uncertainty in the ratio of the event yield in the 0-lepton channel to that in the 2-lepton channel in the $p_{\mathrm{T}}^{V} > 150$ GeV region. For both W + HF and Z + HF, relative acceptance uncertainties are estimated for the ratio of the event yield in the SR to that in the CRs.

For Z + HF, shape uncertainties are derived for m_{bb} and p_{T}^{V}, which are evaluated from comparisons with data in the m_{bb} side-bands ($m_{bb} <$ 80 GeV or $m_{bb} >$ 140 GeV), after subtracting backgrounds other than Z + jets. For W + HF, uncertainties are derived for p_{T}^{V} and the $\mathrm{R_{BDT}}$ method from comparisons of the nominal sample (Sherpa) with an alternative sample (MadGraph5_aMC@NLO+Pythia 8 [111, 112]).

***tt̄* production** In the 0- and 1-lepton channels (jointly referred to as 0+1-lepton channel) separate floating normalisations are used for the 2-jet region and 3-jet region. Uncertainties are derived from comparisons between the nominal sample (Powheg+Pythia 8) and alternative samples corresponding to matrix-element (MadGraph5_aMC@NLO+Pythia 8) and parton-shower (Powheg+Herwig 7 [113]) generator variations.

Relative acceptance uncertainties are estimated for the 0-lepton and 1-lepton channel normalisation ratios. The dominant flavour component of the two b-tagged jets in $t\bar{t}$ is bb. However, there is a sizeable bc component which has a more signal-like topology. Uncertainties in the relative composition of three components, bb, bc, and any other flavour configuration (referred to as 'other') are estimated from the difference in the ratio of the bc or other components to the bb yield between the nominal sample and the alternative matrix element and parton shower generator samples. Shape uncertainties are derived for p_{T}^{V} and using the $\mathrm{R_{BDT}}$ method in the 0+1-lepton channels from comparisons with the alternative parton shower and matrix element generator samples.

In the 2-lepton channel the $t\bar{t}$ background is estimated by a data-driven method as discussed in Sect. 6.1. The uncertainty in this background is dominated by the statistical uncertainty of the $e\mu$ control region data events.

Single-top-quark production In the Wt- and t-channels, uncertainties are derived for the normalisation, relative acceptance and shapes of the m_{bb} and p_{T}^{V} distributions. For the Wt-channel, the estimated modelling uncertainties are applied independently according to the flavour of the two b-tagged jets, due to the different regions of phase space being probed when there are two b-jets (bb) present compared with events where there are fewer b-jets present (referred to as 'other'). Those uncertainties are evaluated from comparisons between the nominal sample (Powheg+Pythia 8 using the diagram removal scheme [114]) and alternative samples with parton-shower variations (Powheg+Herwig++) and a different scheme to account for the interference between Wt and $t\bar{t}$ production (Powheg+Pythia 8 using the diagram

Table 6 Summary of the systematic uncertainties in the background modelling for Z + jets, W + jets, $t\bar{t}$, single-top-quark and multi-jet production. 'ME' indicates a matrix element generator variation and 'PS' indicates a parton shower generator variation. An 'M+S' symbol is used when a shape uncertainty includes a migration effect that allows relative acceptance changes between regions, whilst 'S' indicates that the uncertainty only acts upon the shape in the signal region. Instances where an uncertainty is considered independently in different regions are detailed in parentheses. Where the size of an acceptance systematic uncertainty varies between regions, a range is displayed

Z + jets	
$Z + ll$ normalisation	18%
$Z + cl$ normalisation	23%
Z + HF normalisation	Floating (2-jet, 3-jet) × ($75\,\text{GeV} < p_{\text{T}}^{V} < 150\,\text{GeV}$, $p_{\text{T}}^{V} > 150\,\text{GeV}$)
$Z + bc$-to-$Z + bb$ ratio	30–40%
$Z + cc$-to-$Z + bb$ ratio	13–16%
$Z + bl$-to-$Z + bb$ ratio	20–28%
SR-to-low ΔR CR ratio	3.8–9.9% ($75\,\text{GeV} < p_{\text{T}}^{V} < 150\,\text{GeV}$, $p_{\text{T}}^{V} > 150\,\text{GeV}$)
SR-to-high ΔR CR	2.7–4.1% ($75\,\text{GeV} < p_{\text{T}}^{V} < 150\,\text{GeV}$, $p_{\text{T}}^{V} > 150\,\text{GeV}$)
0-to-2 lepton ratio	7%
p_{T}^{V}	M+S ($75\,\text{GeV} < p_{\text{T}}^{V} < 150\,\text{GeV}$, $p_{\text{T}}^{V} > 150\,\text{GeV}$)
m_{bb}	S ($75\,\text{GeV} < p_{\text{T}}^{V} < 150\,\text{GeV}$, $p_{\text{T}}^{V} > 150\,\text{GeV}$)
W + jets	
$W + ll$ normalisation	32%
$W + cl$ normalisation	37%
W + HF normalisation	Floating (2-jet, 3-jet)
$W + bc$-to-$W + bb$ ratio	15% (0-lepton) and 30% (1-lepton)
$W + cc$-to-$W + bb$ ratio	10% (0-lepton) and 30% (1-lepton)
$W + bl$-to-$W + bb$ ratio	26% (0-lepton) and 23% (1-lepton)
SR-to-CR ratio	3.6–15%
0-to-1 lepton ratio	5%
p_{T}^{V}	M+S (2-jet, 3-jet)
R_{BDT}	S
$t\bar{t}$ (0+1-lepton channels only)	
$t\bar{t}$ normalisation	Floating (2-jet, 3-jet)
0-to-1 lepton ratio	8%
$t\bar{t}$ (flavour composition) bc-to-bb ratio (ME)	7.6–8.2% (0-lepton), 1.3–3.8% (1-lepton)
$t\bar{t}$ (flavour composition) bc-to-bb ratio (PS)	2.1–3.2% (0-lepton), 1.5–7.1% (1-lepton)
$t\bar{t}$ (flavour composition) other-to-bb ratio (ME)	2.8–6.4% (0-lepton), 3.3–5.7% (1-lepton)
$t\bar{t}$ (flavour composition) other-to-bb ratio (PS)	5.6–13% (0-lepton), 0.3–2.1% (1-lepton)
p_{T}^{V}	M+S (2-jet, 3-jet)
R_{BDT} ME variation	M+S (2-jet, 3-jet)
R_{BDT} PS variation	M+S (0-lepton, 1-lepton)
Single top quark	
Cross-section	4.6% (s-channel), 4.4% (t-channel), 6.2% (Wt)
Acceptance 2-jet	17% (t-channel), 55% ($Wt(bb)$), 24% (Wt(other))
Acceptance 3-jet	20% (t-channel), 51% ($Wt(bb)$), 21% (Wt(other))
m_{bb}	M+S (t-channel, $Wt(bb)$, Wt(other))
p_{T}^{V}	M+S (t-channel, $Wt(bb)$, Wt(other))
Multi-jet (1-lepton)	
Normalisation	30–200% (2-jet), 100% (3-jet)
BDT template	M+S

Table 7 Summary of the systematic uncertainties in the background modelling for diboson production. 'PS/UE' indicates parton shower/underlying event. An 'M+S' symbol is used when a shape uncertainty includes a migration effect that allows relative acceptance changes between regions. Instances where an uncertainty is considered independently in different regions are detailed in parentheses. When extracting the $(W/Z)Z$ diboson production signal yield, as the normalisations are unconstrained, the normalisation uncertainties are removed. Where the size of an acceptance systematic uncertainty varies between regions, a range is displayed

ZZ	
Normalisation	20%
0-to-2 lepton ratio	6%
Acceptance from scale variations	10–18%
Acceptance from PS/UE variations for 2 or more jets	6%
Acceptance from PS/UE variations for 3 jets	7% (0-lepton), 3% (2-lepton)
m_{bb} from scale variations	M+S (correlated with WZ uncertainties)
p_{T}^{V} from scale variations	M+S (correlated with WZ uncertainties)
m_{bb} from PS/UE variations	M+S (correlated with WZ uncertainties)
p_{T}^{V} from PS/UE variations	M+S (correlated with WZ uncertainties)
m_{bb} from matrix-element variations	M+S (correlated with WZ uncertainties)
WZ	
Normalisation	26%
0-to-1 lepton ratio	11%
Acceptance from scale variations	13–21%
Acceptance from PS/UE variations for 2 or more jets	4%
Acceptance from PS/UE variations for 3 jets	11%
m_{bb} from scale variations	M+S (correlated with ZZ uncertainties)
p_{T}^{V} from scale variations	M+S (correlated with ZZ uncertainties)
m_{bb} from PS/UE variations	M+S (correlated with ZZ uncertainties)
p_{T}^{V} from PS/UE variations	M+S (correlated with ZZ uncertainties)
m_{bb} from matrix-element variations	M+S (correlated with ZZ uncertainties)
WW	
Normalisation	25%

subtraction scheme) [115]. Only a normalisation uncertainty is derived for the s-channel, since its contribution is at a very low level.

Table 8 Summary of the systematic uncertainties in the signal modelling. 'PS/UE' indicates parton shower/underlying event. An 'M+S' symbol is used when a shape uncertainty includes a migration effect that allows relative acceptance changes between regions. Instances where an uncertainty is considered independently in different regions are detailed in parenthesis. Where the size of an acceptance systematic uncertainty varies between regions, a range is displayed

Signal	
Cross-section (scale)	0.7% (qq), 25% (gg)
$H \to b\bar{b}$ branching fraction	1.7%
Scale variations in STXS bins	3.0–3.9% ($qq \to WH$), 6.7–12% ($qq \to ZH$), 37–100% ($gg \to ZH$)
PS/UE variations in STXS bins	1–5% for $qq \to VH$, 5–20% for $gg \to ZH$
PDF+α_{S} variations in STXS bins	1.8–2.2% ($qq \to WH$), 1.4–1.7% ($qq \to ZH$), 2.9–3.3% ($gg \to ZH$)
m_{bb} from scale variations	M+S ($qq \to VH$, $gg \to ZH$)
m_{bb} from PS/UE variations	M+S
m_{bb} from PDF+α_{S} variations	M+S
p_{T}^{V} from NLO EW correction	M+S

Table 9 Factors applied to the nominal normalisations of the $t\bar{t}$, W+HF and Z+HF backgrounds, as obtained from the global likelihood fit to the 13 TeV data for the nominal multivariate analysis. The errors represent the combined statistical and systematic uncertainties

Process and category	Normalisation factor
$t\bar{t}$ 2-jet	0.98 ± 0.09
$t\bar{t}$ 3-jet	0.93 ± 0.06
W + HF 2-jet	1.06 ± 0.11
W + HF 3-jet	1.15 ± 0.09
Z + HF 2-jet, $75 < p_{\mathrm{T}}^{V} < 150$ GeV	1.28 ± 0.08
Z + HF 3-jet, $75 < p_{\mathrm{T}}^{V} < 150$ GeV	1.17 ± 0.05
Z + HF 2-jet, 150 GeV $< p_{\mathrm{T}}^{V}$	1.16 ± 0.07
Z + HF 3-jet, 150 GeV $< p_{\mathrm{T}}^{V}$	1.09 ± 0.04

Diboson production The diboson backgrounds are composed of three distinct processes: WZ, WW and ZZ production. Given the small contribution from WW production ($< 0.1\%$ of the total background) only a normalisation uncertainty is assigned. For the more important contributions from the WZ and ZZ backgrounds, uncertainties are considered in the overall normalisation, the relative acceptance between regions and the m_{bb} and p_{T}^{V} shapes. These are derived following the procedure described in Ref. [87] and are outlined in Table 7, which includes comparisons of the nominal sample (SHERPA) with alternative samples (POWHEG+PYTHIA 8 and POWHEG+HERWIG++).

Multi-jet background uncertainties The systematic uncertainties in the multi-jet background estimate in the 1-lepton channel are derived by following the procedure outlined in Ref. [33]. Two different uncertainty components are considered, those which alter the normalisation and those which alter the multi-jet BDT template shape.

7.3 Signal uncertainties

The systematic uncertainties that affect the modelling of the signal are summarised in Table 8 and are estimated with procedures that closely follow those outlined in Refs. [27,35,116,117]. The systematic uncertainties in the calculations of the VH production cross-sections and the $H \to b\bar{b}$ branching fraction[7] are assigned following the recommendations of the LHC Higgs Cross Section Working Group [31,70,71,118,119].

Uncertainties in the m_{bb} and p_{T}^{V} signal shape are estimated, as described in Ref. [33], from scale variations, PDF and α_{S} (PDF+α_{S}) uncertainties, from varying the parton shower and underlying event (PS/UE) models using AZNLO tuning variations and from comparisons with alternative parton-shower generator samples (POWHEG+HERWIG 7). In addition, a systematic uncertainty from higher-order EW corrections effects is taken into account as a variation in the shape of the p_{T}^{V} distributions for $qq \to VH$ production. Acceptance uncertainties, evaluated according to STXS regions, correctly accounting for the migration and correlations between regions, are evaluated for the scale variations, PS/UE models and PDF+α_{S}.

For the STXS measurement, the signal uncertainties are separated into two groups, uncertainties in the acceptance and shape of kinematic distributions which alter the signal modelling (theoretical modelling uncertainties) and the uncertainties in the prediction of the production cross-section for each of these regions (theoretical cross-section uncertainties). Whilst theoretical modelling uncertainties enter the STXS measurements, theoretical cross-section uncertainties only affect the predictions with which they are compared, and are therefore not included in the likelihood function.

8 Statistical analysis

The statistical procedure is based on a likelihood function $\mathcal{L}(\mu, \boldsymbol{\theta})$, constructed as the product of Poisson probability terms over the bins of the input distributions, with parameters of interest (POI) extracted by maximising the likelihood. The effects of systematic uncertainties enter the likelihood as nuisance parameters (NP), $\boldsymbol{\theta}$. Most of the uncertainties discussed in Sect. 7 are constrained with Gaussian or log-normal probability density functions. The normalisations of the largest backgrounds, $t\bar{t}$, $W+\mathrm{HF}$ and $Z+\mathrm{HF}$, can be reliably determined by the fit, so they are left unconstrained in the likelihood. The uncertainties due to the limited number of events in the simulated samples used for the background predictions are included using the Beeston–Barlow technique [120]. As detailed in Ref. [121], systematic variations that are subject to large statistical fluctuations are smoothed, and systematic uncertainties that have a negligible impact on the final results are pruned away region-by-region (treating signal and control regions separately).

The global likelihood fit comprises 14 signal regions, defined as the 2- and 3-jet categories in the two high-p_{T}^{V} ($150 < p_{\mathrm{T}}^{V} < 250$ GeV and $p_{\mathrm{T}}^{V} > 250$ GeV) regions for the three channels, and in the medium-p_{T}^{V} region ($75 < p_{\mathrm{T}}^{V} < 150$ GeV) for the 2-lepton channel. The 28 control regions are also input as event yields in all fit configurations.

Three different versions of the analysis are studied, which differ in the distributions input to the fit.

- The nominal analysis, referred to as the multivariate analysis, uses the BDT_{VH} multivariate discriminant output distributions as the inputs to the fit. Three different POI configurations are studied. Firstly, a single-POI fit measures μ_{VH}^{bb}, the signal strength that multiplies the SM Higgs boson VH production cross-section times the branching fraction into $b\bar{b}$. Secondly, a two-POI fit is undertaken, which jointly measures the signal strengths of the WH and ZH components. Finally, a five-POI fit version measures the signal cross-section multiplied by the $H \to b\bar{b}$ and $V \to$ leptons branching fractions in the five STXS regions (see Table 4).
- The dijet-mass cross-check analysis uses the m_{bb} distributions, instead of the BDT_{VH} distributions, as inputs to a single-POI fit to measure μ_{VH}^{bb}.
- The diboson validation analysis, a measurement of the signal strength of the WZ and ZZ processes, uses the BDT_{VZ} output distributions. The SM Higgs boson is included as a background process normalised to the predicted SM cross-section with an uncertainty of 50%, which conservatively encompasses the previous measurement and uncertainty [33]. Two POI configurations are evaluated, firstly a single-POI fit to measure μ_{VZ}^{bb}, the signal strength of the combined WZ and ZZ diboson processes, and secondly a two-POI fit to simultaneously measure the WZ and ZZ signal strengths.

The background predictions in all post-fit distributions and tables are obtained by normalising the backgrounds and set-

[7] These systematic uncertainties are fully degenerate with the signal yield and do not affect the calculation of the significance relative to the background-only prediction and STXS cross-section measurement.

Table 10 The Higgs boson signal, background and data yields for each signal region in the 0- and 1-lepton channels after the full selection. The signal and background yields are normalised to the results of the global likelihood fit. All systematic uncertainties are included in the indicated uncertainties. An entry of "–" indicates that a specific background component is negligible in a certain region, or that no simulated events are left after the analysis selection

Signal regions	0-lepton		0-lepton		1-lepton		1-lepton	
	$150\,\text{GeV} < p_{\text{T}}^{V} < 250\,\text{GeV}$		$p_{\text{T}}^{V} > 250\,\text{GeV}$		$150\,\text{GeV} < p_{\text{T}}^{V} < 250\,\text{GeV}$		$p_{\text{T}}^{V} > 250\,\text{GeV}$	
Sample	2-jet	3-jet	2-jet	3-jet	2-jet	3-jet	2-jet	3-jet
Z + jets	2846 ± 80	3830 ± 160	338 ± 13	533 ± 23	102 ± 5	207 ± 11	10 ± 1	25 ± 2
W + jets	634 ± 63	1500 ± 110	83 ± 9	220 ± 19	1850 ± 160	4080 ± 270	353 ± 33	935 ± 69
Single top	237 ± 35	770 ± 130	9 ± 2	36 ± 8	990 ± 160	3570 ± 600	70 ± 15	313 ± 66
$t\bar{t}$	1157 ± 76	5470 ± 220	39 ± 5	151 ± 16	4600 ± 210	21030 ± 620	188 ± 19	970 ± 58
Diboson	360 ± 55	333 ± 79	86 ± 13	70 ± 17	229 ± 57	264 ± 83	57 ± 15	68 ± 22
Multi-jet	–	–	–	–	130 ± 47	24 ± 14	16 ± 10	7 ± 8
Total bkg.	5234 ± 63	11910 ± 100	554 ± 15	1011 ± 21	7899 ± 82	29170 ± 170	694 ± 23	2318 ± 42
Signal ($\mu = 1.02$)	147 ± 24	130 ± 22	40 ± 6	33 ± 6	148 ± 24	125 ± 21	52 ± 9	44 ± 7
Data	5397	11875	578	1046	8044	29316	727	2378

Table 11 The Higgs boson signal, background and data yields for each signal region in the 2-lepton channel after the full selection. The signal and background yields are normalised to the results of the global likelihood fit. The top background is derived from $e\mu$-CR data. All systematic uncertainties are included in the indicated uncertainties. An entry of "–" indicates that a specific background component is negligible in a certain region, or that no simulated events are left after the analysis selection

Signal regions	2-lepton		2-lepton		2-lepton	
	$75\,\text{GeV} < p_{\text{T}}^{V} < 150\,\text{GeV}$		$150\,\text{GeV} < p_{\text{T}}^{V} < 250\,\text{GeV}$		$p_{\text{T}}^{V} > 250\,\text{GeV}$	
Sample	2-jet	≥3-jet	2-jet	≥3-jet	2-jet	≥3-jet
Z + jets	5900 ± 100	11630 ± 160	716 ± 19	2499 ± 52	84 ± 3	537 ± 16
W + jets	1 ± 0	6 ± 0	< 1	2 ± 0	< 1	< 1
Top	3193 ± 57	8796 ± 87	52 ± 7	389 ± 19	1 ± 1	15 ± 4
Diboson	283 ± 47	443 ± 78	83 ± 14	169 ± 30	20 ± 4	52 ± 10
Total bkg.	9378 ± 86	20880 ± 130	851 ± 19	3058 ± 44	106 ± 4	605 ± 14
Signal ($\mu = 1.02$)	78 ± 14	106 ± 21	34 ± 6	59 ± 12	10 ± 2	18 ± 3
Data	9463	20927	881	3148	123	614

ting the nuisance parameters according to the values determined by the fit used to measure μ_{VH}^{bb}.

9 Results

9.1 Signal strength measurements

The post-fit normalisation factors of the unconstrained backgrounds in the global likelihood fit are shown for the single-POI multivariate analysis in Table 9, the post-fit signal and background yields are shown in Tables 10 and 11, and Fig. 3 shows the BDT_{VH} output distributions in the high-p_{T}^{V} 2-jet SRs, which are most sensitive to the signal.

For a Higgs boson mass of 125 GeV, when all channels are combined, the fitted value of the VH signal strength is:

$$\mu_{VH}^{bb} = 1.02^{+0.18}_{-0.17} = 1.02^{+0.12}_{-0.11}(\text{stat.})^{+0.14}_{-0.13}(\text{syst.}).$$

For the VH production mode the background-only hypothesis is rejected with a significance of 6.7 standard deviations, to be compared with an expectation of 6.7 standard deviations [122].

The results of the combined fit when measuring signal strengths separately for the WH and ZH production processes are shown in Fig. 4. The WH and ZH production modes reject the background-only hypothesis with observed (expected) significances of 4.0 (4.1) and 5.3 (5.1) standard deviations, respectively. The fitted values of the two signal

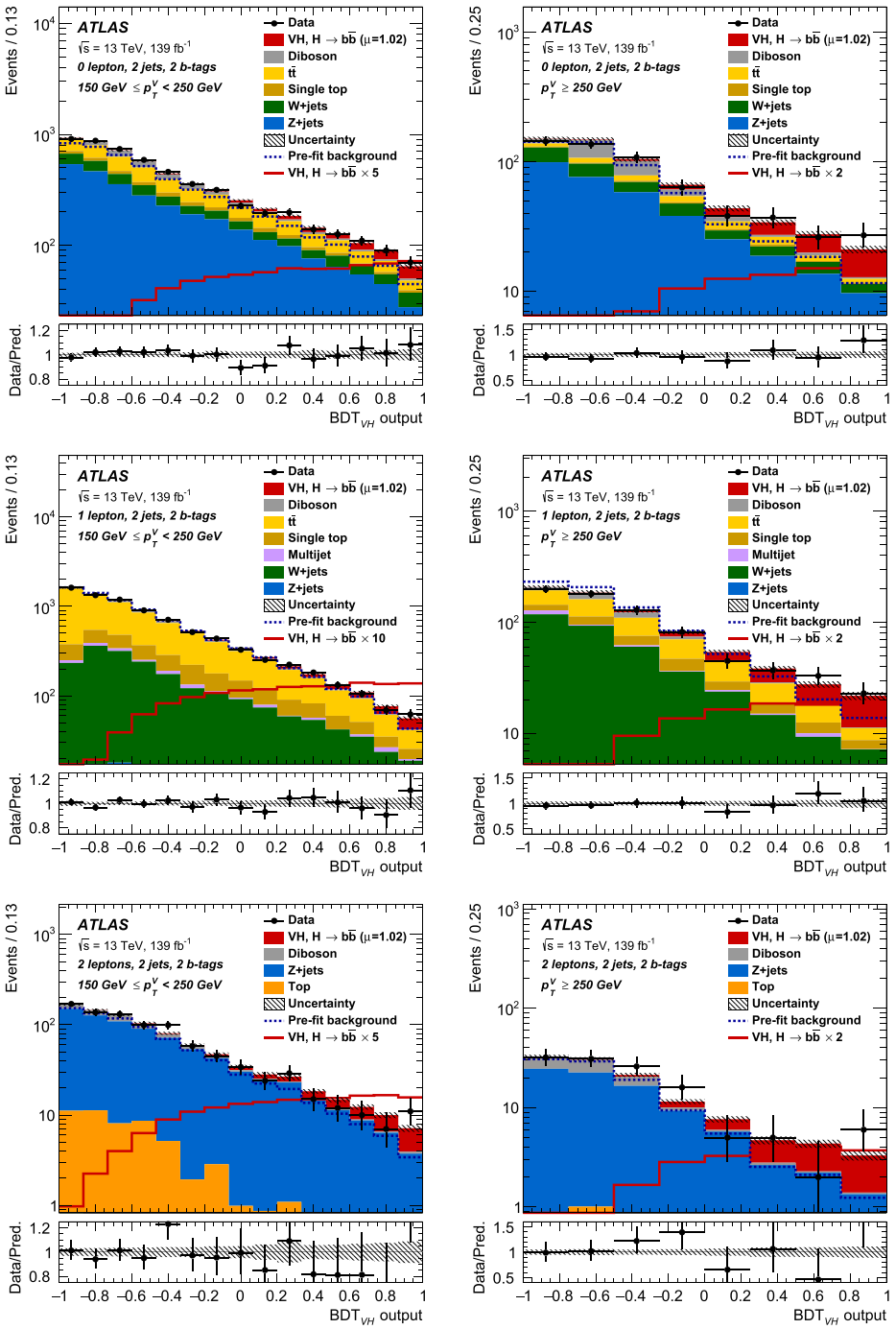

Fig. 3 The BDT_{VH} output post-fit distributions in the 0-lepton (top), 1-lepton (middle) and 2-lepton (bottom) channels for 2-b-tag 2-jet events, for the $150 < p_{\mathrm{T}}^{V} < 250$ GeV (left) and $p_{\mathrm{T}}^{V} > 250$ GeV (right) p_{T}^{V} regions. The background contributions after the global likelihood fit are shown as filled histograms. The Higgs boson signal ($m_H = 125$ GeV) is shown as a filled histogram on top of the fitted backgrounds normalised to the signal yield extracted from data ($\mu = 1.02$), and unstacked as an unfilled histogram, scaled by the factor indicated in the legend. The dashed histogram shows the total pre-fit background. The size of the combined statistical and systematic uncertainty for the sum of the fitted signal and background is indicated by the hatched band. The ratio of the data to the sum of the fitted signal ($\mu = 1.02$) and background is shown in the lower panel. The BDT_{VH} output distributions are shown with the binning used in the global likelihood fit

strengths are:

$$\mu_{WH}^{bb} = 0.95^{+0.27}_{-0.25} = 0.95 \pm 0.18(\mathrm{stat.})^{+0.19}_{-0.18}(\mathrm{syst.}),$$
$$\mu_{ZH}^{bb} = 1.08^{+0.25}_{-0.23} = 1.08 \pm 0.17(\mathrm{stat.})^{+0.18}_{-0.15}(\mathrm{syst.}),$$

with a linear correlation between them of 2.7%.

The effects of systematic uncertainties on the measurement of the VH, WH and ZH signal strengths are displayed in Table 12. The impact of a set of systematic uncertainties is defined as the difference in quadrature between the uncertainty in μ computed when all NPs are fitted and that when the NPs in the set are fixed to their best-fit values. The total statistical uncertainty is defined as the uncertainty in μ when all the NPs are fixed to their best-fit values. The total systematic uncertainty is then defined as the difference in quadrature between the total uncertainty in μ and the total statistical uncertainty. For the WH and ZH signal strength measure-

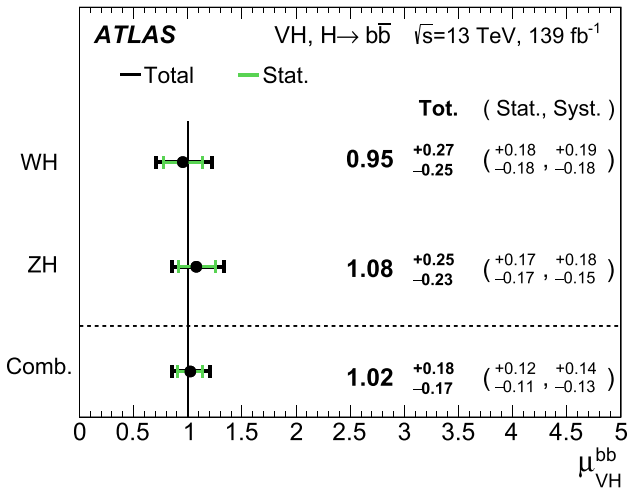

Fig. 4 The fitted values of the Higgs boson signal strength μ_{VH}^{bb} for $m_H = 125$ GeV for the WH and ZH processes and their combination. The individual μ_{VH}^{bb} values for the $(W/Z)H$ processes are obtained from a simultaneous fit with the signal strength for each of the WH and ZH processes floating independently. The probability of compatibility of the individual signal strengths is 71%

ments the total statistical and systematic uncertainties are similar in size, with the b-tagging, jet, $E_{\mathrm{T}}^{\mathrm{miss}}$, background modelling and signal systematic uncertainties all making important contributions to the total systematic uncertainty. The impact of the statistical uncertainty from the simulated event samples has been significantly reduced compared to the previous result [35], due to the measures taken to considerably enhance the number of simulated events.

9.1.1 Dijet-mass cross-check

From the fit to m_{bb}, for all channels combined, the value of the signal strength is

$$\mu_{VH}^{bb} = 1.17^{+0.25}_{-0.23} = 1.17 \pm 0.16(\mathrm{stat.})^{+0.19}_{-0.16}(\mathrm{syst.}).$$

Using the 'bootstrap' method [121], the dijet-mass and nominal multivariate analysis results are found to be statistically compatible at the level of 1.1 standard deviations. The observed excess rejects the background-only hypothesis with a significance of 5.5 standard deviations, compared to an expectation of 4.9 standard deviations. Good agreement is also found when comparing the values of signal strengths in the individual channels from the dijet-mass analysis with those from the multivariate analysis.

The m_{bb} distribution is shown in Fig. 5 summed over all channels and regions, weighted by their respective values of the ratio of fitted Higgs boson signal to background yields and after subtraction of all backgrounds except for the WZ and ZZ diboson processes.

Table 12 Breakdown of the contributions to the uncertainty in μ_{VH}^{bb} for the VH, WH and ZH signal strength measurements. The sum in quadrature of the systematic uncertainties attached to the categories differs from the total systematic uncertainty due to correlations

Source of uncertainty		σ_μ VH	WH	ZH
Total		0.177	0.260	0.240
Statistical		0.115	0.182	0.171
Systematic		0.134	0.186	0.168
Statistical uncertainties				
Data statistical		0.108	0.171	0.157
$t\bar{t}$ $e\mu$ control region		0.014	0.003	0.026
Floating normalisations		0.034	0.061	0.045
Experimental uncertainties				
Jets		0.043	0.050	0.057
$E_{\mathrm{T}}^{\mathrm{miss}}$		0.015	0.045	0.013
Leptons		0.004	0.015	0.005
b-tagging	b-jets	0.045	0.025	0.064
	c-jets	0.035	0.068	0.010
	light-flavour jets	0.009	0.004	0.014
Pile-up		0.003	0.002	0.007
Luminosity		0.016	0.016	0.016
Theoretical and modelling uncertainties				
Signal		0.072	0.060	0.107
Z + jets		0.032	0.013	0.059
W + jets		0.040	0.079	0.009
$t\bar{t}$		0.021	0.046	0.029
Single top quark		0.019	0.048	0.015
Diboson		0.033	0.033	0.039
Multi-jet		0.005	0.017	0.005
MC statistical		0.031	0.055	0.038

9.1.2 Diboson validation

The measurement of VZ production using a multivariate approach, as a validation of the Higgs boson analysis, returns a signal strength of

$$\mu_{VZ}^{bb} = 0.93^{+0.16}_{-0.13} = 0.93^{+0.07}_{-0.06}(\mathrm{stat.})^{+0.14}_{-0.12}(\mathrm{syst.}),$$

in good agreement with the Standard Model prediction. Analogously to the nominal analysis, fits are also performed with separate signal strengths for the WZ and ZZ production modes, and the results are shown in Fig. 6.

9.2 Cross-section measurements

The measured VH cross-sections times the $H \to b\bar{b}$ and $V \to$ leptons branching fractions, $\sigma \times B$, together with the

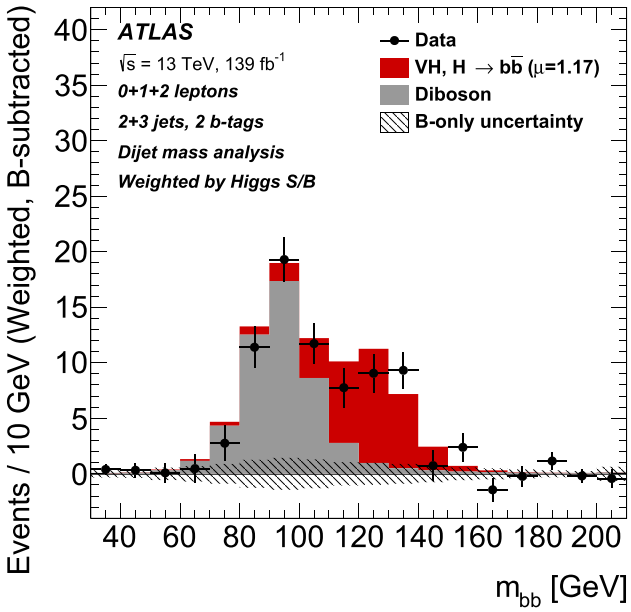

Fig. 5 The distribution of m_{bb} in data after subtraction of all backgrounds except for the WZ and ZZ diboson processes, as obtained with the dijet-mass analysis. The contributions from all lepton channels, p_{T}^{V} regions and number-of-jets categories are summed and weighted by their respective S/B ratios, with S being the total fitted signal and B the total fitted background in each region. The expected contribution of the associated WH and ZH production of a SM Higgs boson with $m_H = 125$ GeV is shown scaled by the measured signal strength ($\mu = 1.17$). The size of the combined statistical and systematic uncertainty for the fitted background is indicated by the hatched band

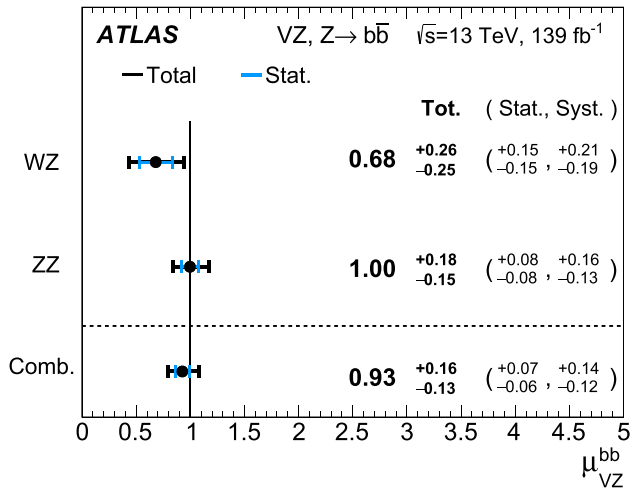

Fig. 6 The fitted values of the VZ signal strength μ_{VZ}^{bb} for the WZ and ZZ processes and their combination. The individual μ_{VZ}^{bb} values for the WZ and ZZ processes are obtained from a simultaneous fit with the signal strengths for each of the WZ and ZZ processes floating independently. The probability of compatibility of the individual signal strengths is 27%

SM predictions in the reduced STXS regions, are summarised in Table 13 and Fig. 7. The cross-sections are all consistent with the Standard Model expectations and are measured with relative uncertainties varying from 30% in the highest p_{T}^{V} region to 85% in the lowest p_{T}^{V} region. The data statistical uncertainty is the largest single uncertainty in all regions, although in the lower p_{T}^{V} regions systematic uncertainties make a sizeable contribution to the total uncertainty. In all regions there are large contributions from the background modelling, b-tagging and jet systematic uncertainties. In the lowest p_{T}^{V} region in both the WH and ZH measurements, the $E_{\mathrm{T}}^{\mathrm{miss}}$ uncertainty is one of the largest uncertainties. For the ZH measurements, the signal uncertainties also make a sizeable contribution due to the limited precision of the theoretical calculations of the $gg \to ZH$ process.

10 Constraints on effective interactions

The strength and tensor structure of the process VH, $H \to b\bar{b}$ are investigated using an effective Lagrangian approach. Extra terms are added to the SM Lagrangian ($\mathcal{L}_{\mathrm{SM}}$) to obtain an effective Lagrangian ($\mathcal{L}_{\mathrm{SMEFT}}$) following the approach in Refs. [124,125]:

$$\mathcal{L}_{\mathrm{SMEFT}} = \mathcal{L}_{\mathrm{SM}} + \sum_i \frac{c_i^{(D)}}{\Lambda^{D-4}} \mathcal{Q}_i^{(D)},$$

where Λ is the energy scale of the new interactions, $\mathcal{Q}_i^{(D)}$ are dimension-D operators, and $c_i^{(D)}$ are numerical Wilson coefficients. Only $D = 6$ operators are considered in this study, since $D = 5$ and $D = 7$ operators violate lepton or baryon number, whilst $D > 7$ operators are further suppressed by powers of Λ.

The STXS measurements are used to constrain the coefficients of the operators in the 'Warsaw' formulation [126], which provides a complete set of independent operators when considering those allowed by the SM gauge symmetries. Thirteen operators directly affect the VH cross-section [127]. This analysis has significant sensitivity to the six operators detailed in Table 14, in addition to the operator which directly affects the $H \to b\bar{b}$ decay width.

Following methodologies similar to those outlined in Ref. [125], a parameterisation of the STXS production cross-section and Higgs boson decay rates in terms of the SMEFT parameters is derived, in this case based upon leading-order predictions made using the SMEFTsim package [125]. The interference terms between the SM and BSM amplitudes are linear in the coefficients and of order $1/\Lambda^2$, while BSM contributions are quadratic in the coefficients and of order $1/\Lambda^4$. Linear terms from $D = 8$ operators are suppressed by the same $1/\Lambda^4$ factor as the quadratic $D = 6$ terms. However, it is currently not possible to include such terms, so results for both the linear and linear plus quadratic $D = 6$ terms are studied to provide some indication of the effect $D = 8$ linear terms could have on the result. Modifications of the

$gg \to ZH$ production cross-section are only introduced by either higher-dimension ($D \geq 8$) operators or corrections that are formally at NNLO in QCD, and are not included in this study. The expected $gg \to ZH$ contribution is fixed to the SM prediction within uncertainties. The dependence of the experimental acceptance in each analysis region on the Wilson coefficients is not accounted for in this study, although it was verified that the impact on the acceptance from the EFT operators was at most 10%.

Maximum-likelihood fits across the STXS regions are performed to determine the Wilson coefficients. All coefficients but one are assumed to vanish, and one-dimensional confidence level (CL) intervals are inferred for the coefficient under study both with and without the quadratic terms. An example negative-log-likelihood one-dimensional projection is shown in Fig. 8 for $c_{Hq}^{(3)}$, and the 68% and 95% CL intervals are summarised in Fig. 9 for the four coefficients to which the analysis has greatest sensitivity, in addition to the c_{dH} coefficient which directly affects the $H \to b\bar{b}$ decay width. As detailed in Table 14, the $\mathcal{Q}_{Hu}$, $\mathcal{Q}_{Hd}$ and $\mathcal{Q}_{Hq}^{(1)}$ operators have a similar impact and as such are found to be highly degenerate, so only a representative result for $\mathcal{Q}_{Hu}$ is shown. The coefficient $c_{Hq}^{(3)}$ is constrained at 68% CL to be no more than a few percent, whilst the constraints on the other three coefficients range from 10–30% to order unity and c_{dH} has much weaker constraints. In most cases the observed constraints are found to significantly depend on the presence of the quadratic terms, indicating that $D = 8$ linear terms could also have a non-negligible effect.

These limits were also produced using the full likelihood and using only the STXS measurement central values and covariance matrix. It was found that the two methods produced results that are consistent with each other within $\sim$ 10%–20% for the majority of operators and to within $\sim$ 30% for the two operators with the weakest constraints, $\mathcal{Q}_{dH}$ and $\mathcal{Q}_{HWB}$.

As there are only five STXS regions, attempting to simultaneously extract constraints on multiple coefficients, some of which have similar effects, leads to unmanageable correlations. An alternative approach is to fit an orthogonal set of linear combinations of the Wilson coefficients of the Warsaw-basis operators. This removes the assumption, inherent in the one-dimensional limits, that only one operator acts at a time. Based upon the procedure outlined in Ref. [127], eigenvectors are determined from the Hessian matrix of the STXS likelihood fit to data, after it has been re-expressed in terms of the Wilson coefficients. This approach only considers the

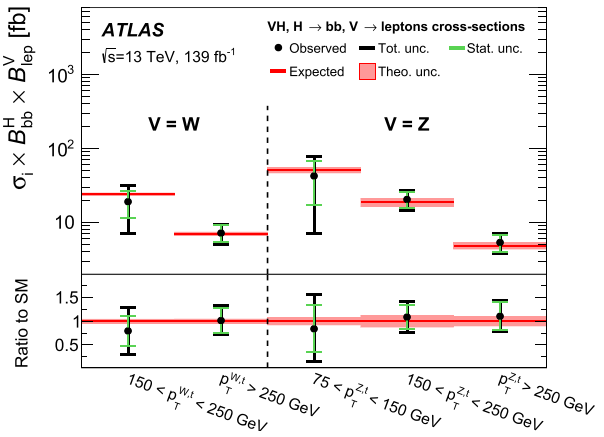

Fig. 7 Measured VH, $V \to$ leptons cross-sections times the $H \to b\bar{b}$ branching fraction in the reduced STXS scheme

Table 13 Best-fit values and uncertainties for the VH, $V \to$ leptons cross-section times the $H \to b\bar{b}$ branching fraction, in the reduced STXS scheme. The SM predictions for each region, computed using the inclusive cross-section calculations and the simulated event samples are also shown. The contributions to the total uncertainty in the measurements from statistical (Stat. unc.) or systematic uncertainties (Syst. unc.) in the signal prediction (Th. sig.), background prediction (Th. bkg.), and in experimental performance (Exp.) are given separately. The total systematic uncertainty, equal to the difference in quadrature between the total uncertainty and the statistical uncertainty, differs from the sum in quadrature of the Th. sig., Th. bkg., and Exp. systematic uncertainties due to correlations. All leptonic decays of the V bosons (including those to τ-leptons, $\ell = e, \mu, \tau$) are considered. These results along with the corresponding correlation matrix are available in the HEPData repository [123]

STXS region		SM prediction	Result	Stat. unc.	Syst. unc. [fb]		
Process	$p_{\mathrm{T}}^{V,\mathrm{t}}$ interval	[fb]	[fb]	[fb]	Th. sig.	Th. bkg.	Exp.
$W(\ell\nu)H$	150–250 GeV	24.0 ± 1.1	19.0 ± 12.1	± 7.7	± 0.9	± 5.5	± 6.0
$W(\ell\nu)H$	> 250 GeV	7.1 ± 0.3	7.2 ± 2.2	± 1.9	± 0.4	± 0.8	± 0.7
$Z(\ell\ell/\nu\nu)H$	75–150 GeV	50.6 ± 4.1	42.5 ± 35.9	± 25.3	± 5.6	± 17.2	± 19.7
$Z(\ell\ell/\nu\nu)H$	150–250 GeV	18.8 ± 2.4	20.5 ± 6.2	± 5.0	± 2.3	± 2.4	± 2.3
$Z(\ell\ell/\nu\nu)H$	>250 GeV	4.9 ± 0.5	5.4 ± 1.7	± 1.5	± 0.5	± 0.5	± 0.3

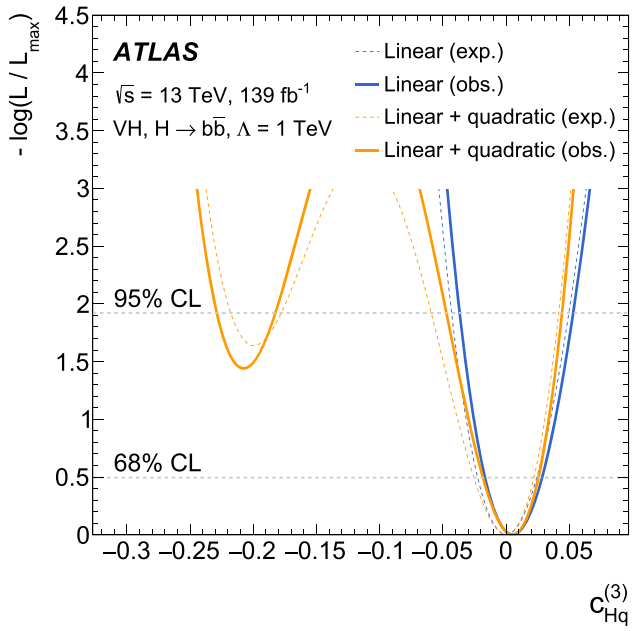

Fig. 8 The observed (solid) and expected (dotted) profiled negative-log-likelihood functions for the one-dimensional fits to constrain the coefficient $c_{Hq}^{(3)}$ of an effective Lagrangian when the other coefficients are assumed to vanish, shown for the case where only linear (blue) or linear and quadratic (orange) terms are considered

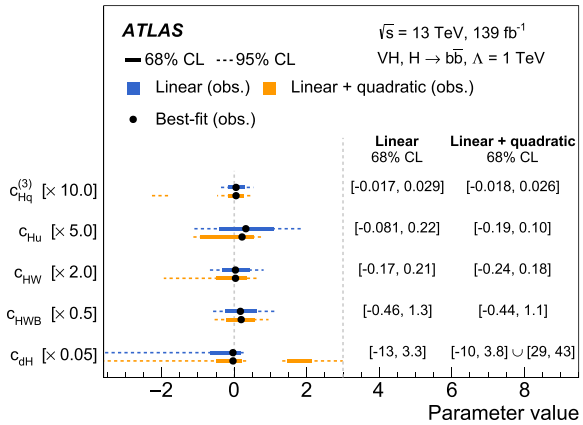

Fig. 9 Summary of the observed best-fit values and one-dimensional confidence intervals for the Wilson coefficients of the Warsaw-basis operators to which this analysis has the greatest sensitivity along with the c_{dH} coefficient which directly affects the $H \to b\bar{b}$ decay width. Limits are shown for the case where only linear (blue) or linear and quadratic (orange) terms are considered and confidence intervals are shown at both 68% CL (solid lines) and 95% CL (dashed lines)

linear terms and the $H \to b\bar{b}$ partial width, with a dedicated independent parameter added to account for the modifications to the total width.

The resulting five eigenvectors are shown in Table 15. They are labelled as E0–E4 and ordered in terms of experimental sensitivity, with E0 having the greatest and E4 the least. The eigenvectors contain information about the sensitivity of the analysis to degenerate deformations of the SM.

Table 14 Wilson coefficients c_i and corresponding dimension-6 SMEFT operators $\mathcal{Q}_i$, to which this analysis is sensitive, in the Warsaw formulation [126]

Wilson coefficient	Operator	Impacted vertex	
		Production	Decay
c_{HWB}	$\mathcal{Q}_{HWB} = H^\dagger \tau^I H W^I_{\mu\nu} B^{\mu\nu}$	HZZ	
c_{HW}	$\mathcal{Q}_{HW} = H^\dagger H W^I_{\mu\nu} W_I^{\mu\nu}$	HZZ, HWW	
$c_{Hq}^{(3)}$	$\mathcal{Q}_{Hq}^{(3)} = (H^\dagger i \overleftrightarrow{D^I_\mu} H)(\bar{q}_p \tau^I \gamma^\mu q_r)$	$qqZH, qq'WH$	
$c_{Hq}^{(1)}$	$\mathcal{Q}_{Hq}^{(1)} = (H^\dagger i \overleftrightarrow{D_\mu} H)(\bar{q}_p \gamma^\mu q_r)$	$qqZH$	
c_{Hu}	$\mathcal{Q}_{Hu} = (H^\dagger i \overleftrightarrow{D_\mu} H)(\bar{u}_p \gamma^\mu u_r)$	$qqZH$	
c_{Hd}	$\mathcal{Q}_{Hd} = (H^\dagger i \overleftrightarrow{D_\mu} H)(\bar{d}_p \gamma^\mu d_r)$	$qqZH$	
c_{dH}	$\mathcal{Q}_{dH} = (H^\dagger H)(\bar{q} d H)$		Hbb

Table 15 The composition and eigenvalues of the eigenvectors, which are composed of a linear combination of the Wilson coefficients of the Warsaw-basis operators [126]. All modifications that alter the branching ratio are absorbed into an additional independent term ($\Delta\mathrm{BR}/\mathrm{BR}_{\mathrm{SM}}$), which linearly alters the branching ratio and all contributions with a coefficient below 0.2 are omitted. The full composition of the eigenvectors is available in the HEPData repository [123]

Wilson coefficient	Eigenvalue	Eigenvector
c_{E0}	2000	$0.98 \cdot c_{Hq}^{(3)}$
c_{E1}	38	$0.85 \cdot c_{Hu} - 0.39 \cdot c_{Hq}^{(1)} - 0.27 \cdot c_{Hd}$
c_{E2}	8.3	$0.70 \cdot \Delta\mathrm{BR}/\mathrm{BR}_{\mathrm{SM}} + 0.62 \cdot c_{HW}$
c_{E3}	0.2	$0.74 \cdot c_{HWB} + 0.53 \cdot c_{Hq}^{(1)} - 0.32 \cdot c_{HW}$
c_{E4}	6.4×10^{-3}	$0.65 \cdot c_{HW} - 0.60 \cdot \Delta\mathrm{BR}/\mathrm{BR}_{\mathrm{SM}} + 0.35 \cdot c_{Hq}^{(1)}$

The leading eigenvector, E0, consists almost exclusively of $c_{Hq}^{(3)}$, which is also the coefficient most constrained in the one-dimensional limits, with similar limits obtained in both cases. The second eigenvector, E1, is dominated by c_{Hu}, but has sizeable contributions from c_{Hd} and $c_{Hq}^{(1)}$, suggesting only a linear combination of these coefficients can be constrained given the degeneracy between them. The eigenvector E2 demonstrates sensitivity to a combination of the branching ratio and c_{HW}, whilst E3 has limited sensitivity to a combination of c_{HWB} and $c_{Hq}^{(1)}$. The analysis has negligible sensitivity to the fifth eigenvector. Figure 10 shows the impact

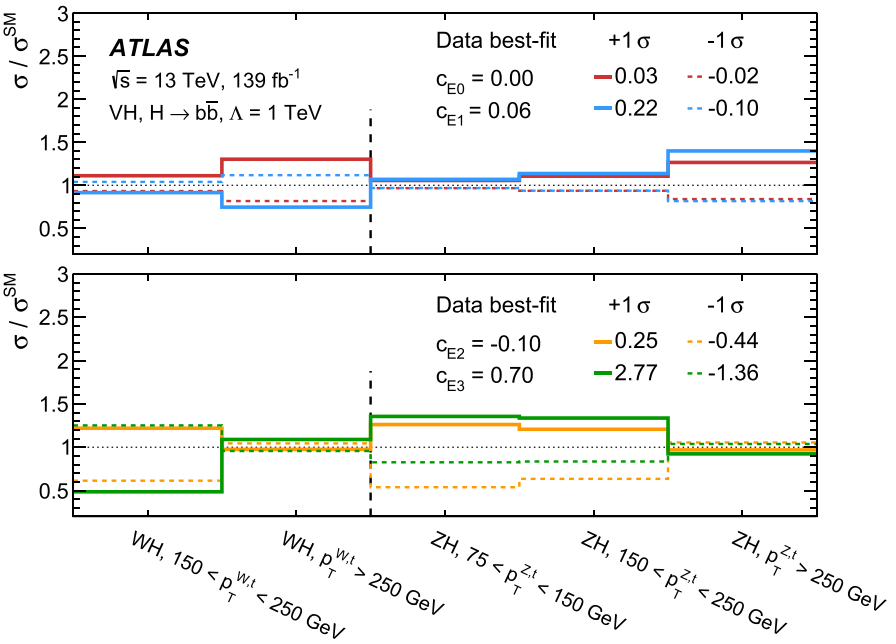

Fig. 10 The impact of the leading four eigenvectors on the STXS cross-section measurements. The change to the cross-section is indicated at the $+1\sigma$ (solid) and -1σ (dashed) limits of the corresponding Wilson coefficients, extracted from a simultaneous fit to data of all five eigenvectors

on the STXS cross-section measurements when varying the coefficients for the four leading eigenvectors within their 1σ bounds. The analysis has greatest sensitivity to coefficients which predominantly increase the cross-section in the higher p_{T}^{V} STXS regions (E0 and E1), with lower sensitivity to those which predominantly impact the lower p_{T}^{V} STXS regions (E2 and E3).

11 Conclusion

Measurements are presented of the Standard Model Higgs boson decaying into a $b\bar{b}$ pair and produced in association with a W or Z boson, using data collected by the ATLAS experiment in proton–proton collisions from Run 2 of the LHC. The data correspond to an integrated luminosity of $139\,\mathrm{fb}^{-1}$ collected at a centre-of-mass energy of $\sqrt{s}$ =13 TeV.

For a Higgs boson with $m_H = 125$ GeV produced in association with either a Z or W boson, an observed (expected) significance of 6.7 (6.7) standard deviations is found and a signal strength relative to the SM prediction of $\mu_{VH}^{bb} = 1.02^{+0.12}_{-0.11}(\mathrm{stat.})^{+0.14}_{-0.13}(\mathrm{syst.})$ is measured. For a Higgs boson produced in association with a W boson, an observed (expected) significance of 4.0 (4.1) standard deviations is found and a signal strength relative to the SM prediction for $m_H = 125$ GeV of $\mu_{WH}^{bb} = 0.95 \pm 0.18(\mathrm{stat.})^{+0.19}_{-0.18}(\mathrm{syst.})$ is measured. For a Higgs boson produced in association with a Z boson an observed (expected) significance of rejecting the background-only hypothesis of 5.3 (5.1) standard deviations is found and a signal strength of $\mu_{ZH}^{bb} = 1.08 \pm 0.17(\mathrm{stat.})^{+0.18}_{-0.15}(\mathrm{syst.})$ is measured.

Cross-sections of associated production of a Higgs boson decaying into bottom quark pairs and an electroweak gauge boson, W or Z, decaying into leptons are measured as a function of the gauge boson transverse momentum in kinematic fiducial volumes in the simplified template cross-section framework. The uncertainties in the measurements vary from 30% in the highest p_{T}^{V} regions to 85% in the lowest, and are in agreement with the Standard Model predictions.

Limits are also set on the coefficients of effective Lagrangian operators which affect the VH production and $H \to b\bar{b}$ decay. Limits are studied for both the variation of a single coefficient and also the simultaneous variation of a set of linear combinations of coefficients. The allowed range of the individual or linear combinations of the coefficients, to which the analysis has the greatest sensitivity, is limited to a few percent.

Acknowledgements We thank CERN for the very successful operation of the LHC, as well as the support staff from our institutions without whom ATLAS could not be operated efficiently. We acknowledge the support of ANPCyT, Argentina; YerPhI, Armenia; ARC, Australia; BMWFW and FWF, Austria; ANAS, Azerbaijan; SSTC, Belarus; CNPq and FAPESP, Brazil; NSERC, NRC and CFI, Canada; CERN; CONICYT, Chile; CAS, MOST and NSFC, China; COLCIENCIAS, Colombia; MSMT CR, MPO CR and VSC CR, Czech Republic; DNRF and DNSRC, Denmark; IN2P3-CNRS and CEA-DRF/IRFU, France; SRNSFG, Georgia; BMBF, HGF and MPG, Germany; GSRT, Greece; RGC and Hong Kong SAR, China; ISF and Benoziyo Center, Israel; INFN, Italy; MEXT and JSPS, Japan; CNRST, Morocco; NWO, Netherlands; RCN, Norway; MNiSW and NCN, Poland; FCT, Portugal; MNE/IFA, Romania; MES of Russia and NRC KI, Russia Federation; JINR; MESTD, Serbia; MSSR, Slovakia; ARRS and MIZŠ, Slovenia; DST/NRF, South Africa; MINECO, Spain; SRC and Wallenberg Foundation, Sweden; SERI, SNSF and Cantons of Bern and Geneva, Switzerland; MOST, Taiwan; TAEK, Turkey; STFC, United

Kingdom; DOE and NSF, United States of America. In addition, individual groups and members have received support from BCKDF, CANARIE, Compute Canada and CRC, Canada; ERC, ERDF, Horizon 2020, Marie Skłodowska-Curie Actions and COST, European Union; Investissements d'Avenir Labex, Investissements d'Avenir Idex and ANR, France; DFG and AvH Foundation, Germany; Herakleitos, Thales and Aristeia programmes co-financed by EU-ESF and the Greek NSRF, Greece; BSF-NSF and GIF, Israel; CERCA Programme Generalitat de Catalunya and PROMETEO Programme Generalitat Valenciana, Spain; Göran Gustafssons Stiftelse, Sweden; The Royal Society and Leverhulme Trust, United Kingdom. The crucial computing support from all WLCG partners is acknowledged gratefully, in particular from CERN, the ATLAS Tier-1 facilities at TRIUMF (Canada), NDGF (Denmark, Norway, Sweden), CC-IN2P3 (France), KIT/GridKA (Germany), INFN-CNAF (Italy), NL-T1 (Netherlands), PIC (Spain), ASGC (Taiwan), RAL (UK) and BNL (USA), the Tier-2 facilities worldwide and large non-WLCG resource providers. Major contributors of computing resources are listed in Ref. [128].

Data Availability Statement This manuscript has no associated data or the data will not be deposited. [Author' comment: All ATLAS scientific output is published in journals, and preliminary results are made available in Conference Notes. All are openly available, without restriction on use by external parties beyond copyright law and the standard conditions agreed by CERN. Data associated with journal publications are also made available: tables and data from plots (e.g. cross section values, likelihood profiles, selection efficiencies, cross section limits, ...) are stored in appropriate repositories such as HEPDATA (http://hepdata.cedar.ac.uk/). ATLAS also strives to make additional material related to the paper available that allows a reinterpretation of the data in the context of new theoretical models. For example, an extended encapsulation of the analysis is often provided for measurements in the framework of RIVET (http://rivet.hepforge.org/)." This information is taken from the ATLAS Data Access Policy, which is a public document that can be downloaded from http://opendata.cern.ch/record/413 [opendata.cern.ch]. The results of this analysis, including the correlation matrix, are available in Ref. [123].]

Funded by SCOAP[3].

References

1. F. Englert, R. Brout, Broken symmetry and the mass of gauge vector mesons. Phys. Rev. Lett. **13**, 321 (1964). https://doi.org/10.1103/PhysRevLett.13.321
2. P.W. Higgs, Broken symmetries, massless particles and gauge fields. Phys. Lett. **12**, 132 (1964). https://doi.org/10.1016/0031-9163(64)91136-9
3. P.W. Higgs, Broken symmetries and the masses of gauge bosons. Phys. Rev. Lett. **13**, 508 (1964). https://doi.org/10.1103/PhysRevLett.13.508
4. G. Guralnik, C. Hagen, T. Kibble, Global conservation laws and massless particles. Phys. Rev. Lett. **13**, 585 (1964). https://doi.org/10.1103/PhysRevLett.13.585
5. P.W. Higgs, Spontaneous symmetry breakdown without massless bosons. Phys. Rev. **145**, 1156 (1966). https://doi.org/10.1103/PhysRev.145.1156
6. T. Kibble, Symmetry breaking in non-abelian gauge theories. Phys. Rev. **155**, 1554 (1967). https://doi.org/10.1103/PhysRev.155.1554
7. ATLAS Collaboration, Observation of a new particle in the search for the Standard Model Higgs boson with the ATLAS detector at the LHC. Phys. Lett. B **716**, 1 (2012). https://doi.org/10.1016/j.physletb.2012.08.020 arXiv:1207.7214 [hep-ex]
8. CMS Collaboration, Observation of a new boson at a mass of 125 GeV with the CMS experiment at the LHC. Phys. Lett. B **716**, 30 (2012). https://doi.org/10.1016/j.physletb.2012.08.021. arXiv:1207.7235 [hep-ex]
9. L. Evans, P. Bryant, LHC Machine, JINST **3**, S08001 (2008). https://doi.org/10.1088/1748-0221/3/08/S08001
10. ATLAS and CMS Collaborations, Combined measurement of the Higgs boson mass in pp collisions at $\sqrt{s} = 7$ and 8 TeV with the ATLAS and CMS experiments. Phys. Rev. Lett. **114**, 191803 (2015). https://doi.org/10.1103/PhysRevLett.114.191803. arXiv:1503.07589 [hep-ex]
11. ATLAS Collaboration, Measurements of Higgs boson properties in the diphoton decay channel with 36 fb^{-1} of pp collision data at $\sqrt{s}$ = 13 TeV with the ATLAS detector. Phys. Rev. D **98**, 052005 (2018). https://doi.org/10.1103/PhysRevD.98.052005. arXiv:1802.04146 [hep-ex]
12. ATLAS Collaboration, Measurement of the Higgs boson coupling properties in the $H \to ZZ^* \to 4\ell$ decay channel at $\sqrt{s} = 13$ TeV with the ATLAS detector. JHEP **03**, 095 (2018). https://doi.org/10.1007/JHEP03(2018)095. arXiv:1712.02304 [hep-ex]
13. ATLAS Collaboration, Measurement of inclusive and differential cross sections in the $H \to ZZ^* \to 4\ell$ decay channel in pp collisions at $\sqrt{s} = 13$ TeV with the ATLAS detector. JHEP **10**, 132 (2017). https://doi.org/10.1007/JHEP10(2017)132. arXiv:1708.02810 [hep-ex]
14. ATLAS Collaboration, Measurement of the Higgs boson mass in the $H \to ZZ^* \to 4\ell$ and $H \to \gamma\gamma$ channels with $\sqrt{s} =$ 13 TeV pp collisions using the ATLAS detector. Phys. Lett. B **784**, 345 (2018). https://doi.org/10.1016/j.physletb.2018.07.050. arXiv:1806.00242 [hep-ex]
15. ATLAS Collaboration, Combined measurement of differential and total cross sections in the $H \to \gamma\gamma$ and the $H \to ZZ^* \to 4\ell$ decay channels at $\sqrt{s} = 13$ TeV with the ATLAS detector. Phys. Lett. B **786**, 114 (2018). https://doi.org/10.1016/j.physletb.2018.09.019. arXiv:1805.10197 [hep-ex]
16. ATLAS Collaboration, Measurements of gluon-gluon fusion and vector-boson fusion Higgs boson production cross-sections in the $H \to WW^* \to e\nu\mu\nu$ decay channel in pp collisions at $\sqrt{s} = 13$ TeV with the ATLAS detector. Phys. Lett. B **789**, 508 (2019). https://doi.org/10.1016/j.physletb.2018.11.064. arXiv:1808.09054 [hep-ex]
17. CMS Collaboration, Measurement of inclusive and differential Higgs boson production cross sections in the diphoton decay channel in proton–proton collisions at $\sqrt{s} = 13$ TeV. JHEP **01**, 183 (2019). https://doi.org/10.1007/JHEP01(2019)183. arXiv:1807.0382 5 [hep-ex]
18. CMS Collaboration, Measurements of Higgs boson properties in the diphoton decay channel in proton–proton collisions at $\sqrt{s} = 13$ TeV. JHEP **11**, 185 (2018). https://doi.org/10.1007/JHEP11(2018)185. arXiv:1804.02716 [hep-ex]
19. CMS Collaboration, Measurements of properties of the Higgs boson decaying into the four-lepton final state in pp collisions

at $\sqrt{s} = 13$ TeV. JHEP **11**, 047 (2017). https://doi.org/10.1007/JHEP11(2017)047. arXiv:1706.09936 [hep-ex]
20. CMS Collaboration, Measurements of properties of the Higgs boson decaying to a W boson pair in pp collisions at $\sqrt{s} = 13$ TeV. Phys. Lett. B **791**, 96 (2019). https://doi.org/10.1016/j.physletb.2018.12.073. arXiv:1806.05246 [hep-ex]
21. ATLAS and CMS Collaborations, Measurements of the Higgs boson production and decay rates and constraints on its couplings from a combined ATLAS and CMS analysis of the LHC pp collision data at $\sqrt{s} = 7$ and 8 TeV. JHEP **08**, 045 (2016). https://doi.org/10.1007/JHEP08(2016)045. arXiv:1606.02266 [hep-ex]
22. ATLAS Collaboration, Cross-section measurements of the Higgs boson decaying into a pair of τ-leptons in proton–proton collisions at $\sqrt{s} = 13$ TeV with the ATLAS detector. Phys. Rev. D **99**, 072001 (2019). https://doi.org/10.1103/PhysRevD.99.072001. arXiv:1811.08856 [hep-ex]
23. CMS Collaboration, Observation of the Higgs boson decay to a pair of τ leptons. Phys. Lett. B **779**, 283 (2018). https://doi.org/10.1016/j.physletb.2018.02.004. arXiv:1708.00373 [hep-ex]
24. ATLAS Collaboration, Observation of Higgs boson production in association with a top quark pair at the LHC with the ATLAS detector. Phys. Lett. B **784**, 173 (2018). https://doi.org/10.1016/j.physletb.2018.07.035. arXiv:1806.00425 [hep-ex]
25. CMS Collaboration, Observation of $t\bar{t}H$ production. Phys. Rev. Lett. **120**, 231801 (2018). https://doi.org/10.1103/PhysRevLett.120.231801. arXiv:1804.02610 [hep-ex]
26. A. Djouadi, J. Kalinowski, M. Spira, HDECAY: a program for Higgs boson decays in the Standard Model and its supersymmetric extension. Comput. Phys. Commun. **108**, 56 (1998). https://doi.org/10.1016/S0010-4655(97)00123-9. arXiv:hep-ph/9704448
27. LHC Higgs Cross Section Working Group, Handbook of LHC Higgs cross sections: 4. Deciphering the nature of the Higgs sector, CERN-2017-002-M (2016). https://doi.org/10.2172/1345634. arXiv:1610.07922 [hep-ph]
28. CMS Collaboration, Inclusive search for a highly boosted Higgs boson decaying to a bottom quark–antiquark pair. Phys. Rev. Lett. **120**, 071802 (2018). https://doi.org/10.1103/PhysRevLett.120.071802. arXiv:1709.05543 [hep-ex]
29. S. Glashow, D.V. Nanopoulos, A. Yildiz, Associated production of Higgs bosons and Z particles. Phys. Rev. D **18**, 1724 (1978). https://doi.org/10.1103/PhysRevD.18.1724
30. R. Lafaye et al., Measuring the Higgs sector. JHEP **08**, 009 (2009). https://doi.org/10.1088/1126-6708/2009/08/009. arXiv:0904.3866 [hep-ph]
31. LHC Higgs Cross Section Working Group, Handbook of LHC Higgs cross sections: 3. Higgs properties, CERN-2013-004 (2013). https://doi.org/10.5170/CERN-2013-004. arXiv:1307.1347 [hep-ph]
32. J. Ellis, V. Sanz, T. You, Complete Higgs sector constraints on dimension-6 operators. JHEP **07**, 036 (2014). https://doi.org/10.1007/JHEP07(2014)036. arXiv:1404.3667 [hep-ph]
33. ATLAS Collaboration, Observation of $H \to b\bar{b}$ decays and VH production with the ATLAS detector. Phys. Lett. B **786**, 59 (2018). https://doi.org/10.1016/j.physletb.2018.09.013. arXiv:1808.08238 [hep-ex]
34. CMS Collaboration, Observation of Higgs boson decay to bottom quarks. Phys. Rev. Lett. **121**, 121801 (2018). https://doi.org/10.1103/PhysRevLett.121.121801. arXiv:1808.08242 [hep-ex]
35. ATLAS Collaboration, Measurement of VH, $H \to b\bar{b}$ production as a function of the vector-boson transverse momentum in 13 TeV pp collisions with the ATLAS detector. JHEP **05**, 141 (2019). https://doi.org/10.1007/JHEP05(2019)141. arXiv:1903.04618 [hep-ex]
36. ATLAS Collaboration, Measurement of the associated production of a Higgs boson decaying to b quarks with a vector boson at high transverse momentum in pp collisions at $\sqrt{s} = 13$ TeV with the ATLAS detector, ATLAS-CONF-2020-007 (2020). https://cds.cern.ch/record/2715063
37. ATLAS Collaboration, The ATLAS experiment at the CERN Large Hadron Collider. JINST **3**, S08003 (2008). https://doi.org/10.1088/1748-0221/3/08/S08003
38. ATLAS Collaboration, ATLAS Insertable B-Layer Technical Design Report, ATLAS-TDR-19 (2010). https://cds.cern.ch/record/1291633 [Addendum: ATLAS Insertable B-Layer Technical Design Report, ATLAS-TDR-19-ADD-1 (2012). https://cds.cern.ch/record/1451888]
39. ATLAS IBL Collaboration, Production and integration of the ATLAS Insertable B-Layer. JINST **13**, T05008 (2018). https://doi.org/10.1088/1748-0221/13/05/T05008. arXiv:1803.00844 [physics.ins-det]
40. ATLAS Collaboration, Performance of the ATLAS trigger system in 2015. Eur. Phys. J. C **77**, 317 (2017). https://doi.org/10.1140/epjc/s10052-017-4852-3. arXiv:1611.09661 [hep-ex]
41. ATLAS Collaboration, Luminosity determination in pp collisions at $\sqrt{s} = 8$ TeV using the ATLAS detector at the LHC. Eur. Phys. J. C **76**, 653 (2016). https://doi.org/10.1140/epjc/s10052-016-4466-1. arXiv:1608.03953 [hep-ex]
42. G. Avoni et al., The new LUCID-2 detector for luminosity measurement and monitoring in ATLAS. JINST **13**, P07017 (2018). https://doi.org/10.1088/1748-0221/13/07/P07017
43. ATLAS Collaboration, The ATLAS simulation infrastructure. Eur. Phys. J. C **70**, 823 (2010). https://doi.org/10.1140/epjc/s10052-010-1429-9. arXiv:1005.4568 [physics.ins-det]
44. S. Agostinelli et al., GEANT4: a simulation toolkit. Nucl. Instrum. Methods A **506**, 250 (2003). https://doi.org/10.1016/S0168-9002(03)01368-8
45. T. Sjostrand, S. Mrenna, P.Z. Skands, A brief introduction to PYTHIA 8.1. Comput. Phys. Commun. **178**, 852 (2008). https://doi.org/10.1016/j.cpc.2008.01.036. arXiv:0710.3820 [hep-ph]
46. ATLAS Collaboration, The Pythia 8 A3 tune description of ATLAS minimum bias and inelastic measurements incorporating the Donnachie–Landshoff diffractive model, ATL-PHYS-PUB-2016-017 (2016). https://cds.cern.ch/record/2206965
47. R.D. Ball et al., Parton distributions with LHC data. Nucl. Phys. B **867**, 244 (2013). https://doi.org/10.1016/j.nuclphysb.2012.10.003. arXiv:1207.1303 [hep-ph]
48. E. Bothmann et al., Event generation with Sherpa 2.2. Sci. Post Phys. **7**, 034 (2019). https://doi.org/10.21468/SciPostPhys.7.3.034. arXiv:1905.09127 [hep-ph]
49. D. Lange, The EvtGen particle decay simulation package. Nucl. Instrum. Methods A **462**, 152 (2001). https://doi.org/10.1016/S0168-9002(01)00089-4
50. J. Butterworth et al., PDF4LHC recommendations for LHC Run II. J. Phys. G **43**, 023001 (2016). https://doi.org/10.1088/0954-3899/43/2/023001. arXiv:1510.03865 [hep-ph]
51. A. Denner, S. Dittmaier, S. Kallweit, A. Muck, Electroweak corrections to Higgs–Strahlung off W/Z bosons at the Tevatron and the LHC with Hawk. JHEP **03**, 075 (2012). https://doi.org/10.1007/JHEP03(2012)075. arXiv:1112.5142 [hep-ph]
52. A. Denner, S. Dittmaier, S. Kallweit, A. Muck, HAWK 2.0: a Monte Carlo program for Higgs production in vector-boson fusion and Higgs Strahlung at hadron colliders. Comput. Phys. Commun. **195**, 161 (2015). https://doi.org/10.1016/j.cpc.2015.04.021. arXiv:1412.5390 [hep-ph]
53. J. de Favereau de Jeneret et al., High energy photon interactions at the LHC (2009). arXiv:0908.2020 [hep-ph]
54. S. Alioli, P. Nason, C. Oleari, E. Re, A general framework for implementing NLO calculations in shower Monte Carlo programs: the POWHEG BOX. JHEP **06**, 043 (2010). https://doi.org/10.1007/JHEP06(2010)043. arXiv:1002.2581 [hep-ph]

55. R.D. Ball et al., Parton distributions for the LHC Run II. JHEP **04**, 040 (2015). https://doi.org/10.1007/JHEP04(2015)040. arXiv:1410.8849 [hep-ph]
56. ATLAS Collaboration, Measurement of the Z/γ^* boson transverse momentum distribution in pp collisions at $\sqrt{s} = 7$ TeV with the ATLAS detector. JHEP **09**, 145 (2014). https://doi.org/10.1007/JHEP09(2014)145. arXiv:1406.3660 [hep-ex]
57. G. Cullen et al., Automated one-loop calculations with GOSAM. Eur. Phys. J. C **72**, 1889 (2012). https://doi.org/10.1140/epjc/s10052-012-1889-1. arXiv:1111.2034 [hep-ph]
58. K. Hamilton, P. Nason, G. Zanderighi, MINLO: multi-scale improved NLO. JHEP **10**, 155 (2012). https://doi.org/10.1007/JHEP10(2012)155. arXiv:1206.3572 [hep-ph]
59. G. Luisoni, P. Nason, C. Oleari, F. Tramontano, $HW^{\pm}/HZ + 0$ and 1 jet at NLO with the POWHEG BOX interfaced to GoSam and their merging within MiNLO. JHEP **10**, 083 (2013). https://doi.org/10.1007/JHEP10(2013)083. arXiv:1306.2542 [hep-ph]
60. M. Ciccolini, S. Dittmaier, M. Kramer, Electroweak radiative corrections to associated WH and ZH production at hadron colliders. Phys. Rev. D **68**, 073003 (2003). https://doi.org/10.1103/PhysRevD.68.073003. arXiv:hep-ph/0306234
61. O. Brein, A. Djouadi, R. Harlander, NNLO QCD corrections to the Higgs–Strahlung processes at hadron colliders. Phys. Lett. B **579**, 149 (2004). https://doi.org/10.1016/j.physletb.2003.10.112. arXiv:hep-ph/0307206
62. G. Ferrera, M. Grazzini, F. Tramontano, Associated Higgs-W-boson production at hadron colliders: a fully exclusive QCD calculation at NNLO. Phys. Rev. Lett. **107**, 152003 (2011). https://doi.org/10.1103/PhysRevLett.107.152003. arXiv:1107.1164 [hep-ph]
63. O. Brein, R. Harlander, M. Wiesemann, T. Zirke, Top-quark mediated effects in hadronic Higgs–Strahlung. Eur. Phys. J. C **72**, 1868 (2012). https://doi.org/10.1140/epjc/s10052-012-1868-6. arXiv:1111.0761 [hep-ph]
64. G. Ferrera, M. Grazzini, F. Tramontano, Higher-order QCD effects for associated WH production and decay at the LHC. JHEP **04**, 039 (2014). https://doi.org/10.1007/JHEP04(2014)039. arXiv:1312.1669 [hep-ph]
65. G. Ferrera, M. Grazzini, F. Tramontano, Associated ZH production at hadron colliders: the fully differential NNLO QCD calculation. Phys. Lett. B **740**, 51 (2015). https://doi.org/10.1016/j.physletb.2014.11.040. arXiv:1407.4747 [hep-ph]
66. J.M. Campbell, R.K. Ellis, C. Williams, Associated production of a Higgs boson at NNLO. JHEP **06**, 179 (2016). https://doi.org/10.1007/JHEP06(2016)179. arXiv:1601.00658 [hep-ph]
67. L. Altenkamp, S. Dittmaier, R.V. Harlander, H. Rzehak, T.J.E. Zirke, Gluon-induced Higgs–Strahlung at next-to-leading order QCD. JHEP **02**, 078 (2013). https://doi.org/10.1007/JHEP02(2013)078. arXiv:1211.5015 [hep-ph]
68. B. Hespel, F. Maltoni, E. Vryonidou, Higgs and Z boson associated production via gluon fusion in the SM and the 2HDM. JHEP **06**, 065 (2015). https://doi.org/10.1007/JHEP06(2015)065. arXiv:1503.01656 [hep-ph]
69. R.V. Harlander, A. Kulesza, V. Theeuwes, T. Zirke, Soft gluon resummation for gluon-induced Higgs Strahlung. JHEP **11**, 082 (2014). https://doi.org/10.1007/JHEP11(2014)082. arXiv:1410.0217 [hep-ph]
70. R.V. Harlander, S. Liebler, T. Zirke, Higgs Strahlung at the Large Hadron Collider in the 2-Higgs-doublet model. JHEP **02**, 023 (2014). https://doi.org/10.1007/JHEP02(2014)023. arXiv:1307.8122 [hep-ph]
71. O. Brein, R.V. Harlander, T.J.E. Zirke, vh@nnlo – Higgs Strahlung at hadron colliders. Comput. Phys. Commun. **184**, 998 (2013). https://doi.org/10.1016/j.cpc.2012.11.002. arXiv:1210.5347 [hep-ph]
72. S. Frixione, P. Nason, G. Ridolfi, A positive-weight next-to-leading-order Monte Carlo for heavy flavour hadron production. JHEP **09**, 126 (2007). https://doi.org/10.1088/1126-6708/2007/09/126. arXiv:0707.3088 [hep-ph]
73. ATLAS Collaboration, ATLAS Pythia 8 tunes to 7 TeV data, ATL-PHYS-PUB-2014-021 (2014). https://cds.cern.ch/record/1966419
74. M. Czakon, A. Mitov, Top++: a program for the calculation of the top-pair cross-section at hadron colliders. Comput. Phys. Commun. **185**, 2930 (2014). https://doi.org/10.1016/j.cpc.2014.06.021. arXiv:1112.5675 [hep-ph]
75. S. Alioli, P. Nason, C. Oleari, E. Re, NLO single-top production matched with shower in POWHEG: s- and t-channel contributions. JHEP **09**, 111 (2009). https://doi.org/10.1088/1126-6708/2009/09/111 [Erratum: JHEP 02 (2010) 011]. arXiv:0907.4076 [hep-ph]
76. N. Kidonakis, Next-to-next-to-leading resummation for s-channel single top quark production. Phys. Rev. D **81**, 054028 (2010). https://doi.org/10.1103/PhysRevD.81.054028. arXiv:1001.5034 [hep-ph]
77. N. Kidonakis, Next-to-next-to-leading-order collinear and soft gluon corrections for t-channel single top quark production. Phys. Rev. D **83**, 091503 (2011). https://doi.org/10.1103/PhysRevD.83.091503. arXiv:1103.2792 [hep-ph]
78. E. Re, Single-top Wt-channel production matched with parton showers using the POWHEG method. Eur. Phys. J. C **71**, 1547 (2011). https://doi.org/10.1140/epjc/s10052-011-1547-z. arXiv:1009.2450 [hep-ph]
79. N. Kidonakis, Two-loop soft anomalous dimensions for single top quark associated production with a W^- or H^-. Phys. Rev. D **82**, 054018 (2010). https://doi.org/10.1103/PhysRevD.82.054018. arXiv:1005.4451 [hep-ph]
80. F. Cascioli, P. Maierhofer, S. Pozzorini, Scattering amplitudes with open loops. Phys. Rev. Lett. **108**, 111601 (2012). https://doi.org/10.1103/PhysRevLett.108.111601. arXiv:1111.5206 [hep-ph]
81. T. Gleisberg, S. Hoche, Comix, a new matrix element generator. JHEP **12**, 039 (2008). https://doi.org/10.1088/1126-6708/2008/12/039. arXiv:0808.3674 [hep-ph]
82. S. Schumann, F. Krauss, A parton shower algorithm based on Catani–Seymour dipole factorisation. JHEP **03**, 038 (2008). https://doi.org/10.1088/1126-6708/2008/03/038. arXiv:0709.1027 [hep-ph]
83. S. Hoche, F. Krauss, M. Schonherr, F. Siegert, QCD matrix elements + parton showers. The NLO case. JHEP **04**, 027 (2013). https://doi.org/10.1007/JHEP04(2013)027. arXiv:1207.5030 [hep-ph]
84. S. Catani, L. Cieri, G. Ferrera, D. de Florian, M. Grazzini, Vector boson production at hadron colliders: a fully exclusive QCD calculation at next-to-next-to-leading order. Phys. Rev. Lett. **103**, 082001 (2009). https://doi.org/10.1103/PhysRevLett.103.082001. arXiv:0903.2120 [hep-ph]
85. ATLAS Collaboration, Reconstruction of primary vertices at the ATLAS experiment in Run 1 proton-proton collisions at the LHC. Eur. Phys. J. C **77**, 332 (2017). https://doi.org/10.1140/epjc/s10052-017-4887-5. arXiv:1611.10235 [physics.ins-det]
86. ATLAS Collaboration, Electron and photon performance measurements with the ATLAS detector using the 2015–2017 LHC proton–proton collision data. JINST **14**, P12006 (2019). https://doi.org/10.1088/1748-0221/14/12/P12006. arXiv:1908.00005 [hep-ex]
87. ATLAS Collaboration, Evidence for the $H \to b\bar{b}$ decay with the ATLAS detector. JHEP **12**, 024 (2017). https://doi.org/10.1007/JHEP12(2017)024. arXiv:1708.03299 [hep-ex]
88. ATLAS Collaboration, Muon reconstruction performance of the ATLAS detector in proton–proton collision data at $\sqrt{s} = 13$

TeV. Eur. Phys. J. C **76**, 292 (2016). https://doi.org/10.1140/epjc/s10052-016-4120-y. arXiv:1603.05598 [hep-ex]
89. ATLAS Collaboration, Reconstruction of hadronic decay products of tau leptons with the ATLAS experiment. Eur. Phys. J. C **76**, 295 (2016). https://doi.org/10.1140/epjc/s10052-016-4110-0. arXiv:1512.05955 [hep-ex]
90. ATLAS Collaboration, Measurement of the tau lepton reconstruction and identification performance in the ATLAS experiment using pp collisions at $\sqrt{s} = 13$ TeV, ATLAS-CONF-2017-029 (2017). https://cds.cern.ch/record/2261772
91. W. Lampl et al., Calorimeter clustering algorithms: description and performance, ATL-LARG-PUB-2008-002 (2008). https://cds.cern.ch/record/1099735
92. M. Cacciari, G.P. Salam, G. Soyez, The anti-k_t jet clustering algorithm. JHEP **04**, 063 (2008). https://doi.org/10.1088/1126-6708/2008/04/063. arXiv:0802.1189 [hep-ph]
93. ATLAS Collaboration, Selection of jets produced in 13 TeV proton–proton collisions with the ATLAS detector, ATLAS-CONF-2015-029 (2015). https://cds.cern.ch/record/2037702
94. ATLAS Collaboration, Performance of pile-up mitigation techniques for jets in pp collisions at $\sqrt{s} = 8$ TeV using the ATLAS detector. Eur. Phys. J. C **76**, 581 (2016). https://doi.org/10.1140/epjc/s10052-016-4395-z. arXiv:1510.03823 [hep-ex]
95. ATLAS Collaboration, ATLAS b-jet identification performance and efficiency measurement with $t\bar{t}$ events in pp collisions at $\sqrt{s} = 13$ TeV. Eur. Phys. J. C **79**, 970 (2019). https://doi.org/10.1140/epjc/s10052-019-7450-8. arXiv:1907.05120 [hep-ex]
96. ATLAS Collaboration, Jet energy scale measurements and their systematic uncertainties in proton-proton collisions at $\sqrt{s} = 13$ TeV with the ATLAS detector. Phys. Rev. D **96**, 072002 (2017). https://doi.org/10.1103/PhysRevD.96.072002. arXiv:1703.09665 [hep-ex]
97. ATLAS Collaboration, Performance of missing transverse momentum reconstruction with the ATLAS detector using proton–proton collisions at $\sqrt{s} = 13$ TeV. Eur. Phys. J. C **78**, 903 (2018). https://doi.org/10.1140/epjc/s10052-018-6288-9. arXiv:1802.08168 [hep-ex]
98. J.M. Butterworth, A.R. Davison, M. Rubin, G.P. Salam, Jet substructure as a new Higgs-search channel at the Large Hadron Collider. Phys. Rev. Lett. **100**, 242001 (2008). https://doi.org/10.1103/PhysRevLett.100.242001. arXiv:0802.2470 [hep-ph]
99. ATLAS Collaboration, ATLAS sensitivity to the Standard Model Higgs in the HW and HZ channels at high transverse momenta, ATL-PHYS-PUB-2009-088 (2009). https://cds.cern.ch/record/1201444
100. S. Badger et al., Les Houches 2015: Physics at TeV Colliders Standard Model Working Group Report (2016). arXiv:1605.04692 [hep-ph]. https://lss.fnal.gov/archive/2016/conf/fermilab-conf-16-175-ppd-t.pdf
101. N. Berger et al., Simplified template cross sections—stage 1.1 (2019). arXiv:1906.02754 [hep-ph]
102. ATLAS Collaboration, Measurement of b-tagging efficiency of c-jets in $t\bar{t}$ events using a likelihood approach with the ATLAS detector, ATLAS-CONF-2018-001 (2018). https://cds.cern.ch/record/2306649
103. ATLAS Collaboration, Calibration of light-flavour b-jet mistagging rates using ATLAS proton–proton collision data at $\sqrt{s} = 13$ TeV, ATLAS-CONF-2018-006 (2018). https://cds.cern.ch/record/2314418
104. D. Gonçalves, J. Nakamura, Role of the Z polarization in the $H \to b\bar{b}$ measurement. Phys. Rev. D **98**, 093005 (2018). https://doi.org/10.1103/PhysRevD.98.093005. arXiv:1805.06385 [hep-ph]
105. A. Hoecker et al., TMVA - toolkit for multivariate data analysis (2007). arXiv:0703039 [physics.data-an]
106. ATLAS Collaboration, Jet energy resolution in proton-proton collisions at $\sqrt{s} = 7$ TeV recorded in 2010 with the ATLAS detector. Eur. Phys. J. C **73**, 2306 (2013). https://doi.org/10.1140/epjc/s10052-013-2306-0. arXiv:1210.6210 [hep-ex]
107. ATLAS Collaboration, Electron reconstruction and identification in the ATLAS experiment using the 2015 and 2016 LHC proton–proton collision data at $\sqrt{s} = 13$ TeV. Eur. Phys. J. C **79**, 639 (2019). https://doi.org/10.1140/epjc/s10052-019-7140-6. arXiv:1902.04655 [hep-ex]
108. ATLAS Collaboration, $E_{\mathrm{T}}^{\mathrm{miss}}$ performance in the ATLAS detector using 2015-2016 LHC pp collisions, ATLAS-CONF-2018-023 (2018). https://cds.cern.ch/record/2625233
109. ATLAS Collaboration, Measurement of the inelastic proton–proton cross section at $\sqrt{s} = 13$ TeV with the ATLAS Detector at the LHC. Phys. Rev. Lett. **117**, 182002 (2016). https://doi.org/10.1103/PhysRevLett.117.182002. arXiv:1606.02625 [hep-ex]
110. K. Cranmer, J. Pavez, G. Louppe, Approximating likelihood ratios with calibrated discriminative classifiers (2015). arXiv:1506.02169 [stat.AP]
111. J. Alwall et al., The automated computation of tree-level and next-to-leading order differential cross sections, and their matching to parton shower simulations. JHEP **07**, 79 (2014). https://doi.org/10.1007/JHEP07(2014)079. arXiv:1405.0301 [hep-ph]
112. M. Bahr et al., Herwig++ physics and manual. Eur. Phys. J. C **58**, 639 (2008). https://doi.org/10.1140/epjc/s10052-008-0798-9. arXiv:0803.0883 [hep-ph]
113. J. Bellm et al., Herwig 7.0/Herwig++ 3.0 release note. Eur. Phys. J. C **76**, 196 (2016). https://doi.org/10.1140/epjc/s10052-016-4018-8. arXiv:1512.01178 [hep-ph]
114. S. Frixione, E. Laenen, P. Motylinski, B.R. Webber, C.D. White, Single-top hadroproduction in association with a W boson. JHEP **07**, 029 (2008). https://doi.org/10.1088/1126-6708/2008/07/029. arXiv:0805.3067 [hep-ph]
115. S. Frixione, P. Nason, C. Oleari, Matching NLO QCD computations with Parton Shower simulations: the POWHEG method. JHEP **11**, 070 (2007). https://doi.org/10.1088/1126-6708/2007/11/070. arXiv:0709.2092 [hep-ph]
116. ATLAS Collaboration, Evaluation of theoretical uncertainties for simplified template cross section measurements of V-associated production of the Higgs boson, ATL-PHYS-PUB-2018-035 (2018). https://cds.cern.ch/record/2649241
117. J. Bendavid et al., Les Houches 2017: Physics at TeV Colliders Standard Model Working Group Report (2018). arXiv:1803.07977 [hep-ph]. https://lss.fnal.gov/archive/2018/conf/fermilab-conf-18-122-cd-t.pdf
118. LHC Higgs Cross Section Working Group, S. Dittmaier, C. Mariotti, G. Passarino, R. Tanaka (Eds.) Handbook of LHC Higgs cross sections: 1. Inclusive observables, CERN-2011-002 (2011). https://doi.org/10.5170/CERN-2011-002. arXiv:1101.0593 [hep-ph]
119. LHC Higgs Cross Section Working Group, S. Dittmaier, C. Mariotti, G. Passarino, R. Tanaka (Eds.) Handbook of LHC Higgs cross sections: 2. Differential distributions, CERN-2012-002 (2012). https://doi.org/10.5170/CERN-2012-002. arXiv:1201.3084 [hep-ph]
120. R.J. Barlow, C. Beeston, Fitting using finite Monte Carlo samples. Comput. Phys. Commun. **77**, 219 (1993). https://doi.org/10.1016/0010-4655(93)90005-W
121. ATLAS Collaboration, Search for the $b\bar{b}$ decay of the Standard Model Higgs boson in associated $(W/Z)H$ production with the ATLAS detector. JHEP **01**, 069 (2015). https://doi.org/10.1007/JHEP01(2015)069. arXiv:1409.6212 [hep-ex]

122. G. Cowan, K. Cranmer, E. Gross, O. Vitells, Asymptotic formulae for likelihood-based tests of new physics. Eur. Phys. J. C **71**, 1554 (2011). https://doi.org/10.1140/epjc/s10052-011-1554-0, [Erratum: Eur. Phys. J. C 73 (2013) 2501]. arXiv:1007.1727 [physics.data-an]
123. ATLAS Collaboration, Measurements of WH and ZH production in the $H \to b\bar{b}$ decay channel in pp collisions at 13 TeV with the ATLAS detector, HEPData (2020). https://doi.org/10.17182/hepdata.94800
124. R. Contino, M. Ghezzi, C. Grojean, M. Muhlleitner, M. Spira, Effective Lagrangian for a light Higgs-like scalar. JHEP **07**, 035 (2013). https://doi.org/10.1007/JHEP07(2013)035. arXiv:1303.3876 [hep-ph]
125. I. Brivio, Y. Jiang, M. Trott, The SMEFTsim package, theory and tools. JHEP **12**, 070 (2017). https://doi.org/10.1007/JHEP12(2017)070. arXiv:1709.06492 [hep-ph]
126. B. Grzadkowski, M. Iskrzynski, M. Misiak, J. Rosiek, Dimension-six terms in the Standard Model Lagrangian. JHEP **10**, 085 (2010). https://doi.org/10.1007/JHEP10(2010)085. arXiv:1008.4884 [hep-ph]
127. ATLAS Collaboration, Methodology for the EFT interpretation of Higgs boson simplified template cross-section results in ATLAS, ATL-PHYS-PUB-2019-042 (2019). https://cds.cern.ch/record/2694284
128. ATLAS Collaboration, ATLAS Computing Acknowledgements, ATL-GEN-PUB-2016-002. https://cds.cern.ch/record/2202407

ATLAS Collaboration

G. Aad[102], B. Abbott[128], D.C. Abbott[103], A. Abed Abud[36], K. Abeling[53], D.K. Abhayasinghe[94], S.H. Abidi[166], O.S. AbouZeid[40], N.L. Abraham[155], H. Abramowicz[160], H. Abreu[159], Y. Abulaiti[6], B.S. Acharya[67a,67b,n], B. Achkar[53], L. Adam[100], C. Adam Bourdarios[5], L. Adamczyk[84a], L. Adamek[166], J. Adelman[121], M. Adersberger[114], A. Adiguzel[12c], S. Adorni[54], T. Adye[143], A.A. Affolder[145], Y. Afik[159], C. Agapopoulou[65], M.N. Agaras[38], A. Aggarwal[119], C. Agheorghiesei[27c], J.A. Aguilar-Saavedra[139f,139a,ad], A. Ahmad[36], F. Ahmadov[80], W.S. Ahmed[104], X. Ai[18], G. Aielli[74a,74b], S. Akatsuka[86], M. Akbiyik[100], T.P.A. Åkesson[97], E. Akilli[54], A.V. Akimov[111], K. Al Khoury[65], G.L. Alberghi[23b,23a], J. Albert[175], M.J. Alconada Verzini[160], S. Alderweireldt[36], M. Aleksa[36], I.N. Aleksandrov[80], C. Alexa[27b], T. Alexopoulos[10], A. Alfonsi[120], F. Alfonsi[23b,23a], M. Alhroob[128], B. Ali[141], S. Ali[157], M. Aliev[165], G. Alimonti[69a], C. Allaire[36], B.M.M. Allbrooke[155], B.W. Allen[131], P.P. Allport[21], A. Aloisio[70a,70b], F. Alonso[89], C. Alpigiani[147], E. Alunno Camelia[74a,74b], M. Alvarez Estevez[99], M.G. Alviggi[70a,70b], Y. Amaral Coutinho[81b], A. Ambler[104], L. Ambroz[134], C. Amelung[26], D. Amidei[106], S.P. Amor Dos Santos[139a], S. Amoroso[46], C.S. Amrouche[54], F. An[79], C. Anastopoulos[148], N. Andari[144], T. Andeen[11], J.K. Anders[20], S.Y. Andrean[45a,45b], A. Andreazza[69a,69b], V. Andrei[61a], C.R. Anelli[175], S. Angelidakis[9], A. Angerami[39], A.V. Anisenkov[122b,122a], A. Annovi[72a], C. Antel[54], M.T. Anthony[148], E. Antipov[129], M. Antonelli[51], D.J.A. Antrim[170], F. Anulli[73a], M. Aoki[82], J.A. Aparisi Pozo[173], M.A. Aparo[155], L. Aperio Bella[46], N. Aranzabal[36], V. Araujo Ferraz[81a], R. Araujo Pereira[81b], C. Arcangeletti[51], A.T.H. Arce[49], F.A. Arduh[89], J.-F. Arguin[110], S. Argyropoulos[52], J.-H. Arling[46], A.J. Armbruster[36], A. Armstrong[170], O. Arnaez[166], H. Arnold[120], Z.P. Arrubarrena Tame[114], G. Artoni[134], K. Asai[126], S. Asai[162], T. Asawatavonvanich[164], N. Asbah[59], E.M. Asimakopoulou[171], L. Asquith[155], J. Assahsah[35d], K. Assamagan[29], R. Astalos[28a], R.J. Atkin[33a], M. Atkinson[172], N.B. Atlay[19], H. Atmani[65], K. Augsten[141], V.A. Austrup[181], G. Avolio[36], M.K. Ayoub[15a], G. Azuelos[110,al], H. Bachacou[144], K. Bachas[161], M. Backes[134], F. Backman[45a,45b], P. Bagnaia[73a,73b], M. Bahmani[85], H. Bahrasemani[151], A.J. Bailey[173], V.R. Bailey[172], J.T. Baines[143], C. Bakalis[10], O.K. Baker[182], P.J. Bakker[120], E. Bakos[16], D. Bakshi Gupta[8], S. Balaji[156], E.M. Baldin[122b,122a], P. Balek[179], F. Balli[144], W.K. Balunas[134], J. Balz[100], E. Banas[85], M. Bandieramonte[138], A. Bandyopadhyay[24], Sw. Banerjee[180,i], L. Barak[160], W.M. Barbe[38], E.L. Barberio[105], D. Barberis[55b,55a], M. Barbero[102], G. Barbour[95], T. Barillari[115], M.-S. Barisits[36], J. Barkeloo[131], T. Barklow[152], R. Barnea[159], B.M. Barnett[143], R.M. Barnett[18], Z. Barnovska-Blenessy[60a], A. Baroncelli[60a], G. Barone[29], A.J. Barr[134], L. Barranco Navarro[45a,45b], F. Barreiro[99], J. Barreiro Guimarães da Costa[15a], U. Barron[160], S. Barsov[137], F. Bartels[61a], R. Bartoldus[152], G. Bartolini[102], A.E. Barton[90], P. Bartos[28a], A. Basalaev[46], A. Basan[100], A. Bassalat[65,ai], M.J. Basso[166], R.L. Bates[57], S. Batlamous[35e], J.R. Batley[32], B. Batool[150], M. Battaglia[145], M. Bauce[73a,73b], F. Bauer[144], K.T. Bauer[170], P. Bauer[24], H.S. Bawa[31], A. Bayirli[12c], J.B. Beacham[49], T. Beau[135], P.H. Beauchemin[169], F. Becherer[52], P. Bechtle[24], H.C. Beck[53], H.P. Beck[20,p], K. Becker[177], C. Becot[46], A. Beddall[12d], A.J. Beddall[12a], V.A. Bednyakov[80], M. Bedognetti[120], C.P. Bee[154], T.A. Beermann[181], M. Begalli[81b], M. Begel[29], A. Behera[154], J.K. Behr[46], F. Beisiegel[24], M. Belfkir[5], A.S. Bell[95], G. Bella[160], L. Bellagamba[23b], A. Bellerive[34], P. Bellos[9], K. Beloborodov[122b,122a], K. Belotskiy[112], N.L. Belyaev[112], D. Benchekroun[35a], N. Benekos[10], Y. Benhammou[160], D.P. Benjamin[6], M. Benoit[54], J.R. Bensinger[26], S. Bentvelsen[120], L. Beresford[134], M. Beretta[51], D. Berge[19], E. Bergeaas Kuutmann[171], N. Berger[5],

B. Bergmann[141], L.J. Bergsten[26], J. Beringer[18], S. Berlendis[7], G. Bernardi[135], C. Bernius[152], F.U. Bernlochner[24], T. Berry[94], P. Berta[100], C. Bertella[15a], A. Berthold[48], I.A. Bertram[90], O. Bessidskaia Bylund[181], N. Besson[144], A. Bethani[101], S. Bethke[115], A. Betti[42], A.J. Bevan[93], J. Beyer[115], D.S. Bhattacharya[176], P. Bhattarai[26], V.S. Bhopatkar[6], R. Bi[138], R.M. Bianchi[138], O. Biebel[114], D. Biedermann[19], R. Bielski[36], K. Bierwagen[100], N.V. Biesuz[72a,72b], M. Biglietti[75a], T.R.V. Billoud[110], M. Bindi[53], A. Bingul[12d], C. Bini[73a,73b], S. Biondi[23b,23a], C.J. Birch-sykes[101], M. Birman[179], T. Bisanz[36], J.P. Biswal[3], D. Biswas[180,i], A. Bitadze[101], C. Bittrich[48], K. Bjørke[133], T. Blazek[28a], I. Bloch[46], C. Blocker[26], A. Blue[57], U. Blumenschein[93], G.J. Bobbink[120], V.S. Bobrovnikov[122b,122a], S.S. Bocchetta[97], D. Bogavac[14], A.G. Bogdanchikov[122b,122a], C. Bohm[45a], V. Boisvert[94], P. Bokan[53], T. Bold[84a], A.E. Bolz[61b], M. Bomben[135], M. Bona[93], J.S. Bonilla[131], M. Boonekamp[144], C.D. Booth[94], A.G. Borbély[57], H.M. Borecka-Bielska[91], L.S. Borgna[95], A. Borisov[123], G. Borissov[90], D. Bortoletto[134], D. Boscherini[23b], M. Bosman[14], J.D. Bossio Sola[104], K. Bouaouda[35a], J. Boudreau[138], E.V. Bouhova-Thacker[90], D. Boumediene[38], S.K. Boutle[57], A. Boveia[127], J. Boyd[36], D. Boye[33c], I.R. Boyko[80], A.J. Bozson[94], J. Bracinik[21], N. Brahimi[60d], G. Brandt[181], O. Brandt[32], F. Braren[46], B. Brau[103], J.E. Brau[131], W.D. Breaden Madden[57], K. Brendlinger[46], R. Brener[159], L. Brenner[36], R. Brenner[171], S. Bressler[179], B. Brickwedde[100], D.L. Briglin[21], D. Britton[57], D. Britzger[115], I. Brock[24], R. Brock[107], G. Brooijmans[39], W.K. Brooks[146d], E. Brost[29], P.A. Bruckman de Renstrom[85], B. Brüers[46], D. Bruncko[28b], A. Bruni[23b], G. Bruni[23b], L.S. Bruni[120], S. Bruno[74a,74b], M. Bruschi[23b], N. Bruscino[73a,73b], L. Bryngemark[152], T. Buanes[17], Q. Buat[154], P. Buchholz[150], A.G. Buckley[57], I.A. Budagov[80], M.K. Bugge[133], F. Bührer[52], O. Bulekov[112], B.A. Bullard[59], T.J. Burch[121], S. Burdin[91], C.D. Burgard[120], A.M. Burger[129], B. Burghgrave[8], J.T.P. Burr[46], C.D. Burton[11], J.C. Burzynski[103], V. Büscher[100], E. Buschmann[53], P.J. Bussey[57], J.M. Butler[25], C.M. Buttar[57], J.M. Butterworth[95], P. Butti[36], W. Buttinger[36], C.J. Buxo Vazquez[107], A. Buzatu[157], A.R. Buzykaev[122b,122a], G. Cabras[23b,23a], S. Cabrera Urbán[173], D. Caforio[56], H. Cai[138], V.M.M. Cairo[152], O. Cakir[4a], N. Calace[36], P. Calafiura[18], G. Calderini[135], P. Calfayan[66], G. Callea[57], L.P. Caloba[81b], A. Caltabiano[74a,74b], S. Calvente Lopez[99], D. Calvet[38], S. Calvet[38], T.P. Calvet[102], M. Calvetti[72a,72b], R. Camacho Toro[135], S. Camarda[36], D. Camarero Munoz[99], P. Camarri[74a,74b], M.T. Camerlingo[75a,75b], D. Cameron[133], C. Camincher[36], S. Campana[36], M. Campanelli[95], A. Camplani[40], V. Canale[70a,70b], A. Canesse[104], M. Cano Bret[78], J. Cantero[129], T. Cao[160], Y. Cao[172], M.D.M. Capeans Garrido[36], M. Capua[41b,41a], R. Cardarelli[74a], F. Cardillo[148], G. Carducci[41b,41a], I. Carli[142], T. Carli[36], G. Carlino[70a], B.T. Carlson[138], E.M. Carlson[175,167a], L. Carminati[69a,69b], R.M.D. Carney[152], S. Caron[119], E. Carquin[146d], S. Carrá[46], G. Carratta[23b,23a], J.W.S. Carter[166], T.M. Carter[50], M.P. Casado[14,f], A.F. Casha[166], F.L. Castillo[173], L. Castillo Garcia[14], V. Castillo Gimenez[173], N.F. Castro[139a,139e], A. Catinaccio[36], J.R. Catmore[133], A. Cattai[36], V. Cavaliere[29], V. Cavasinni[72a,72b], E. Celebi[12b], F. Celli[134], K. Cerny[130], A.S. Cerqueira[81a], A. Cerri[155], L. Cerrito[74a,74b], F. Cerutti[18], A. Cervelli[23b,23a], S.A. Cetin[12b], Z. Chadi[35a], D. Chakraborty[121], J. Chan[180], W.S. Chan[120], W.Y. Chan[91], J.D. Chapman[32], B. Chargeishvili[158b], D.G. Charlton[21], T.P. Charman[93], C.C. Chau[34], S. Che[127], S. Chekanov[6], S.V. Chekulaev[167a], G.A. Chelkov[80,ag], B. Chen[79], C. Chen[60a], C.H. Chen[79], H. Chen[29], J. Chen[60a], J. Chen[39], J. Chen[26], S. Chen[136], S.J. Chen[15c], X. Chen[15b], Y. Chen[60a], Y.-H. Chen[46], H.C. Cheng[63a], H.J. Cheng[15a], A. Cheplakov[80], E. Cheremushkina[123], R. Cherkaoui El Moursli[35e], E. Cheu[7], K. Cheung[64], T.J.A. Chevalérias[144], L. Chevalier[144], V. Chiarella[51], G. Chiarelli[72a], G. Chiodini[68a], A.S. Chisholm[21], A. Chitan[27b], I. Chiu[162], Y.H. Chiu[175], M.V. Chizhov[80], K. Choi[11], A.R. Chomont[73a,73b], Y.S. Chow[120], L.D. Christopher[33e], M.C. Chu[63a], X. Chu[15a,15d], J. Chudoba[140], J.J. Chwastowski[85], L. Chytka[130], D. Cieri[115], K.M. Ciesla[85], D. Cinca[47], V. Cindro[92], I.A. Cioară[27b], A. Ciocio[18], F. Cirotto[70a,70b], Z.H. Citron[179,j], M. Citterio[69a], D.A. Ciubotaru[27b], B.M. Ciungu[166], A. Clark[54], M.R. Clark[39], P.J. Clark[50], S.E. Clawson[101], C. Clement[45a,45b], Y. Coadou[102], M. Cobal[67a,67c], A. Coccaro[55b], J. Cochran[79], R. Coelho Lopes De Sa[103], H. Cohen[160], A.E.C. Coimbra[36], B. Cole[39], A.P. Colijn[120], J. Collot[58], P. Conde Muiño[139a,139h], S.H. Connell[33c], I.A. Connelly[57], S. Constantinescu[27b], F. Conventi[70a,am], A.M. Cooper-Sarkar[134], F. Cormier[174], K.J.R. Cormier[166], L.D. Corpe[95], M. Corradi[73a,73b], E.E. Corrigan[97], F. Corriveau[104,ab], M.J. Costa[173], F. Costanza[5], D. Costanzo[148], G. Cowan[94], J.W. Cowley[32], J. Crane[101], K. Cranmer[125], R.A. Creager[136], S. Crépé-Renaudin[58], F. Crescioli[135], M. Cristinziani[24], V. Croft[169], G. Crosetti[41b,41a], A. Cueto[5], T. Cuhadar Donszelmann[170], H. Cui[15a,15d], A.R. Cukierman[152], W.R. Cunningham[57], S. Czekierda[85], P. Czodrowski[36], M.M. Czurylo[61b], M.J. Da Cunha Sargedas De Sousa[60b], J.V. Da Fonseca Pinto[81b], C. Da Via[101], W. Dabrowski[84a], F. Dachs[36], T. Dado[47], S. Dahbi[33e], T. Dai[106], C. Dallapiccola[103], M. Dam[40], G. D'amen[29], V. D'Amico[75a,75b],

J. Damp[100], J.R. Dandoy[136], M.F. Daneri[30], M. Danninger[151], V. Dao[36], G. Darbo[55b], O. Dartsi[5], A. Dattagupta[131], T. Daubney[46], S. D'Auria[69a,69b], C. David[167b], T. Davidek[142], D.R. Davis[49], I. Dawson[148], K. De[8], R. De Asmundis[70a], M. De Beurs[120], S. De Castro[23b,23a], N. De Groot[119], P. de Jong[120], H. De la Torre[107], A. De Maria[15c], D. De Pedis[73a], A. De Salvo[73a], U. De Sanctis[74a,74b], M. De Santis[74a,74b], A. De Santo[155], J.B. De Vivie De Regie[65], C. Debenedetti[145], D.V. Dedovich[80], A.M. Deiana[42], J. Del Peso[99], Y. Delabat Diaz[46], D. Delgove[65], F. Deliot[144], C.M. Delitzsch[7], M. Della Pietra[70a,70b], D. Della Volpe[54], A. Dell'Acqua[36], L. Dell'Asta[74a,74b], M. Delmastro[5], C. Delporte[65], P.A. Delsart[58], D.A. DeMarco[166], S. Demers[182], M. Demichev[80], G. Demontigny[110], S.P. Denisov[123], L. D'Eramo[121], D. Derendarz[85], J.E. Derkaoui[35d], F. Derue[135], P. Dervan[91], K. Desch[24], K. Dette[166], C. Deutsch[24], M.R. Devesa[30], P.O. Deviveiros[36], F.A. Di Bello[73a,73b], A. Di Ciaccio[74a,74b], L. Di Ciaccio[5], W.K. Di Clemente[136], C. Di Donato[70a,70b], A. Di Girolamo[36], G. Di Gregorio[72a,72b], B. Di Micco[75a,75b], R. Di Nardo[75a,75b], K.F. Di Petrillo[59], R. Di Sipio[166], C. Diaconu[102], F.A. Dias[120], T. Dias Do Vale[139a], M.A. Diaz[146a], F.G. Diaz Capriles[24], J. Dickinson[18], M. Didenko[165], E.B. Diehl[106], J. Dietrich[19], S. Díez Cornell[46], C. Diez Pardos[150], A. Dimitrievska[18], W. Ding[15b], J. Dingfelder[24], S.J. Dittmeier[61b], F. Dittus[36], F. Djama[102], T. Djobava[158b], J.I. Djuvsland[17], M.A.B. Do Vale[81c], M. Dobre[27b], D. Dodsworth[26], C. Doglioni[97], J. Dolejsi[142], Z. Dolezal[142], M. Donadelli[81d], B. Dong[60c], J. Donini[38], A. D'onofrio[15c], M. D'Onofrio[91], J. Dopke[143], A. Doria[70a], M.T. Dova[89], A.T. Doyle[57], E. Drechsler[151], E. Dreyer[151], T. Dreyer[53], A.S. Drobac[169], D. Du[60b], T.A. du Pree[120], Y. Duan[60d], F. Dubinin[111], M. Dubovsky[28a], A. Dubreuil[54], E. Duchovni[179], G. Duckeck[114], O.A. Ducu[36], D. Duda[115], A. Dudarev[36], A.C. Dudder[100], E.M. Duffield[18], M. D'uffizi[101], L. Duflot[65], M. Dührssen[36], C. Dülsen[181], M. Dumancic[179], A.E. Dumitriu[27b], M. Dunford[61a], A. Duperrin[102], H. Duran Yildiz[4a], M. Düren[56], A. Durglishvili[158b], D. Duschinger[48], B. Dutta[46], D. Duvnjak[1], G.I. Dyckes[136], M. Dyndal[36], S. Dysch[101], B.S. Dziedzic[85], M.G. Eggleston[49], T. Eifert[8], G. Eigen[17], K. Einsweiler[18], T. Ekelof[171], H. El Jarrari[35e], V. Ellajosyula[171], M. Ellert[171], F. Ellinghaus[181], A.A. Elliot[93], N. Ellis[36], J. Elmsheuser[29], M. Elsing[36], D. Emeliyanov[143], A. Emerman[39], Y. Enari[162], M.B. Epland[49], J. Erdmann[47], A. Ereditato[20], P.A. Erland[85], M. Errenst[181], M. Escalier[65], C. Escobar[173], O. Estrada Pastor[173], E. Etzion[160], H. Evans[66], M.O. Evans[155], A. Ezhilov[137], F. Fabbri[57], L. Fabbri[23b,23a], V. Fabiani[119], G. Facini[177], R.M. Fakhrutdinov[123], S. Falciano[73a], P.J. Falke[24], S. Falke[36], J. Faltova[142], Y. Fang[15a], Y. Fang[15a], G. Fanourakis[44], M. Fanti[69a,69b], M. Faraj[67a,67c,q], A. Farbin[8], A. Farilla[75a], E.M. Farina[71a,71b], T. Farooque[107], S.M. Farrington[50], P. Farthouat[36], F. Fassi[35e], P. Fassnacht[36], D. Fassouliotis[9], M. Faucci Giannelli[50], W.J. Fawcett[32], L. Fayard[65], O.L. Fedin[137,o], W. Fedorko[174], A. Fehr[20], M. Feickert[172], L. Feligioni[102], A. Fell[148], C. Feng[60b], M. Feng[49], M.J. Fenton[170], A.B. Fenyuk[123], S.W. Ferguson[43], J. Ferrando[46], A. Ferrante[172], A. Ferrari[171], P. Ferrari[120], R. Ferrari[71a], D.E. Ferreira de Lima[61b], A. Ferrer[173], D. Ferrere[54], C. Ferretti[106], F. Fiedler[100], A. Filipčič[92], F. Filthaut[119], K.D. Finelli[25], M.C.N. Fiolhais[139a,139c,a], L. Fiorini[173], F. Fischer[114], J. Fischer[100], W.C. Fisher[107], T. Fitschen[21], I. Fleck[150], P. Fleischmann[106], T. Flick[181], B.M. Flierl[114], L. Flores[136], L.R. Flores Castillo[63a], F.M. Follega[76a,76b], N. Fomin[17], J.H. Foo[166], G.T. Forcolin[76a,76b], B.C. Forland[66], A. Formica[144], F.A. Förster[14], A.C. Forti[101], E. Fortin[102], M.G. Foti[134], D. Fournier[65], H. Fox[90], P. Francavilla[72a,72b], S. Francescato[73a,73b], M. Franchini[23b,23a], S. Franchino[61a], D. Francis[36], L. Franco[5], L. Franconi[20], M. Franklin[59], G. Frattari[73a,73b], A.N. Fray[93], P.M. Freeman[21], B. Freund[110], W.S. Freund[81b], E.M. Freundlich[47], D.C. Frizzell[128], D. Froidevaux[36], J.A. Frost[134], M. Fujimoto[126], C. Fukunaga[163], E. Fullana Torregrosa[173], T. Fusayasu[116], J. Fuster[173], A. Gabrielli[23b,23a], A. Gabrielli[36], S. Gadatsch[54], P. Gadow[115], G. Gagliardi[55b,55a], L.G. Gagnon[110], G.E. Gallardo[134], E.J. Gallas[134], B.J. Gallop[143], R. Gamboa Goni[93], K.K. Gan[127], S. Ganguly[179], J. Gao[60a], Y. Gao[50], Y.S. Gao[31,l], F.M. Garay Walls[146a], C. García[173], J.E. García Navarro[173], J.A. García Pascual[15a], C. Garcia-Argos[52], M. Garcia-Sciveres[18], R.W. Gardner[37], N. Garelli[152], S. Gargiulo[52], C.A. Garner[166], V. Garonne[133], S.J. Gasiorowski[147], P. Gaspar[81b], A. Gaudiello[55b,55a], G. Gaudio[71a], I.L. Gavrilenko[111], A. Gavrilyuk[124], C. Gay[174], G. Gaycken[46], E.N. Gazis[10], A.A. Geanta[27b], C.M. Gee[145], C.N.P. Gee[143], J. Geisen[97], M. Geisen[100], C. Gemme[55b], M.H. Genest[58], C. Geng[106], S. Gentile[73a,73b], S. George[94], T. Geralis[44], L.O. Gerlach[53], P. Gessinger-Befurt[100], G. Gessner[47], S. Ghasemi[150], M. Ghasemi Bostanabad[175], M. Ghneimat[150], A. Ghosh[65], A. Ghosh[78], B. Giacobbe[23b], S. Giagu[73a,73b], N. Giangiacomi[23b,23a], P. Giannetti[72a], A. Giannini[70a,70b], G. Giannini[14], S.M. Gibson[94], M. Gignac[145], D.T. Gil[84b], B.J. Gilbert[39], D. Gillberg[34], G. Gilles[181], D.M. Gingrich[3,al], M.P. Giordani[67a,67c], P.F. Giraud[144], G. Giugliarelli[67a,67c], D. Giugni[69a], F. Giuli[74a,74b], S. Gkaitatzis[161], I. Gkialas[9,g], E.L. Gkougkousis[14], P. Gkountoumis[10],

L.K. Gladilin[113], C. Glasman[99], J. Glatzer[14], P.C.F. Glaysher[46], A. Glazov[46], G.R. Gledhill[131], I. Gnesi[41b,b], M. Goblirsch-Kolb[26], D. Godin[110], S. Goldfarb[105], T. Golling[54], D. Golubkov[123], A. Gomes[139a,139b], R. Goncalves Gama[53], R. Gonçalo[139a,139c], G. Gonella[131], L. Gonella[21], A. Gongadze[80], F. Gonnella[21], J.L. Gonski[39], S. González de la Hoz[173], S. Gonzalez Fernandez[14], R. Gonzalez Lopez[91], C. Gonzalez Renteria[18], R. Gonzalez Suarez[171], S. Gonzalez-Sevilla[54], G.R. Gonzalvo Rodriguez[173], L. Goossens[36], N.A. Gorasia[21], P.A. Gorbounov[124], H.A. Gordon[29], B. Gorini[36], E. Gorini[68a,68b], A. Gorišek[92], A.T. Goshaw[49], M.I. Gostkin[80], C.A. Gottardo[119], M. Gouighri[35b], A.G. Goussiou[147], N. Govender[33c], C. Goy[5], I. Grabowska-Bold[84a], E.C. Graham[91], J. Gramling[170], E. Gramstad[133], S. Grancagnolo[19], M. Grandi[155], V. Gratchev[137], P.M. Gravila[27f], F.G. Gravili[68a,68b], C. Gray[57], H.M. Gray[18], C. Grefe[24], K. Gregersen[97], I.M. Gregor[46], P. Grenier[152], K. Grevtsov[46], C. Grieco[14], N.A. Grieser[128], A.A. Grillo[145], K. Grimm[31,k], S. Grinstein[14,w], J.-F. Grivaz[65], S. Groh[100], E. Gross[179], J. Grosse-Knetter[53], Z.J. Grout[95], C. Grud[106], A. Grummer[118], J.C. Grundy[134], L. Guan[106], W. Guan[180], C. Gubbels[174], J. Guenther[36], A. Guerguichon[65], J.G.R. Guerrero Rojas[173], F. Guescini[115], D. Guest[170], R. Gugel[100], A. Guida[46], T. Guillemin[5], S. Guindon[36], U. Gul[57], J. Guo[60c], W. Guo[106], Y. Guo[60a], Z. Guo[102], R. Gupta[46], S. Gurbuz[12c], G. Gustavino[128], M. Guth[52], P. Gutierrez[128], C. Gutschow[95], C. Guyot[144], C. Gwenlan[134], C.B. Gwilliam[91], E.S. Haaland[133], A. Haas[125], C. Haber[18], H.K. Hadavand[8], A. Hadef[60a], M. Haleem[176], J. Haley[129], J.J. Hall[148], G. Halladjian[107], G.D. Hallewell[102], K. Hamano[175], H. Hamdaoui[35e], M. Hamer[24], G.N. Hamity[50], K. Han[60a,v], L. Han[60a], S. Han[18], Y.F. Han[166], K. Hanagaki[82,t], M. Hance[145], D.M. Handl[114], M.D. Hank[37], R. Hankache[135], E. Hansen[97], J.B. Hansen[40], J.D. Hansen[40], M.C. Hansen[24], P.H. Hansen[40], E.C. Hanson[101], K. Hara[168], T. Harenberg[181], S. Harkusha[108], P.F. Harrison[177], N.M. Hartman[152], N.M. Hartmann[114], Y. Hasegawa[149], A. Hasib[50], S. Hassani[144], S. Haug[20], R. Hauser[107], L.B. Havener[39], M. Havranek[141], C.M. Hawkes[21], R.J. Hawkings[36], S. Hayashida[117], D. Hayden[107], C. Hayes[106], R.L. Hayes[174], C.P. Hays[134], J.M. Hays[93], H.S. Hayward[91], S.J. Haywood[143], F. He[60a], Y. He[164], M.P. Heath[50], V. Hedberg[97], S. Heer[24], A.L. Heggelund[133], C. Heidegger[52], K.K. Heidegger[52], W.D. Heidorn[79], J. Heilman[34], S. Heim[46], T. Heim[18], B. Heinemann[46,aj], J.G. Heinlein[136], J.J. Heinrich[131], L. Heinrich[36], J. Hejbal[140], L. Helary[46], A. Held[125], S. Hellesund[133], C.M. Helling[145], S. Hellman[45a,45b], C. Helsens[36], R.C.W. Henderson[90], Y. Heng[180], L. Henkelmann[32], A.M. Henriques Correia[36], H. Herde[26], Y. Hernández Jiménez[33e], H. Herr[100], M.G. Herrmann[114], T. Herrmann[48], G. Herten[52], R. Hertenberger[114], L. Hervas[36], T.C. Herwig[136], G.G. Hesketh[95], N.P. Hessey[167a], H. Hibi[83], A. Higashida[162], S. Higashino[82], E. Higón-Rodriguez[173], K. Hildebrand[37], J.C. Hill[32], K.K. Hill[29], K.H. Hiller[46], S.J. Hillier[21], M. Hils[48], I. Hinchliffe[18], F. Hinterkeuser[24], M. Hirose[132], S. Hirose[52], D. Hirschbuehl[181], B. Hiti[92], O. Hladik[140], D.R. Hlaluku[33e], J. Hobbs[154], N. Hod[179], M.C. Hodgkinson[148], A. Hoecker[36], D. Hohn[52], D. Hohov[65], T. Holm[24], T.R. Holmes[37], M. Holzbock[114], L.B.A.H. Hommels[32], T.M. Hong[138], J.C. Honig[52], A. Hönle[115], B.H. Hooberman[172], W.H. Hopkins[6], Y. Horii[117], P. Horn[48], L.A. Horyn[37], S. Hou[157], A. Hoummada[35a], J. Howarth[57], J. Hoya[89], M. Hrabovsky[130], J. Hrdinka[77], J. Hrivnac[65], A. Hrynevich[109], T. Hryn'ova[5], P.J. Hsu[64], S.-C. Hsu[147], Q. Hu[29], S. Hu[60c], Y.F. Hu[15a,15d,an], D.P. Huang[95], Y. Huang[60a], Y. Huang[15a], Z. Hubacek[141], F. Hubaut[102], M. Huebner[24], F. Huegging[24], T.B. Huffman[134], M. Huhtinen[36], R. Hulsken[58], R.F.H. Hunter[34], P. Huo[154], N. Huseynov[80,ac], J. Huston[107], J. Huth[59], R. Hyneman[152], S. Hyrych[28a], G. Iacobucci[54], G. Iakovidis[29], I. Ibragimov[150], L. Iconomidou-Fayard[65], P. Iengo[36], R. Ignazzi[40], O. Igonkina[120,y,*], R. Iguchi[162], T. Iizawa[54], Y. Ikegami[82], M. Ikeno[82], N. Ilic[119,166,ab], F. Iltzsche[48], H. Imam[35a], G. Introzzi[71a,71b], M. Iodice[75a], K. Iordanidou[167a], V. Ippolito[73a,73b], M.F. Isacson[171], M. Ishino[162], W. Islam[129], C. Issever[19,46], S. Istin[159], F. Ito[168], J.M. Iturbe Ponce[63a], R. Iuppa[76a,76b], A. Ivina[179], H. Iwasaki[82], J.M. Izen[43], V. Izzo[70a], P. Jacka[140], P. Jackson[1], R.M. Jacobs[46], B.P. Jaeger[151], V. Jain[2], G. Jäkel[181], K.B. Jakobi[100], K. Jakobs[52], T. Jakoubek[179], J. Jamieson[57], K.W. Janas[84a], R. Jansky[54], M. Janus[53], P.A. Janus[84a], G. Jarlskog[97], A.E. Jaspan[91], N. Javadov[80,ac], T. Javůrek[36], M. Javurkova[103], F. Jeanneau[144], L. Jeanty[131], J. Jejelava[158a], P. Jenni[52,c], N. Jeong[46], S. Jézéquel[5], H. Ji[180], J. Jia[154], H. Jiang[79], Y. Jiang[60a], Z. Jiang[152], S. Jiggins[52], F.A. Jimenez Morales[38], J. Jimenez Pena[115], S. Jin[15c], A. Jinaru[27b], O. Jinnouchi[164], H. Jivan[33e], P. Johansson[148], K.A. Johns[7], C.A. Johnson[66], R.W.L. Jones[90], S.D. Jones[155], T.J. Jones[91], J. Jongmanns[61a], J. Jovicevic[36], X. Ju[18], J.J. Junggeburth[115], A. Juste Rozas[14,w], A. Kaczmarska[85], M. Kado[73a,73b], H. Kagan[127], M. Kagan[152], A. Kahn[39], C. Kahra[100], T. Kaji[178], E. Kajomovitz[159], C.W. Kalderon[29], A. Kaluza[100], A. Kamenshchikov[123], M. Kaneda[162], N.J. Kang[145], S. Kang[79], Y. Kano[117], J. Kanzaki[82], L.S. Kaplan[180], D. Kar[33e], K. Karava[134], M.J. Kareem[167b], I. Karkanias[161], S.N. Karpov[80], Z.M. Karpova[80], V. Kartvelishvili[90], A.N. Karyukhin[123],

E. Kasimi[161], A. Kastanas[45a,45b], C. Kato[60d,60c], J. Katzy[46], K. Kawade[149], K. Kawagoe[88], T. Kawaguchi[117], T. Kawamoto[144], G. Kawamura[53], E.F. Kay[175], S. Kazakos[14], V.F. Kazanin[122b,122a], R. Keeler[175], R. Kehoe[42], J.S. Keller[34], E. Kellermann[97], D. Kelsey[155], J.J. Kempster[21], J. Kendrick[21], K.E. Kennedy[39], O. Kepka[140], S. Kersten[181], B.P. Kerševan[92], S. Ketabchi Haghighat[166], M. Khader[172], F. Khalil-Zada[13], M. Khandoga[144], A. Khanov[129], A.G. Kharlamov[122b,122a], T. Kharlamova[122b,122a], E.E. Khoda[174], A. Khodinov[165], T.J. Khoo[54], G. Khoriauli[176], E. Khramov[80], J. Khubua[158b], S. Kido[83], M. Kiehn[36], C.R. Kilby[94], E. Kim[164], Y.K. Kim[37], N. Kimura[95], A. Kirchhoff[53], D. Kirchmeier[48], J. Kirk[143], A.E. Kiryunin[115], T. Kishimoto[162], D.P. Kisliuk[166], V. Kitali[46], C. Kitsaki[10], O. Kivernyk[24], T. Klapdor-Kleingrothaus[52], M. Klassen[61a], C. Klein[34], M.H. Klein[106], M. Klein[91], U. Klein[91], K. Kleinknecht[100], P. Klimek[121], A. Klimentov[29], T. Klingl[24], T. Klioutchnikova[36], F.F. Klitzner[114], P. Kluit[120], S. Kluth[115], E. Kneringer[77], E.B.F.G. Knoops[102], A. Knue[52], D. Kobayashi[88], M. Kobel[48], M. Kocian[152], T. Kodama[162], P. Kodys[142], D.M. Koeck[155], P.T. Koenig[24], T. Koffas[34], N.M. Köhler[36], M. Kolb[144], I. Koletsou[5], T. Komarek[130], T. Kondo[82], K. Köneke[52], A.X.Y. Kong[1], A.C. König[119], T. Kono[126], V. Konstantinides[95], N. Konstantinidis[95], B. Konya[97], R. Kopeliansky[66], S. Koperny[84a], K. Korcyl[85], K. Kordas[161], G. Koren[160], A. Korn[95], I. Korolkov[14], E.V. Korolkova[148], N. Korotkova[113], O. Kortner[115], S. Kortner[115], V.V. Kostyukhin[148,165], A. Kotsokechagia[65], A. Kotwal[49], A. Koulouris[10], A. Kourkoumeli-Charalampidi[71a,71b], C. Kourkoumelis[9], E. Kourlitis[6], V. Kouskoura[29], R. Kowalewski[175], W. Kozanecki[101], A.S. Kozhin[123], V.A. Kramarenko[113], G. Kramberger[92], D. Krasnopevtsev[60a], M.W. Krasny[135], A. Krasznahorkay[36], D. Krauss[115], J.A. Kremer[100], J. Kretzschmar[91], P. Krieger[166], F. Krieter[114], A. Krishnan[61b], M. Krivos[142], K. Krizka[18], K. Kroeninger[47], H. Kroha[115], J. Kroll[140], J. Kroll[136], K.S. Krowpman[107], U. Kruchonak[80], H. Krüger[24], N. Krumnack[79], M.C. Kruse[49], J.A. Krzysiak[85], A. Kubota[164], O. Kuchinskaia[165], S. Kuday[4b], D. Kuechler[46], J.T. Kuechler[46], S. Kuehn[36], T. Kuhl[46], V. Kukhtin[80], Y. Kulchitsky[108,ae], S. Kuleshov[146b], Y.P. Kulinich[172], M. Kuna[58], T. Kunigo[86], A. Kupco[140], T. Kupfer[47], O. Kuprash[52], H. Kurashige[83], L.L. Kurchaninov[167a], Y.A. Kurochkin[108], A. Kurova[112], M.G. Kurth[15a,15d], E.S. Kuwertz[36], M. Kuze[164], A.K. Kvam[147], J. Kvita[130], T. Kwan[104], F. La Ruffa[41b,41a], C. Lacasta[173], F. Lacava[73a,73b], D.P.J. Lack[101], H. Lacker[19], D. Lacour[135], E. Ladygin[80], R. Lafaye[5], B. Laforge[135], T. Lagouri[146c], S. Lai[53], I.K. Lakomiec[84a], J.E. Lambert[128], S. Lammers[66], W. Lampl[7], C. Lampoudis[161], E. Lançon[29], U. Landgraf[52], M.P.J. Landon[93], M.C. Lanfermann[54], V.S. Lang[52], J.C. Lange[53], R.J. Langenberg[103], A.J. Lankford[170], F. Lanni[29], K. Lantzsch[24], A. Lanza[71a], A. Lapertosa[55b,55a], J.F. Laporte[144], T. Lari[69a], F. Lasagni Manghi[23b,23a], M. Lassnig[36], T.S. Lau[63a], A. Laudrain[65], A. Laurier[34], M. Lavorgna[70a,70b], S.D. Lawlor[94], M. Lazzaroni[69a,69b], B. Le[101], E. Le Guirriec[102], A. Lebedev[79], M. LeBlanc[7], T. LeCompte[6], F. Ledroit-Guillon[58], A.C.A. Lee[95], C.A. Lee[29], G.R. Lee[17], L. Lee[59], S.C. Lee[157], S. Lee[79], B. Lefebvre[167a], H.P. Lefebvre[94], M. Lefebvre[175], C. Leggett[18], K. Lehmann[151], N. Lehmann[20], G. Lehmann Miotto[36], W.A. Leight[46], A. Leisos[161,u], M.A.L. Leite[81d], C.E. Leitgeb[114], R. Leitner[142], D. Lellouch[179,*], K.J.C. Leney[42], T. Lenz[24], S. Leone[72a], C. Leonidopoulos[50], A. Leopold[135], C. Leroy[110], R. Les[107], C.G. Lester[32], M. Levchenko[137], J. Levêque[5], D. Levin[106], L.J. Levinson[179], D.J. Lewis[21], B. Li[15b], B. Li[106], C.-Q. Li[60a], F. Li[60c], H. Li[60a], H. Li[60b], J. Li[60c], K. Li[147], L. Li[60c], M. Li[15a,15d], Q. Li[15a,15d], Q.Y. Li[60a], S. Li[60d,60c], X. Li[46], Y. Li[46], Z. Li[60b], Z. Li[134], Z. Li[104], Z. Liang[15a], M. Liberatore[46], B. Liberti[74a], A. Liblong[166], K. Lie[63c], S. Lim[29], C.Y. Lin[32], K. Lin[107], R.A. Linck[66], R.E. Lindley[7], J.H. Lindon[21], A. Linss[46], A.L. Lionti[54], E. Lipeles[136], A. Lipniacka[17], T.M. Liss[172,ak], A. Lister[174], J.D. Little[8], B. Liu[79], B.X. Liu[6], H.B. Liu[29], J.B. Liu[60a], J.K.K. Liu[37], K. Liu[60d], M. Liu[60a], P. Liu[15a], X. Liu[60a], Y. Liu[46], Y. Liu[15a,15d], Y.L. Liu[106], Y.W. Liu[60a], M. Livan[71a,71b], A. Lleres[58], J. Llorente Merino[151], S.L. Lloyd[93], C.Y. Lo[63b], E.M. Lobodzinska[46], P. Loch[7], S. Loffredo[74a,74b], T. Lohse[19], K. Lohwasser[148], M. Lokajicek[140], J.D. Long[172], R.E. Long[90], I. Longarini[73a,73b], L. Longo[36], K.A. Looper[127], I. Lopez Paz[101], A. Lopez Solis[148], J. Lorenz[114], N. Lorenzo Martinez[5], A.M. Lory[114], P.J. Lösel[114], A. Lösle[52], X. Lou[46], X. Lou[15a], A. Lounis[65], J. Love[6], P.A. Love[90], J.J. Lozano Bahilo[173], M. Lu[60a], Y.J. Lu[64], H.J. Lubatti[147], C. Luci[73a,73b], F.L. Lucio Alves[15c], A. Lucotte[58], F. Luehring[66], I. Luise[135], L. Luminari[73a], B. Lund-Jensen[153], M.S. Lutz[160], D. Lynn[29], H. Lyons[91], R. Lysak[140], E. Lytken[97], F. Lyu[15a], V. Lyubushkin[80], T. Lyubushkina[80], H. Ma[29], L.L. Ma[60b], Y. Ma[95], D.M. Mac Donell[175], G. Maccarrone[51], A. Macchiolo[115], C.M. Macdonald[148], J.C. MacDonald[148], J. Machado Miguens[136], D. Madaffari[173], R. Madar[38], W.F. Mader[48], M. Madugoda Ralalage Don[129], N. Madysa[48], J. Maeda[83], T. Maeno[29], M. Maerker[48], V. Magerl[52], N. Magini[79], J. Magro[67a,67c,q], D.J. Mahon[39], C. Maidantchik[81b], T. Maier[114], A. Maio[139a,139b,139d], K. Maj[84a], O. Majersky[28a], S. Majewski[131], Y. Makida[82], N. Makovec[65], B. Malaescu[135], Pa. Malecki[85], V.P. Maleev[137], F. Malek[58],

D. Malito[41b,41a], U. Mallik[78], D. Malon[6], C. Malone[32], S. Maltezos[10], S. Malyukov[80], J. Mamuzic[173], G. Mancini[70a,70b], I. Mandić[92], L. Manhaes de Andrade Filho[81a], I.M. Maniatis[161], J. Manjarres Ramos[48], K.H. Mankinen[97], A. Mann[114], A. Manousos[77], B. Mansoulie[144], I. Manthos[161], S. Manzoni[120], A. Marantis[161], G. Marceca[30], L. Marchese[134], G. Marchiori[135], M. Marcisovsky[140], L. Marcoccia[74a,74b], C. Marcon[97], C.A. Marin Tobon[36], M. Marjanovic[128], Z. Marshall[18], M.U.F. Martensson[171], S. Marti-Garcia[173], C.B. Martin[127], T.A. Martin[177], V.J. Martin[50], B. Martin dit Latour[17], L. Martinelli[75a,75b], M. Martinez[14,w], P. Martinez Agullo[173], V.I. Martinez Outschoorn[103], S. Martin-Haugh[143], V.S. Martoiu[27b], A.C. Martyniuk[95], A. Marzin[36], S.R. Maschek[115], L. Masetti[100], T. Mashimo[162], R. Mashinistov[111], J. Masik[101], A.L. Maslennikov[122b,122a], L. Massa[23b,23a], P. Massarotti[70a,70b], P. Mastrandrea[72a,72b], A. Mastroberardino[41b,41a], T. Masubuchi[162], D. Matakias[29], A. Matic[114], N. Matsuzawa[162], P. Mättig[24], J. Maurer[27b], B. Maček[92], D.A. Maximov[122b,122a], R. Mazini[157], I. Maznas[161], S.M. Mazza[145], J.P. Mc Gowan[104], S.P. Mc Kee[106], T.G. McCarthy[115], W.P. McCormack[18], E.F. McDonald[105], J.A. Mcfayden[36], G. Mchedlidze[158b], M.A. McKay[42], K.D. McLean[175], S.J. McMahon[143], P.C. McNamara[105], C.J. McNicol[177], R.A. McPherson[175,ab], J.E. Mdhluli[33e], Z.A. Meadows[103], S. Meehan[36], T. Megy[38], S. Mehlhase[114], A. Mehta[91], B. Meirose[43], D. Melini[159], B.R. Mellado Garcia[33e], J.D. Mellenthin[53], M. Melo[28a], F. Meloni[46], A. Melzer[24], E.D. Mendes Gouveia[139a,139e], L. Meng[36], X.T. Meng[106], S. Menke[115], E. Meoni[41b,41a], S. Mergelmeyer[19], S.A.M. Merkt[138], C. Merlassino[134], P. Mermod[54], L. Merola[70a,70b], C. Meroni[69a], G. Merz[106], O. Meshkov[113,111], J.K.R. Meshreki[150], J. Metcalfe[6], A.S. Mete[6], C. Meyer[66], J.-P. Meyer[144], M. Michetti[19], R.P. Middleton[143], L. Mijović[50], G. Mikenberg[179], M. Mikestikova[140], M. Mikuž[92], H. Mildner[148], A. Milic[166], C.D. Milke[42], D.W. Miller[37], A. Milov[179], D.A. Milstead[45a,45b], R.A. Mina[152], A.A. Minaenko[123], I.A. Minashvili[158b], A.I. Mincer[125], B. Mindur[84a], M. Mineev[80], Y. Minegishi[162], L.M. Mir[14], M. Mironova[134], A. Mirto[68a,68b], K.P. Mistry[136], T. Mitani[178], J. Mitrevski[114], V.A. Mitsou[173], M. Mittal[60c], O. Miu[166], A. Miucci[20], P.S. Miyagawa[93], A. Mizukami[82], J.U. Mjörnmark[97], T. Mkrtchyan[61a], M. Mlynarikova[142], T. Moa[45a,45b], S. Mobius[53], K. Mochizuki[110], P. Mogg[114], S. Mohapatra[39], R. Moles-Valls[24], K. Mönig[46], E. Monnier[102], A. Montalbano[151], J. Montejo Berlingen[36], M. Montella[95], F. Monticelli[89], S. Monzani[69a], N. Morange[65], A.L. Moreira De Carvalho[139a], D. Moreno[22a], M. Moreno Llácer[173], C. Moreno Martinez[14], P. Morettini[55b], M. Morgenstern[159], S. Morgenstern[48], D. Mori[151], M. Morii[59], M. Morinaga[178], V. Morisbak[133], A.K. Morley[36], G. Mornacchi[36], A.P. Morris[95], L. Morvaj[154], P. Moschovakos[36], B. Moser[120], M. Mosidze[158b], T. Moskalets[144], J. Moss[31,m], E.J.W. Moyse[103], S. Muanza[102], J. Mueller[138], R.S.P. Mueller[114], D. Muenstermann[90], G.A. Mullier[97], D.P. Mungo[69a,69b], J.L. Munoz Martinez[14], F.J. Munoz Sanchez[101], P. Murin[28b], W.J. Murray[177,143], A. Murrone[69a,69b], J.M. Muse[128], M. Muškinja[18], C. Mwewa[33a], A.G. Myagkov[123,ag], A.A. Myers[138], G. Myers[66], J. Myers[131], M. Myska[141], B.P. Nachman[18], O. Nackenhorst[47], A.Nag Nag[48], K. Nagai[134], K. Nagano[82], Y. Nagasaka[62], J.L. Nagle[29], E. Nagy[102], A.M. Nairz[36], Y. Nakahama[117], K. Nakamura[82], T. Nakamura[162], H. Nanjo[132], F. Napolitano[61a], R.F. Naranjo Garcia[46], R. Narayan[42], I. Naryshkin[137], T. Naumann[46], G. Navarro[22a], P.Y. Nechaeva[111], F. Nechansky[46], T.J. Neep[21], A. Negri[71a,71b], M. Negrini[23b], C. Nellist[119], C. Nelson[104], M.E. Nelson[45a,45b], S. Nemecek[140], M. Nessi[36,e], M.S. Neubauer[172], F. Neuhaus[100], M. Neumann[181], R. Newhouse[174], P.R. Newman[21], C.W. Ng[138], Y.S. Ng[19], Y.W.Y. Ng[170], B. Ngair[35e], H.D.N. Nguyen[102], T. Nguyen Manh[110], E. Nibigira[38], R.B. Nickerson[134], R. Nicolaidou[144], D.S. Nielsen[40], J. Nielsen[145], M. Niemeyer[53], N. Nikiforou[11], V. Nikolaenko[123,ag], I. Nikolic-Audit[135], K. Nikolopoulos[21], P. Nilsson[29], H.R. Nindhito[54], Y. Ninomiya[82], A. Nisati[73a], N. Nishu[60c], R. Nisius[115], I. Nitsche[47], T. Nitta[178], T. Nobe[162], D.L. Noel[32], Y. Noguchi[86], I. Nomidis[135], M.A. Nomura[29], M. Nordberg[36], J. Novak[92], T. Novak[92], O. Novgorodova[48], R. Novotny[141], L. Nozka[130], K. Ntekas[170], E. Nurse[95], F.G. Oakham[34,al], H. Oberlack[115], J. Ocariz[135], A. Ochi[83], I. Ochoa[39], J.P. Ochoa-Ricoux[146a], K. O'Connor[26], S. Oda[88], S. Odaka[82], S. Oerdek[53], A. Ogrodnik[84a], A. Oh[101], C.C. Ohm[153], H. Oide[164], M.L. Ojeda[166], H. Okawa[168], Y. Okazaki[86], M.W. O'Keefe[91], Y. Okumura[162], T. Okuyama[82], A. Olariu[27b], L.F. Oleiro Seabra[139a], S.A. Olivares Pino[146a], D. Oliveira Damazio[29], J.L. Oliver[1], M.J.R. Olsson[170], A. Olszewski[85], J. Olszowska[85], Ö.O. Öncel[24], D.C. O'Neil[151], A.P. O'neill[134], A. Onofre[139a,139e], P.U.E. Onyisi[11], H. Oppen[133], R.G. Oreamuno Madriz[121], M.J. Oreglia[37], G.E. Orellana[89], D. Orestano[75a,75b], N. Orlando[14], R.S. Orr[166], V. O'Shea[57], R. Ospanov[60a], G. Otero y Garzon[30], H. Otono[88], P.S. Ott[61a], G.J. Ottino[18], M. Ouchrif[35d], J. Ouellette[29], F. Ould-Saada[133], A. Ouraou[144,*], Q. Ouyang[15a], M. Owen[57], R.E. Owen[143], V.E. Ozcan[12c], N. Ozturk[8], J. Pacalt[130], H.A. Pacey[32], K. Pachal[49], A. Pacheco Pages[14], C. Padilla Aranda[14], S. Pagan Griso[18], G. Palacino[66],

S. Palazzo[50], S. Palestini[36], M. Palka[84b], P. Palni[84a], C.E. Pandini[54], J.G. Panduro Vazquez[94], P. Pani[46], G. Panizzo[67a,67c], L. Paolozzi[54], C. Papadatos[110], K. Papageorgiou[9,g], S. Parajuli[42], A. Paramonov[6], C. Paraskevopoulos[10], D. Paredes Hernandez[63b], S.R. Paredes Saenz[134], B. Parida[179], T.H. Park[166], A.J. Parker[31], M.A. Parker[32], F. Parodi[55b,55a], E.W. Parrish[121], J.A. Parsons[39], U. Parzefall[52], L. Pascual Dominguez[135], V.R. Pascuzzi[18], J.M.P. Pasner[145], F. Pasquali[120], E. Pasqualucci[73a], S. Passaggio[55b], F. Pastore[94], P. Pasuwan[45a,45b], S. Pataraia[100], J.R. Pater[101], A. Pathak[180,i], J. Patton[91], T. Pauly[36], J. Pearkes[152], B. Pearson[115], M. Pedersen[133], L. Pedraza Diaz[119], R. Pedro[139a], T. Peiffer[53], S.V. Peleganchuk[122b,122a], O. Penc[140], H. Peng[60a], B.S. Peralva[81a], M.M. Perego[65], A.P. Pereira Peixoto[139a], L. Pereira Sanchez[45a,45b], D.V. Perepelitsa[29], E. Perez Codina[167a], F. Peri[19], L. Perini[69a,69b], H. Pernegger[36], S. Perrella[36], A. Perrevoort[120], K. Peters[46], R.F.Y. Peters[101], B.A. Petersen[36], T.C. Petersen[40], E. Petit[102], V. Petousis[141], A. Petridis[1], C. Petridou[161], F. Petrucci[75a,75b], M. Pettee[182], N.E. Pettersson[103], K. Petukhova[142], A. Peyaud[144], R. Pezoa[146d], L. Pezzotti[71a,71b], T. Pham[105], F.H. Phillips[107], P.W. Phillips[143], M.W. Phipps[172], G. Piacquadio[154], E. Pianori[18], A. Picazio[103], R.H. Pickles[101], R. Piegaia[30], D. Pietreanu[27b], J.E. Pilcher[37], A.D. Pilkington[101], M. Pinamonti[67a,67c], J.L. Pinfold[3], C. Pitman Donaldson[95], M. Pitt[160], L. Pizzimento[74a,74b], A. Pizzini[120], M.-A. Pleier[29], V. Plesanovs[52], V. Pleskot[142], E. Plotnikova[80], P. Podberezko[122b,122a], R. Poettgen[97], R. Poggi[54], L. Poggioli[135], I. Pogrebnyak[107], D. Pohl[24], I. Pokharel[53], G. Polesello[71a], A. Poley[151,167a], A. Policicchio[73a,73b], R. Polifka[142], A. Polini[23b], C.S. Pollard[46], V. Polychronakos[29], D. Ponomarenko[112], L. Pontecorvo[36], S. Popa[27a], G.A. Popeneciu[27d], L. Portales[5], D.M. Portillo Quintero[58], S. Pospisil[141], K. Potamianos[46], I.N. Potrap[80], C.J. Potter[32], H. Potti[11], T. Poulsen[97], J. Poveda[173], T.D. Powell[148], G. Pownall[46], M.E. Pozo Astigarraga[36], P. Pralavorio[102], S. Prell[79], D. Price[101], M. Primavera[68a], M.L. Proffitt[147], N. Proklova[112], K. Prokofiev[63c], F. Prokoshin[80], S. Protopopescu[29], J. Proudfoot[6], M. Przybycien[84a], D. Pudzha[137], A. Puri[172], P. Puzo[65], D. Pyatiizbyantseva[112], J. Qian[106], Y. Qin[101], A. Quadt[53], M. Queitsch-Maitland[36], M. Racko[28a], F. Ragusa[69a,69b], G. Rahal[98], J.A. Raine[54], S. Rajagopalan[29], A. Ramirez Morales[93], K. Ran[15a,15d], D.M. Rauch[46], F. Rauscher[114], S. Rave[100], B. Ravina[148], I. Ravinovich[179], J.H. Rawling[101], M. Raymond[36], A.L. Read[133], N.P. Readioff[148], M. Reale[68a,68b], D.M. Rebuzzi[71a,71b], G. Redlinger[29], K. Reeves[43], J. Reichert[136], D. Reikher[160], A. Reiss[100], A. Rej[150], C. Rembser[36], A. Renardi[46], M. Renda[27b], M.B. Rendel[115], A.G. Rennie[57], S. Resconi[69a], E.D. Resseguie[18], S. Rettie[95], B. Reynolds[127], E. Reynolds[21], O.L. Rezanova[122b,122a], P. Reznicek[142], E. Ricci[76a,76b], R. Richter[115], S. Richter[46], E. Richter-Was[84b], M. Ridel[135], P. Rieck[115], O. Rifki[46], M. Rijssenbeek[154], A. Rimoldi[71a,71b], M. Rimoldi[46], L. Rinaldi[23b], T.T. Rinn[172], G. Ripellino[153], I. Riu[14], P. Rivadeneira[46], J.C. Rivera Vergara[175], F. Rizatdinova[129], E. Rizvi[93], C. Rizzi[36], S.H. Robertson[104,ab], M. Robin[46], D. Robinson[32], C.M. Robles Gajardo[146d], M. Robles Manzano[100], A. Robson[57], A. Rocchi[74a,74b], E. Rocco[100], C. Roda[72a,72b], S. Rodriguez Bosca[173], A.M. Rodríguez Vera[167b], S. Roe[36], J. Roggel[181], O. Røhne[133], R. Röhrig[115], R.A. Rojas[146d], B. Roland[52], C.P.A. Roland[66], J. Roloff[29], A. Romaniouk[112], M. Romano[23b,23a], N. Rompotis[91], M. Ronzani[125], L. Roos[135], S. Rosati[73a], G. Rosin[103], B.J. Rosser[136], E. Rossi[46], E. Rossi[75a,75b], E. Rossi[70a,70b], L.P. Rossi[55b], L. Rossini[46], R. Rosten[14], M. Rotaru[27b], B. Rottler[52], D. Rousseau[65], G. Rovelli[71a,71b], A. Roy[11], D. Roy[33e], A. Rozanov[102], Y. Rozen[159], X. Ruan[33e], T.A. Ruggeri[1], F. Rühr[52], A. Ruiz-Martinez[173], A. Rummler[36], Z. Rurikova[52], N.A. Rusakovich[80], H.L. Russell[104], L. Rustige[38,47], J.P. Rutherfoord[7], E.M. Rüttinger[148], M. Rybar[142], G. Rybkin[65], E.B. Rye[133], A. Ryzhov[123], J.A. Sabater Iglesias[46], P. Sabatini[53], L. Sabetta[73a,73b], S. Sacerdoti[65], H.F-W. Sadrozinski[145], R. Sadykov[80], F. Safai Tehrani[73a], B. Safarzadeh Samani[155], M. Safdari[152], P. Saha[121], S. Saha[104], M. Sahinsoy[115], A. Sahu[181], M. Saimpert[36], M. Saito[162], T. Saito[162], H. Sakamoto[162], D. Salamani[54], G. Salamanna[75a,75b], A. Salnikov[152], J. Salt[173], A. Salvador Salas[14], D. Salvatore[41b,41a], F. Salvatore[155], A. Salvucci[63a,63b,63c], A. Salzburger[36], J. Samarati[36], D. Sammel[52], D. Sampsonidis[161], D. Sampsonidou[161], J. Sánchez[173], A. Sanchez Pineda[67a,36,67c], H. Sandaker[133], C.O. Sander[46], I.G. Sanderswood[90], M. Sandhoff[181], C. Sandoval[22b], D.P.C. Sankey[143], M. Sannino[55b,55a], Y. Sano[117], A. Sansoni[51], C. Santoni[38], H. Santos[139a,139b], S.N. Santpur[18], A. Santra[173], K.A. Saoucha[148], A. Sapronov[80], J.G. Saraiva[139a,139d], O. Sasaki[82], K. Sato[168], F. Sauerburger[52], E. Sauvan[5], P. Savard[166,al], R. Sawada[162], C. Sawyer[143], L. Sawyer[96,af], I. Sayago Galvan[173], C. Sbarra[23b], A. Sbrizzi[67a,67c], T. Scanlon[95], J. Schaarschmidt[147], P. Schacht[115], D. Schaefer[37], L. Schaefer[136], S. Schaepe[36], U. Schäfer[100], A.C. Schaffer[65], D. Schaile[114], R.D. Schamberger[154], E. Schanet[114], C. Scharf[19], N. Scharmberg[101], V.A. Schegelsky[137], D. Scheirich[142], F. Schenck[19], M. Schernau[170], C. Schiavi[55b,55a], L.K. Schildgen[24], Z.M. Schillaci[26],

E.J. Schioppa[68a,68b], M. Schioppa[41b,41a], K.E. Schleicher[52], S. Schlenker[36], K.R. Schmidt-Sommerfeld[115], K. Schmieden[36], C. Schmitt[100], S. Schmitt[46], J.C. Schmoeckel[46], L. Schoeffel[144], A. Schoening[61b], P.G. Scholer[52], E. Schopf[134], M. Schott[100], J.F.P. Schouwenberg[119], J. Schovancova[36], S. Schramm[54], F. Schroeder[181], A. Schulte[100], H.-C. Schultz-Coulon[61a], M. Schumacher[52], B.A. Schumm[145], Ph. Schune[144], A. Schwartzman[152], T.A. Schwarz[106], Ph. Schwemling[144], R. Schwienhorst[107], A. Sciandra[145], G. Sciolla[26], M. Scornajenghi[41b,41a], F. Scuri[72a], F. Scutti[105], L.M. Scyboz[115], C.D. Sebastiani[91], P. Seema[19], S.C. Seidel[118], A. Seiden[145], B.D. Seidlitz[29], T. Seiss[37], C. Seitz[46], J.M. Seixas[81b], G. Sekhniaidze[70a], S.J. Sekula[42], N. Semprini-Cesari[23b,23a], S. Sen[49], C. Serfon[29], L. Serin[65], L. Serkin[67a,67b], M. Sessa[60a], H. Severini[128], S. Sevova[152], F. Sforza[55b,55a], A. Sfyrla[54], E. Shabalina[53], J.D. Shahinian[145], N.W. Shaikh[45a,45b], D. Shaked Renous[179], L.Y. Shan[15a], M. Shapiro[18], A. Sharma[134], A.S. Sharma[1], P.B. Shatalov[124], K. Shaw[155], S.M. Shaw[101], M. Shehade[179], Y. Shen[128], A.D. Sherman[25], P. Sherwood[95], L. Shi[95], S. Shimizu[82], C.O. Shimmin[182], Y. Shimogama[178], M. Shimojima[116], I.P.J. Shipsey[134], S. Shirabe[164], M. Shiyakova[80,z], J. Shlomi[179], A. Shmeleva[111], M.J. Shochet[37], J. Shojaii[105], D.R. Shope[153], S. Shrestha[127], E.M. Shrif[33e], E. Shulga[179], P. Sicho[140], A.M. Sickles[172], E. Sideras Haddad[33e], O. Sidiropoulou[36], A. Sidoti[23b,23a], F. Siegert[48], Dj. Sijacki[16], M.Jr. Silva[180], M.V. Silva Oliveira[36], S.B. Silverstein[45a], S. Simion[65], R. Simoniello[100], C.J. Simpson-allsop[21], S. Simsek[12b], P. Sinervo[166], V. Sinetckii[113], S. Singh[151], M. Sioli[23b,23a], I. Siral[131], S.Yu. Sivoklokov[113], J. Sjölin[45a,45b], A. Skaf[53], E. Skorda[97], P. Skubic[128], M. Slawinska[85], K. Sliwa[169], R. Slovak[142], V. Smakhtin[179], B.H. Smart[143], J. Smiesko[28b], N. Smirnov[112], S.Yu. Smirnov[112], Y. Smirnov[112], L.N. Smirnova[113,r], O. Smirnova[97], E.A. Smith[37], H.A. Smith[134], M. Smizanska[90], K. Smolek[141], A. Smykiewicz[85], A.A. Snesarev[111], H.L. Snoek[120], I.M. Snyder[131], S. Snyder[29], R. Sobie[175,ab], A. Soffer[160], A. Søgaard[50], F. Sohns[53], C.A. Solans Sanchez[36], E.Yu. Soldatov[112], U. Soldevila[173], A.A. Solodkov[123], A. Soloshenko[80], O.V. Solovyanov[123], V. Solovyev[137], P. Sommer[148], H. Son[169], W. Song[143], W.Y. Song[167b], A. Sopczak[141], A.L. Sopio[95], F. Sopkova[28b], S. Sottocornola[71a,71b], R. Soualah[67a,67c], A.M. Soukharev[122b,122a], D. South[46], S. Spagnolo[68a,68b], M. Spalla[115], M. Spangenberg[177], F. Spanò[94], D. Sperlich[52], T.M. Spieker[61a], G. Spigo[36], M. Spina[155], D.P. Spiteri[57], M. Spousta[142], A. Stabile[69a,69b], B.L. Stamas[121], R. Stamen[61a], M. Stamenkovic[120], E. Stanecka[85], B. Stanislaus[134], M.M. Stanitzki[46], M. Stankaityte[134], B. Stapf[120], E.A. Starchenko[123], G.H. Stark[145], J. Stark[58], P. Staroba[140], P. Starovoitov[61a], S. Stärz[104], R. Staszewski[85], G. Stavropoulos[44], M. Stegler[46], P. Steinberg[29], A.L. Steinhebel[131], B. Stelzer[151,167a], H.J. Stelzer[138], O. Stelzer-Chilton[167a], H. Stenzel[56], T.J. Stevenson[155], G.A. Stewart[36], M.C. Stockton[36], G. Stoicea[27b], M. Stolarski[139a], S. Stonjek[115], A. Straessner[48], J. Strandberg[153], S. Strandberg[45a,45b], M. Strauss[128], T. Strebler[102], P. Strizenec[28b], R. Ströhmer[176], D.M. Strom[131], R. Stroynowski[42], A. Strubig[50], S.A. Stucci[29], B. Stugu[17], J. Stupak[128], N.A. Styles[46], D. Su[152], W. Su[60c,147], X. Su[60a], V.V. Sulin[111], M.J. Sullivan[91], D.M.S. Sultan[54], S. Sultansoy[4c], T. Sumida[86], S. Sun[106], X. Sun[101], K. Suruliz[155], C.J.E. Suster[156], M.R. Sutton[155], S. Suzuki[82], M. Svatos[140], M. Swiatlowski[167a], S.P. Swift[2], T. Swirski[176], A. Sydorenko[100], I. Sykora[28a], M. Sykora[142], T. Sykora[142], D. Ta[100], K. Tackmann[46,x], J. Taenzer[160], A. Taffard[170], R. Tafirout[167a], E. Tagiev[123], R. Takashima[87], K. Takeda[83], T. Takeshita[149], E.P. Takeva[50], Y. Takubo[82], M. Talby[102], A.A. Talyshev[122b,122a], K.C. Tam[63b], N.M. Tamir[160], J. Tanaka[162], R. Tanaka[65], S. Tapia Araya[172], S. Tapprogge[100], A. Tarek Abouelfadl Mohamed[107], S. Tarem[159], K. Tariq[60b], G. Tarna[27b,d], G.F. Tartarelli[69a], P. Tas[142], M. Tasevsky[140], T. Tashiro[86], E. Tassi[41b,41a], A. Tavares Delgado[139a], Y. Tayalati[35e], A.J. Taylor[50], G.N. Taylor[105], W. Taylor[167b], H. Teagle[91], A.S. Tee[90], R. Teixeira De Lima[152], P. Teixeira-Dias[94], H. Ten Kate[36], J.J. Teoh[120], S. Terada[82], K. Terashi[162], J. Terron[99], S. Terzo[14], M. Testa[51], R.J. Teuscher[166,ab], S.J. Thais[182], N. Themistokleous[50], T. Theveneaux-Pelzer[46], F. Thiele[40], D.W. Thomas[94], J.O. Thomas[42], J.P. Thomas[21], E.A. Thompson[46], P.D. Thompson[21], E. Thomson[136], E.J. Thorpe[93], R.E. Ticse Torres[53], V.O. Tikhomirov[111,ah], Yu.A. Tikhonov[122b,122a], S. Timoshenko[112], P. Tipton[182], S. Tisserant[102], K. Todome[23b,23a], S. Todorova-Nova[142], S. Todt[48], J. Tojo[88], S. Tokár[28a], K. Tokushuku[82], E. Tolley[127], R. Tombs[32], K.G. Tomiwa[33e], M. Tomoto[117], L. Tompkins[152], P. Tornambe[103], E. Torrence[131], H. Torres[48], E. Torró Pastor[147], C. Tosciri[134], J. Toth[102,aa], D.R. Tovey[148], A. Traeet[17], C.J. Treado[125], T. Trefzger[176], F. Tresoldi[155], A. Tricoli[29], I.M. Trigger[167a], S. Trincaz-Duvoid[135], D.A. Trischuk[174], W. Trischuk[166], B. Trocmé[58], A. Trofymov[65], C. Troncon[69a], F. Trovato[155], L. Truong[33c], M. Trzebinski[85], A. Trzupek[85], F. Tsai[46], J.C.-L. Tseng[134], P.V. Tsiareshka[108,ae], A. Tsirigotis[161,u], V. Tsiskaridze[154], E.G. Tskhadadze[158a], M. Tsopoulou[161], I.I. Tsukerman[124], V. Tsulaia[18], S. Tsuno[82], D. Tsybychev[154], Y. Tu[63b], A. Tudorache[27b], V. Tudorache[27b], T.T. Tulbure[27a], A.N. Tuna[59], S. Turchikhin[80], D. Turgeman[179], I. Turk Cakir[4b,s], R.J. Turner[21],

R. Turra[69a], P.M. Tuts[39], S. Tzamarias[161], E. Tzovara[100], K. Uchida[162], F. Ukegawa[168], G. Unal[36], M. Unal[11], A. Undrus[29], G. Unel[170], F.C. Ungaro[105], Y. Unno[82], K. Uno[162], J. Urban[28b], P. Urquijo[105], G. Usai[8], Z. Uysal[12d], V. Vacek[141], B. Vachon[104], K.O.H. Vadla[133], T. Vafeiadis[36], A. Vaidya[95], C. Valderanis[114], E. Valdes Santurio[45a,45b], M. Valente[54], S. Valentinetti[23b,23a], A. Valero[173], L. Valéry[46], R.A. Vallance[21], A. Vallier[36], J.A. Valls Ferrer[173], T.R. Van Daalen[14], P. Van Gemmeren[6], S. Van Stroud[95], I. Van Vulpen[120], M. Vanadia[74a,74b], W. Vandelli[36], M. Vandenbroucke[144], E.R. Vandewall[129], A. Vaniachine[165], D. Vannicola[73a,73b], R. Vari[73a], E.W. Varnes[7], C. Varni[55b,55a], T. Varol[157], D. Varouchas[65], K.E. Varvell[156], M.E. Vasile[27b], G.A. Vasquez[175], F. Vazeille[38], D. Vazquez Furelos[14], T. Vazquez Schroeder[36], J. Veatch[53], V. Vecchio[101], M.J. Veen[120], L.M. Veloce[166], F. Veloso[139a,139c], S. Veneziano[73a], A. Ventura[68a,68b], A. Verbytskyi[115], V. Vercesi[71a], M. Verducci[72a,72b], C.M. Vergel Infante[79], C. Vergis[24], W. Verkerke[120], A.T. Vermeulen[120], J.C. Vermeulen[120], C. Vernieri[152], M.C. Vetterli[151,al], N. Viaux Maira[146d], T. Vickey[148], O.E. Vickey Boeriu[148], G.H.A. Viehhauser[134], L. Vigani[61b], M. Villa[23b,23a], M. Villaplana Perez[3], E.M. Villhauer[50], E. Vilucchi[51], M.G. Vincter[34], G.S. Virdee[21], A. Vishwakarma[50], C. Vittori[23b,23a], I. Vivarelli[155], M. Vogel[181], P. Vokac[141], S.E. von Buddenbrock[33e], E. Von Toerne[24], V. Vorobel[142], K. Vorobev[112], M. Vos[173], J.H. Vossebeld[91], M. Vozak[101], N. Vranjes[16], M. Vranjes Milosavljevic[16], V. Vrba[141], M. Vreeswijk[120], R. Vuillermet[36], I. Vukotic[37], S. Wada[168], P. Wagner[24], W. Wagner[181], J. Wagner-Kuhr[114], S. Wahdan[181], H. Wahlberg[89], R. Wakasa[168], V.M. Walbrecht[115], J. Walder[143], R. Walker[114], S.D. Walker[94], W. Walkowiak[150], V. Wallangen[45a,45b], A.M. Wang[59], A.Z. Wang[180], C. Wang[60a], C. Wang[60c], F. Wang[180], H. Wang[18], H. Wang[3], J. Wang[63a], P. Wang[42], Q. Wang[128], R.-J. Wang[100], R. Wang[60a], R. Wang[6], S.M. Wang[157], W.T. Wang[60a], W. Wang[15c], W.X. Wang[60a], Y. Wang[60a], Z. Wang[106], C. Wanotayaroj[46], A. Warburton[104], C.P. Ward[32], D.R. Wardrope[95], N. Warrack[57], A.T. Watson[21], M.F. Watson[21], G. Watts[147], B.M. Waugh[95], A.F. Webb[11], C. Weber[29], M.S. Weber[20], S.A. Weber[34], S.M. Weber[61a], A.R. Weidberg[134], J. Weingarten[47], M. Weirich[100], C. Weiser[52], P.S. Wells[36], T. Wenaus[29], B. Wendland[47], T. Wengler[36], S. Wenig[36], N. Wermes[24], M. Wessels[61a], T.D. Weston[20], K. Whalen[131], A.M. Wharton[90], A.S. White[106], A. White[8], M.J. White[1], D. Whiteson[170], B.W. Whitmore[90], W. Wiedenmann[180], C. Wiel[48], M. Wielers[143], N. Wieseotte[100], C. Wiglesworth[40], L.A.M. Wiik-Fuchs[52], H.G. Wilkens[36], L.J. Wilkins[94], H.H. Williams[136], S. Williams[32], S. Willocq[103], P.J. Windischhofer[134], I. Wingerter-Seez[5], E. Winkels[155], F. Winklmeier[131], B.T. Winter[52], M. Wittgen[152], M. Wobisch[96], A. Wolf[100], R. Wölker[134], J. Wollrath[52], M.W. Wolter[85], H. Wolters[139a,139c], V.W.S. Wong[174], N.L. Woods[145], S.D. Worm[46], B.K. Wosiek[85], K.W. Woźniak[85], K. Wraight[57], S.L. Wu[180], X. Wu[54], Y. Wu[60a], J. Wuerzinger[134], T.R. Wyatt[101], B.M. Wynne[50], S. Xella[40], L. Xia[177], J. Xiang[63c], X. Xiao[106], X. Xie[60a], I. Xiotidis[155], D. Xu[15a], H. Xu[60a], H. Xu[60a], L. Xu[29], T. Xu[144], W. Xu[106], Z. Xu[60b], Z. Xu[152], B. Yabsley[156], S. Yacoob[33a], K. Yajima[132], D.P. Yallup[95], N. Yamaguchi[88], Y. Yamaguchi[164], A. Yamamoto[82], M. Yamatani[162], T. Yamazaki[162], Y. Yamazaki[83], J. Yan[60c], Z. Yan[25], H.J. Yang[60c,60d], H.T. Yang[18], S. Yang[60a], T. Yang[63c], X. Yang[60b,58], Y. Yang[162], Z. Yang[60a], W.-M. Yao[18], Y.C. Yap[46], Y. Yasu[82], E. Yatsenko[60c], H. Ye[15c], J. Ye[42], S. Ye[29], I. Yeletskikh[80], M.R. Yexley[90], E. Yigitbasi[25], P. Yin[39], K. Yorita[178], K. Yoshihara[79], C.J.S. Young[36], C. Young[152], J. Yu[79], R. Yuan[60b,h], X. Yue[61a], M. Zaazoua[35e], B. Zabinski[85], G. Zacharis[10], E. Zaffaroni[54], J. Zahreddine[135], A.M. Zaitsev[123,ag], T. Zakareishvili[158b], N. Zakharchuk[34], S. Zambito[36], D. Zanzi[36], D.R. Zaripovas[57], S.V. Zeißner[47], C. Zeitnitz[181], G. Zemaityte[134], J.C. Zeng[172], O. Zenin[123], T. Ženiš[28a], D. Zerwas[65], M. Zgubič[134], B. Zhang[15c], D.F. Zhang[15b], G. Zhang[15b], J. Zhang[6], K. Zhang[15a], L. Zhang[15c], L. Zhang[60a], M. Zhang[172], R. Zhang[180], S. Zhang[106], X. Zhang[60c], X. Zhang[60b], Y. Zhang[15a,15d], Z. Zhang[63a], Z. Zhang[65], P. Zhao[49], Z. Zhao[60a], A. Zhemchugov[80], Z. Zheng[106], D. Zhong[172], B. Zhou[106], C. Zhou[180], H. Zhou[7], M.S. Zhou[15a,15d], M. Zhou[154], N. Zhou[60c], Y. Zhou[7], C.G. Zhu[60b], C. Zhu[15a,15d], H.L. Zhu[60a], H. Zhu[15a], J. Zhu[106], Y. Zhu[60a], X. Zhuang[15a], K. Zhukov[111], V. Zhulanov[122b,122a], D. Zieminska[66], N.I. Zimine[80], S. Zimmermann[52], Z. Zinonos[115], M. Ziolkowski[150], L. Živković[16], G. Zobernig[180], A. Zoccoli[23b,23a], K. Zoch[53], T.G. Zorbas[148], R. Zou[37], L. Zwalinski[36]

[1] Department of Physics, University of Adelaide, Adelaide, Australia
[2] Physics Department, SUNY Albany, Albany, NY, USA
[3] Department of Physics, University of Alberta, Edmonton, AB, Canada
[4] [(a)]Department of Physics, Ankara University, Ankara, Turkey; [(b)]Istanbul Aydin University, Application and Research Center for Advanced Studies, Istanbul, Turkey; [(c)]Division of Physics, TOBB University of Economics and Technology, Ankara, Turkey

[5] LAPP, Université Grenoble Alpes, Université Savoie Mont Blanc, CNRS/IN2P3, Annecy, France
[6] High Energy Physics Division, Argonne National Laboratory, Argonne, IL, USA
[7] Department of Physics, University of Arizona, Tucson, AZ, USA
[8] Department of Physics, University of Texas at Arlington, Arlington, TX, USA
[9] Physics Department, National and Kapodistrian University of Athens, Athens, Greece
[10] Physics Department, National Technical University of Athens, Zografou, Greece
[11] Department of Physics, University of Texas at Austin, Austin, TX, USA
[12] [(a)]Faculty of Engineering and Natural Sciences, Bahcesehir University, Istanbul, Turkey; [(b)]Faculty of Engineering and Natural Sciences, Istanbul Bilgi University, Istanbul, Turkey; [(c)]Department of Physics, Bogazici University, Istanbul, Turkey; [(d)]Department of Physics Engineering, Gaziantep University, Gaziantep, Turkey
[13] Institute of Physics, Azerbaijan Academy of Sciences, Baku, Azerbaijan
[14] Institut de Física d'Altes Energies (IFAE), Barcelona Institute of Science and Technology, Barcelona, Spain
[15] [(a)]Institute of High Energy Physics, Chinese Academy of Sciences, Beijing, China; [(b)]Physics Department, Tsinghua University, Beijing, China; [(c)]Department of Physics, Nanjing University, Nanjing, China; [(d)]University of Chinese Academy of Science (UCAS), Beijing, China
[16] Institute of Physics, University of Belgrade, Belgrade, Serbia
[17] Department for Physics and Technology, University of Bergen, Bergen, Norway
[18] Physics Division, Lawrence Berkeley National Laboratory and University of California, Berkeley, CA, USA
[19] Institut für Physik, Humboldt Universität zu Berlin, Berlin, Germany
[20] Albert Einstein Center for Fundamental Physics and Laboratory for High Energy Physics, University of Bern, Bern, Switzerland
[21] School of Physics and Astronomy, University of Birmingham, Birmingham, UK
[22] [(a)]Facultad de Ciencias y Centro de Investigaciónes, Universidad Antonio Nariño, Bogotá, Colombia; [(b)]Departamento de Física, Universidad Nacional de Colombia, Bogotá, Colombia
[23] [(a)]Dipartimento di Fisica, INFN Bologna and Universita' di Bologna, Bologna, Italy; [(b)]INFN Sezione di Bologna, Bologna, Italy
[24] Physikalisches Institut, Universität Bonn, Bonn, Germany
[25] Department of Physics, Boston University, Boston, MA, USA
[26] Department of Physics, Brandeis University, Waltham, MA, USA
[27] [(a)]Transilvania University of Brasov, Brasov, Romania; [(b)]Horia Hulubei National Institute of Physics and Nuclear Engineering, Bucharest, Romania; [(c)]Department of Physics, Alexandru Ioan Cuza University of Iasi, Iasi, Romania; [(d)]Physics Department, National Institute for Research and Development of Isotopic and Molecular Technologies, Cluj-Napoca, Romania; [(e)]University Politehnica Bucharest, Bucharest, Romania; [(f)]West University in Timisoara, Timisoara, Romania
[28] [(a)]Faculty of Mathematics, Physics and Informatics, Comenius University, Bratislava, Slovakia; [(b)]Department of Subnuclear Physics, Institute of Experimental Physics of the Slovak Academy of Sciences, Kosice, Slovak Republic
[29] Physics Department, Brookhaven National Laboratory, Upton, NY, USA
[30] Departamento de Física, Universidad de Buenos Aires, Buenos Aires, Argentina
[31] California State University, Long Beach, CA, USA
[32] Cavendish Laboratory, University of Cambridge, Cambridge, UK
[33] [(a)]Department of Physics, University of Cape Town, Cape Town, South Africa; [(b)]iThemba Labs, Western Cape, South Africa; [(c)]Department of Mechanical Engineering Science, University of Johannesburg, Johannesburg, South Africa; [(d)]University of South Africa, Department of Physics, Pretoria, South Africa; [(e)]School of Physics, University of the Witwatersrand, Johannesburg, South Africa
[34] Department of Physics, Carleton University, Ottawa, ON, Canada
[35] [(a)]Faculté des Sciences Ain Chock, Réseau Universitaire de Physique des Hautes Energies, Université Hassan II, Casablanca, Morocco; [(b)]Faculté des Sciences, Université Ibn-Tofail, Kénitra, Morocco; [(c)]Faculté des Sciences Semlalia, Université Cadi Ayyad, LPHEA-Marrakech, Morocco; [(d)]Faculté des Sciences, Université Mohamed Premier and LPTPM, Oujda, Morocco; [(e)]Faculté des sciences, Université Mohammed V, Rabat, Morocco
[36] CERN, Geneva, Switzerland
[37] Enrico Fermi Institute, University of Chicago, Chicago, IL, USA
[38] LPC, Université Clermont Auvergne, CNRS/IN2P3, Clermont-Ferrand, France
[39] Nevis Laboratory, Columbia University, Irvington, NY, USA

[40] Niels Bohr Institute, University of Copenhagen, Copenhagen, Denmark
[41] [(a)]Dipartimento di Fisica, Università della Calabria, Rende, Italy; [(b)]INFN Gruppo Collegato di Cosenza, Laboratori Nazionali di Frascati, Italy
[42] Physics Department, Southern Methodist University, Dallas, TX, USA
[43] Physics Department, University of Texas at Dallas, Richardson, TX, USA
[44] National Centre for Scientific Research "Demokritos", Agia Paraskevi, Greece
[45] [(a)]Department of Physics, Stockholm University, Stockholm, Sweden; [(b)]Oskar Klein Centre, Stockholm, Sweden
[46] Deutsches Elektronen-Synchrotron DESY, Hamburg and Zeuthen, Germany
[47] Lehrstuhl für Experimentelle Physik IV, Technische Universität Dortmund, Dortmund, Germany
[48] Institut für Kern- und Teilchenphysik, Technische Universität Dresden, Dresden, Germany
[49] Department of Physics, Duke University, Durham, NC, USA
[50] SUPA-School of Physics and Astronomy, University of Edinburgh, Edinburgh, UK
[51] INFN e Laboratori Nazionali di Frascati, Frascati, Italy
[52] Physikalisches Institut, Albert-Ludwigs-Universität Freiburg, Freiburg, Germany
[53] II. Physikalisches Institut, Georg-August-Universität Göttingen, Göttingen, Germany
[54] Département de Physique Nucléaire et Corpusculaire, Université de Genève, Geneva, Switzerland
[55] [(a)]Dipartimento di Fisica, Università di Genova, Genoa, Italy; [(b)]INFN Sezione di Genova, Genoa, Italy
[56] II. Physikalisches Institut, Justus-Liebig-Universität Giessen, Giessen, Germany
[57] SUPA - School of Physics and Astronomy, University of Glasgow, Glasgow, UK
[58] LPSC, Université Grenoble Alpes, CNRS/IN2P3, Grenoble INP, Grenoble, France
[59] Laboratory for Particle Physics and Cosmology, Harvard University, Cambridge, MA, USA
[60] [(a)]Department of Modern Physics and State Key Laboratory of Particle Detection and Electronics, University of Science and Technology of China, Hefei, China; [(b)]Institute of Frontier and Interdisciplinary Science and Key Laboratory of Particle Physics and Particle Irradiation (MOE), Shandong University, Qingdao, China; [(c)]School of Physics and Astronomy, Shanghai Jiao Tong University, KLPPAC-MoE, SKLPPC, Shanghai, China; [(d)]Tsung-Dao Lee Institute, Shanghai, China
[61] [(a)]Kirchhoff-Institut für Physik, Ruprecht-Karls-Universität Heidelberg, Heidelberg, Germany; [(b)]Physikalisches Institut, Ruprecht-Karls-Universität Heidelberg, Heidelberg, Germany
[62] Faculty of Applied Information Science, Hiroshima Institute of Technology, Hiroshima, Japan
[63] [(a)]Department of Physics, Chinese University of Hong Kong, Shatin, N.T., Hong Kong; [(b)]Department of Physics, University of Hong Kong, Pok Fu Lam, Hong Kong; [(c)]Department of Physics and Institute for Advanced Study, Hong Kong University of Science and Technology, Clear Water Bay, Kowloon, Hong Kong, China
[64] Department of Physics, National Tsing Hua University, Hsinchu, Taiwan
[65] IJCLab, Université Paris-Saclay, CNRS/IN2P3, 91405 Orsay, France
[66] Department of Physics, Indiana University, Bloomington, IN, USA
[67] [(a)]INFN Gruppo Collegato di Udine, Sezione di Trieste, Udine, Italy; [(b)]ICTP, Trieste, Italy; [(c)]Dipartimento Politecnico di Ingegneria e Architettura, Università di Udine, Udine, Italy
[68] [(a)]INFN Sezione di Lecce, Lecce, Italy; [(b)]Dipartimento di Matematica e Fisica, Università del Salento, Lecce, Italy
[69] [(a)]INFN Sezione di Milano, Milan, Italy; [(b)]Dipartimento di Fisica, Università di Milano, Milan, Italy
[70] [(a)]INFN Sezione di Napoli, Naples, Italy; [(b)]Dipartimento di Fisica, Università di Napoli, Naples, Italy
[71] [(a)]INFN Sezione di Pavia, Pavia, Italy; [(b)]Dipartimento di Fisica, Università di Pavia, Pavia, Italy
[72] [(a)]INFN Sezione di Pisa, Pisa, Italy; [(b)]Dipartimento di Fisica E. Fermi, Università di Pisa, Pisa, Italy
[73] [(a)]INFN Sezione di Roma, Rome, Italy; [(b)]Dipartimento di Fisica, Sapienza Università di Roma, Rome, Italy
[74] [(a)]INFN Sezione di Roma Tor Vergata, Rome, Italy; [(b)]Dipartimento di Fisica, Università di Roma Tor Vergata, Rome, Italy
[75] [(a)]INFN Sezione di Roma Tre, Rome, Italy; [(b)]Dipartimento di Matematica e Fisica, Università Roma Tre, Rome, Italy
[76] [(a)]INFN-TIFPA, Trento, Italy; [(b)]Università degli Studi di Trento, Trento, Italy
[77] Institut für Astro- und Teilchenphysik, Leopold-Franzens-Universität, Innsbruck, Austria
[78] University of Iowa, Iowa City, IA, USA
[79] Department of Physics and Astronomy, Iowa State University, Ames, IA, USA
[80] Joint Institute for Nuclear Research, Dubna, Russia
[81] [(a)]Departamento de Engenharia Elétrica, Universidade Federal de Juiz de Fora (UFJF), Juiz de Fora,

Brazil; [b]Universidade Federal do Rio De Janeiro COPPE/EE/IF, Rio de Janeiro, Brazil; [c]Universidade Federal de São João del Rei (UFSJ), São João del Rei, Brazil; [d]Instituto de Física, Universidade de São Paulo, São Paulo, Brazil
[82] KEK, High Energy Accelerator Research Organization, Tsukuba, Japan
[83] Graduate School of Science, Kobe University, Kobe, Japan
[84] [a]Faculty of Physics and Applied Computer Science, AGH University of Science and Technology, Krakow, Poland; [b]Marian Smoluchowski Institute of Physics, Jagiellonian University, Krakow, Poland
[85] Institute of Nuclear Physics Polish Academy of Sciences, Krakow, Poland
[86] Faculty of Science, Kyoto University, Kyoto, Japan
[87] Kyoto University of Education, Kyoto, Japan
[88] Research Center for Advanced Particle Physics and Department of Physics, Kyushu University, Fukuoka, Japan
[89] Instituto de Física La Plata, Universidad Nacional de La Plata and CONICET, La Plata, Argentina
[90] Physics Department, Lancaster University, Lancaster, UK
[91] Oliver Lodge Laboratory, University of Liverpool, Liverpool, UK
[92] Department of Experimental Particle Physics, Jožef Stefan Institute and Department of Physics, University of Ljubljana, Ljubljana, Slovenia
[93] School of Physics and Astronomy, Queen Mary University of London, London, UK
[94] Department of Physics, Royal Holloway University of London, Egham, UK
[95] Department of Physics and Astronomy, University College London, London, UK
[96] Louisiana Tech University, Ruston, LA, USA
[97] Fysiska institutionen, Lunds universitet, Lund, Sweden
[98] Centre de Calcul de l'Institut National de Physique Nucléaire et de Physique des Particules (IN2P3), Villeurbanne, France
[99] Departamento de Física Teorica C-15 and CIAFF, Universidad Autónoma de Madrid, Madrid, Spain
[100] Institut für Physik, Universität Mainz, Mainz, Germany
[101] School of Physics and Astronomy, University of Manchester, Manchester, UK
[102] CPPM, Aix-Marseille Université, CNRS/IN2P3, Marseille, France
[103] Department of Physics, University of Massachusetts, Amherst, MA, USA
[104] Department of Physics, McGill University, Montreal, QC, Canada
[105] School of Physics, University of Melbourne, Melbourne, VIC, Australia
[106] Department of Physics, University of Michigan, Ann Arbor, MI, USA
[107] Department of Physics and Astronomy, Michigan State University, East Lansing, MI, USA
[108] B.I. Stepanov Institute of Physics, National Academy of Sciences of Belarus, Minsk, Belarus
[109] Research Institute for Nuclear Problems of Byelorussian State University, Minsk, Belarus
[110] Group of Particle Physics, University of Montreal, Montreal, QC, Canada
[111] P.N. Lebedev Physical Institute of the Russian Academy of Sciences, Moscow, Russia
[112] National Research Nuclear University MEPhI, Moscow, Russia
[113] D.V. Skobeltsyn Institute of Nuclear Physics, M.V. Lomonosov Moscow State University, Moscow, Russia
[114] Fakultät für Physik, Ludwig-Maximilians-Universität München, Munich, Germany
[115] Max-Planck-Institut für Physik (Werner-Heisenberg-Institut), Munich, Germany
[116] Nagasaki Institute of Applied Science, Nagasaki, Japan
[117] Graduate School of Science and Kobayashi-Maskawa Institute, Nagoya University, Nagoya, Japan
[118] Department of Physics and Astronomy, University of New Mexico, Albuquerque, NM, USA
[119] Institute for Mathematics, Astrophysics and Particle Physics, Radboud University Nijmegen/Nikhef, Nijmegen, The Netherlands
[120] Nikhef National Institute for Subatomic Physics and University of Amsterdam, Amsterdam, The Netherlands
[121] Department of Physics, Northern Illinois University, DeKalb, IL, USA
[122] [a]Budker Institute of Nuclear Physics and NSU, SB RAS, Novosibirsk, Russia; [b]Novosibirsk State University, Novosibirsk, Russia
[123] Institute for High Energy Physics of the National Research Centre Kurchatov Institute, Protvino, Russia
[124] Institute for Theoretical and Experimental Physics named by A.I. Alikhanov of National Research Centre "Kurchatov Institute", Moscow, Russia
[125] Department of Physics, New York University, New York, NY, USA
[126] Ochanomizu University, Otsuka, Bunkyo-ku, Tokyo, Japan

[127] Ohio State University, Columbus, OH, USA
[128] Homer L. Dodge Department of Physics and Astronomy, University of Oklahoma, Norman, OK, USA
[129] Department of Physics, Oklahoma State University, Stillwater, OK, USA
[130] Palacký University, RCPTM, Joint Laboratory of Optics, Olomouc, Czech Republic
[131] Institute for Fundamental Science, University of Oregon, Eugene, OR, USA
[132] Graduate School of Science, Osaka University, Osaka, Japan
[133] Department of Physics, University of Oslo, Oslo, Norway
[134] Department of Physics, Oxford University, Oxford, UK
[135] LPNHE, Sorbonne Université, Université de Paris, CNRS/IN2P3, Paris, France
[136] Department of Physics, University of Pennsylvania, Philadelphia, PA, USA
[137] Konstantinov Nuclear Physics Institute of National Research Centre "Kurchatov Institute", PNPI, St. Petersburg, Russia
[138] Department of Physics and Astronomy, University of Pittsburgh, Pittsburgh, PA, USA
[139] [(a)]Laboratório de Instrumentação e Física Experimental de Partículas-LIP, Lisbon, Portugal; [(b)]Departamento de Física, Faculdade de Ciências, Universidade de Lisboa, Lisbon, Portugal; [(c)]Departamento de Física, Universidade de Coimbra, Coimbra, Portugal; [(d)]Centro de Física Nuclear da Universidade de Lisboa, Lisbon, Portugal; [(e)]Departamento de Física, Universidade do Minho, Braga, Portugal; [(f)]Departamento de Física Teórica y del Cosmos, Universidad de Granada, Granada, Spain; [(g)]Dep Física and CEFITEC of Faculdade de Ciências e Tecnologia, Universidade Nova de Lisboa, Caparica, Portugal; [(h)]Instituto Superior Técnico, Universidade de Lisboa, Lisbon, Portugal
[140] Institute of Physics of the Czech Academy of Sciences, Prague, Czech Republic
[141] Czech Technical University in Prague, Prague, Czech Republic
[142] Faculty of Mathematics and Physics, Charles University, Prague, Czech Republic
[143] Particle Physics Department, Rutherford Appleton Laboratory, Didcot, UK
[144] IRFU, CEA, Université Paris-Saclay, Gif-sur-Yvette, France
[145] Santa Cruz Institute for Particle Physics, University of California Santa Cruz, Santa Cruz, CA, USA
[146] [(a)]Departamento de Física, Pontificia Universidad Católica de Chile, Santiago, Chile; [(b)]Universidad Andres Bello, Department of Physics, Santiago, Chile; [(c)]Instituto de Alta Investigación, Universidad de Tarapacá, Arica, Chile; [(d)]Departamento de Física, Universidad Técnica Federico Santa María, Valparaíso, Chile
[147] Department of Physics, University of Washington, Seattle, WA, USA
[148] Department of Physics and Astronomy, University of Sheffield, Sheffield, UK
[149] Department of Physics, Shinshu University, Nagano, Japan
[150] Department Physik, Universität Siegen, Siegen, Germany
[151] Department of Physics, Simon Fraser University, Burnaby, BC, Canada
[152] SLAC National Accelerator Laboratory, Stanford, CA, USA
[153] Physics Department, Royal Institute of Technology, Stockholm, Sweden
[154] Departments of Physics and Astronomy, Stony Brook University, Stony Brook, NY, USA
[155] Department of Physics and Astronomy, University of Sussex, Brighton, UK
[156] School of Physics, University of Sydney, Sydney, Australia
[157] Institute of Physics, Academia Sinica, Taipei, Taiwan
[158] [(a)]E. Andronikashvili Institute of Physics, Iv. Javakhishvili Tbilisi State University, Tbilisi, Georgia; [(b)]High Energy Physics Institute, Tbilisi State University, Tbilisi, Georgia
[159] Department of Physics, Technion, Israel Institute of Technology, Haifa, Israel
[160] Raymond and Beverly Sackler School of Physics and Astronomy, Tel Aviv University, Tel Aviv, Israel
[161] Department of Physics, Aristotle University of Thessaloniki, Thessaloniki, Greece
[162] International Center for Elementary Particle Physics and Department of Physics, University of Tokyo, Tokyo, Japan
[163] Graduate School of Science and Technology, Tokyo Metropolitan University, Tokyo, Japan
[164] Department of Physics, Tokyo Institute of Technology, Tokyo, Japan
[165] Tomsk State University, Tomsk, Russia
[166] Department of Physics, University of Toronto, Toronto, ON, Canada
[167] [(a)]TRIUMF, Vancouver, BC, Canada; [(b)]Department of Physics and Astronomy, York University, Toronto, ON, Canada
[168] Division of Physics and Tomonaga Center for the History of the Universe, Faculty of Pure and Applied Sciences, University of Tsukuba, Tsukuba, Japan
[169] Department of Physics and Astronomy, Tufts University, Medford, MA, USA
[170] Department of Physics and Astronomy, University of California Irvine, Irvine, CA, USA

[171] Department of Physics and Astronomy, University of Uppsala, Uppsala, Sweden
[172] Department of Physics, University of Illinois, Urbana, IL, USA
[173] Instituto de Física Corpuscular (IFIC), Centro Mixto Universidad de Valencia - CSIC, Valencia, Spain
[174] Department of Physics, University of British Columbia, Vancouver, BC, Canada
[175] Department of Physics and Astronomy, University of Victoria, Victoria, BC, Canada
[176] Fakultät für Physik und Astronomie, Julius-Maximilians-Universität Würzburg, Würzburg, Germany
[177] Department of Physics, University of Warwick, Coventry, UK
[178] Waseda University, Tokyo, Japan
[179] Department of Particle Physics and Astrophysics, Weizmann Institute of Science, Rehovot, Israel
[180] Department of Physics, University of Wisconsin, Madison, WI, USA
[181] Fakultät für Mathematik und Naturwissenschaften, Fachgruppe Physik, Bergische Universität Wuppertal, Wuppertal, Germany
[182] Department of Physics, Yale University, New Haven, CT, USA

[a] Also at Borough of Manhattan Community College, City University of New York, New York, NY, USA
[b] Also at Centro Studi e Ricerche Enrico Fermi, Rome, Italy
[c] Also at CERN, Geneva, Switzerland
[d] Also at CPPM, Aix-Marseille Université, CNRS/IN2P3, Marseille, France
[e] Also at Département de Physique Nucléaire et Corpusculaire, Université de Genève, Geneva, Switzerland
[f] Also at Departament de Fisica de la Universitat Autonoma de Barcelona, Barcelona, Spain
[g] Also at Department of Financial and Management Engineering, University of the Aegean, Chios, Greece
[h] Also at Department of Physics and Astronomy, Michigan State University, East Lansing, MI, USA
[i] Also at Department of Physics and Astronomy, University of Louisville, Louisville, KY, USA
[j] Also at Department of Physics, Ben Gurion University of the Negev, Beer Sheva, Israel.
[k] Also at Department of Physics, California State University, East Bay, USA
[l] Also at Department of Physics, California State University, Fresno, USA
[m] Also at Department of Physics, California State University, Sacramento, USA
[n] Also at Department of Physics, King's College London, London, UK
[o] Also at Department of Physics, St. Petersburg State Polytechnical University, St. Petersburg, Russia
[p] Also at Department of Physics, University of Fribourg, Fribourg, Switzerland
[q] Also at Dipartimento di Matematica, Informatica e Fisica, Università di Udine, Udine, Italy
[r] Also at Faculty of Physics, M.V. Lomonosov Moscow State University, Moscow, Russia
[s] Also at Giresun University, Faculty of Engineering, Giresun, Turkey
[t] Also at Graduate School of Science, Osaka University, Osaka, Japan
[u] Also at Hellenic Open University, Patras, Greece
[v] Also at IJCLab, Université Paris-Saclay, CNRS/IN2P3, 91405 Orsay, France
[w] Also at Institucio Catalana de Recerca i Estudis Avancats, ICREA, Barcelona, Spain
[x] Also at Institut für Experimentalphysik, Universität Hamburg, Hamburg, Germany
[y] Also at Institute for Mathematics, Astrophysics and Particle Physics, Radboud University Nijmegen/Nikhef, Nijmegen, The Netherlands
[z] Also at Institute for Nuclear Research and Nuclear Energy (INRNE) of the Bulgarian Academy of Sciences, Sofia, Bulgaria
[aa] Also at Institute for Particle and Nuclear Physics, Wigner Research Centre for Physics, Budapest, Hungary
[ab] Also at Institute of Particle Physics (IPP), Montreal, Canada
[ac] Also at Institute of Physics, Azerbaijan Academy of Sciences, Baku, Azerbaijan
[ad] Also at Instituto de Fisica Teorica, IFT-UAM/CSIC, Madrid, Spain
[ae] Also at Joint Institute for Nuclear Research, Dubna, Russia
[af] Also at Louisiana Tech University, Ruston, LA, USA
[ag] Also at Moscow Institute of Physics and Technology State University, Dolgoprudny, Russia
[ah] Also at National Research Nuclear University MEPhI, Moscow, Russia
[ai] Also at Physics Department, An-Najah National University, Nablus, Palestine
[aj] Also at Physikalisches Institut, Albert-Ludwigs-Universität Freiburg, Freiburg, Germany
[ak] Also at The City College of New York, New York, NY, USA

[al] Also at TRIUMF, Vancouver, BC, Canada
[am] Also at Universita di Napoli Parthenope, Naples, Italy
[an] Also at University of Chinese Academy of Sciences (UCAS), Beijing, China
*Deceased